UNIVERSIDADE DE SÃO PAULO
INSTITUTO DE FÍSICA DE SÃO CARLOS

Clara Maria Gonçalves de Faria

Photobiomodulation effects and applications in oncology

São Carlos

2021

Clara Maria Gonçalves de Faria

Photobiomodulation effects and applications in oncology

Thesis presented to the Graduate Program in Physics at the Instituto de Física de São Carlos da Universidade de São Paulo, to obtain the degree of Doctor in Science.

Concentration area: Applied Physics

Advisor: Prof. Dr. Vanderlei Salvador Bagnato

Original version

São Carlos

2021

Ficha catalográfica revisada pelo Serviço de Biblioteca e Informação Prof. Bernhard Gross, com os dados fornecidos pelo(a) autor(a)

de Faria, Clara M G
S856m Photobiomodulation effects and applications in oncology / Clara Maria Gonçalves de Faria ; orientador Vanderlei Salvador Bagnato. – São Carlos, 2021.
76 p. : il. (algumas color.) ; 30 cm.

Thesis (Doctorate - Graduate Program in Applied Physics) – Instituto de Física de São Carlos, Universidade de São Paulo, 2021.

1. Photobiomodulation therapy. 2. Radiotherapy. 3. Photodynamic therapy 4. Oncology. I. Bagnato, Vanderlei Salvador, orient. II. Título.

FOLHA DE APROVAÇÃO

Clara Maria Gonçalves de Faria

Tese apresentada ao Instituto de Física de São Carlos da Universidade de São Paulo para obtenção do título de Doutora em Ciências. Área de Concentração: Física Aplicada.

Aprovado(a) em: 23/07/2021

Comissão Julgadora

Dr(a). Vanderlei Salvador Bagnato

Instituição: (IFSC/USP)

Dr(a). Manoela Domingues Martins

Instituição: (UFRGS/Porto Alegre)

Dr(a). Martha Simões Ribeiro

Instituição: (IPEN/São Paulo)

Dr(a). Roberto Santana da Silva

Instituição: (FCFRP/USP)

Dr(a). Luciano Bachmann

Instituição: (FFCLRP/USP)

ACKNOWLEDGEMENTS

This work would not be possible without the contribution of many dear people. Firstly, I would like to thank my family and friends, who provided the love, opportunities, and stability needed to walk this long and challenging path. Secondly, I'd like to acknowledge the support of my research group, from my colleagues, to technicians and professors. For all the help with paper work, advices, and all the learning I got from you. Then, I must thank the colleagues and friends who contributed directly to the project as co-authors of the articles: Camilla S Costa, Claudia Barrera-Patiño, Heloísa Ciol, Lucas De Pretto, Lucimar De Avó and Sebastião Pratavieira. It is known that one person cannot know it all, so you were fundamental to make this a cohesive interdisciplinary work. At last, I thank my advisor professor Vanderlei S Bagnato, for the opportunities, advices and guidance and for never doubting the potential of this projects as well as my own.

THIS STUDY WAS FINANCED IN PART BY THE COORDENAÇÃO DE APERFEIÇOAMENTO DE PESSOAL DE NÍVEL SUPERIOR - BRASIL (CAPES) - FINANCE CODE 001 AND BY THE FUNDAÇÃO DE AMPARO À PESQUISA DO ESTADO DE SÃO PAULO (FAPESP) PROCESS NUMBER 2017/14182-4.

ABSTRACT

DE FARIA, C. **Photobiomodulation effects and applications in oncology**. 2021. 76p. Thesis (Doctor in Science) - Instituto de Física de São Carlos, Universidade de São Paulo, São Carlos, 2021.

Photobiomodulation therapy employs light with low energy densities to treat several conditions, from wounds to neural diseases. The molecular basis of its effects is being unveiled, but it is stated that the cytochrome-c oxidase enzyme in mitochondria, a photon acceptor of PBMT, contributes to an increase in ATP production and modulates the reduction and oxidation of electron carriers NADH and FAD. Since its effects are not fully understood, PBMT is not used on tumors. Thus, it is interesting to investigate if its effects correlate to mitochondrial metabolism. This study indicates that PBMT decreases the redox state of oral cancer by possibly increasing glycolysis and affects normal and tumor cells through distinct pathways. Additionally, since the combination of metabolic modifications and photodynamic therapy is very attractive, the current study investigates the effects of near-infrared PBMT combined with porphyrin-based photodynamic therapy (PDT) in squamous cell carcinoma cell lines SCC-25 and SCC-4. PBMT enhanced PDT action in SCC-25 cells by increasing photosensitizer (PS) uptake and production of reactive oxygen species (ROS), while the equivalent was not seen in SCC-4 cells compared to the PDT only group. Finally, since the most successful PBMT application is in the prevention and reduction of morbidities in radiotherapy patients, such as oral mucositis, we have investigated its potential in sensitizing tumors to radiation. Here, we demonstrate its potential for skin cancer treatment using a 780-nm light source and an X-ray irradiator by showing increased DNA damage and death in cells and a 30% increase in median survival in mice. Our results indicate that the mechanism underlying these results is likely to be the modulation of the cell cycle and angiogenesis, causing an increase in necrosis when combined with radiation. Therefore, we believe the combination of PBMT and other oncological modalities is worth exploring, for its benefit-cost ratio and simple protocols, along with the possibility of improvement in treatment results.

Keywords: Photobiomodulation therapy. Radiotherapy. Photodynamic therapy. Oncology.

RESUMO

DE FARIA, C. **Efeitos e aplicações da fotobiomodulação na oncologia**. 2021. 76p. Tese (Doutor em Ciências) - Instituto de Física de São Carlos, Universidade de São Paulo, São Carlos, 2021.

A terapia de fotobiomodulação emprega luz com baixa densidade de energia para tratar diversas condições, desde feridas até doenças neurais. A base molecular de seus efeitos está sendo desvendada, mas afirma-se que a enzima citocromo-c oxidase na mitocôndria, aceptora de fótons da PBMT, contribui para o aumento da produção de ATP e modula a redução e oxidação dos portadores de elétrons NADH e FAD. Uma vez que seus efeitos não são totalmente compreendidos, a PBMT não é usado em tumores. Assim, é interessante investigar se seus efeitos se correlacionam com o metabolismo mitocondrial. Este estudo indica que a PBMT diminui o estado redox do câncer oral, possivelmente aumentando a glicólise, e afeta as células normais e tumorais por meio de vias distintas. Além disso, uma vez que a combinação de modificações metabólicas e terapia fotodinâmica é muito atraente, o presente estudo investiga os efeitos da PBMT combinada a terapia fotodinâmica (PDT) usando porfirina em linhagens celulares de carcinoma de células escamosas SCC-25 e SCC-4. A PBMT aumentou a ação da PDT em células SCC-25 aumentando a captação do fotossensibilizador (PS) e a produção de espécies reativas de oxigênio (ROS), enquanto o equivalente não foi visto nas células SCC-4 em comparação com o grupo somente PDT. Finalmente, uma vez que a aplicação de PBMT mais bem-sucedida é na prevenção e redução de morbidades em pacientes com radioterapia, como a mucosite oral, investigamos seu efeito para sensibilizar tumores à radiação. Aqui, demonstramos seu potencial para o tratamento do câncer de pele usando uma fonte de luz de 780 nm e um irradiador de raios-X, mostrando aumento de danos ao DNA e morte em células e um aumento de 30 % na sobrevida média em camundongos. Nossos resultados indicam que o mecanismo subjacente a esses resultados é provavelmente a modulação do ciclo celular e a angiogênese, causando um aumento da necrose quando combinada com a radiação. Em síntese, acreditamos que vale a pena explorar a combinação do PBMT com outras modalidades oncológicas, por sua relação custo-benefício e protocolos simples, além da possibilidade de melhora nos resultados do tratamento.

Palavras-chave: Terapia de fotobiomodulação. Radioterapia. Terapia fotodinâmica. Oncologia.

LIST OF FIGURES

CONTENTS

1 INTRODUCTION

1.1 Photobiomodulation Therapy

Light stimulation, in relatively low fluences, has been used in clinical practice for more than fifty years. It has been previously known as low-level laser (or light) therapy (LLLT), low-intensity laser therapy, low-power laser therapy, cold laser, soft laser, and photobiostimulation. The nomenclature changed to remove the ambiguity of the words "low" and "level", since the first is not accurately definable and the latter is no longer appropriate, as other types of light devices are also used. (1) A nomenclature consensus was achieved in a joint conference of the North American Association for Light Therapy (NAALT) and the World Association for Laser Therapy (WALT) in 2014 and "Photobiomodulation Therapy" was chosen. Since then, a more comprehensive definition for the term has been suggested as "a form of light therapy that utilizes non-ionizing forms of light sources, including lasers, LEDs, and broadband light, in the visible and infrared spectrum. It is a nonthermal process involving endogenous chromophores eliciting photophysical (i.e., linear and nonlinear) and photochemical events at various biological scales. This process results in beneficial therapeutic outcomes including but not limited to the alleviation of pain or inflammation, immunomodulation, and pro-motion of wound healing and tissue regeneration". (2) Its main effects are: increased intracellular concentration of (adenosine triphosphate) ATP, calcium ions (Ca2 +), nitric oxide (NO) and production of reactive oxygen species (ROSs) by the mitochondria, as a superoxide anion radical (O2- $\cdot$). As a consequence, activation of pro-survival mechanisms, protein synthesis, migration, vasodilation and several other metabolic changes are observed. (3) Several evidence support the hypothesis that the enzyme citocrom c oxidase (COX) is the primary acceptor of light in PBM. (4) The retrograde mithocondrial signaling suggests that after photon absorption by COX, the mithocondrial membrane potential is altered resulting in changes in the metabolic basal rate resulting in ROS, NO, Ca2+ and ATP synthesis modulation, given the increase in protons in the intermembranes space. Other action sites of PBM are the light sensitive ion channels, which depolarize the membrane when activated, and the excitation of transcription factors, which modulate the expression of several genes regulatin inflammatory response, proliferation and stress response. (5) Some of them are mentioned and further explained in the text. One of the reasons for general resistance to PBMT is the lack of protocol standardization: wavelengths vary from 600 to 1000 nm, fluences from 1 to 1000 J/cm^2, and the intervals for irradiance are also wide. Because PBMT is dependent on light absorption under specific conditions, as it must match the chromophore excitation wavelength, this variation causes significant differences in results among studies. (6) Additionally, PBM follows a biphasic dose-response according to the

Arndt-Schulz law, meaning that at a specific interval cell activation is proportional to the energy of light, and after the peak, the increase in this stimulus results in the absence of response or an inhibitory one. (7) Therefore, at high or low fluences, it is observed none of the expected effects or the occurrence of others, sometimes undesirable (Figure 1). The tricky part is that the definition of the PBM action interval, defining the limits of low or high fluences, depends on the combination of wavelength and excitation intensity and the cell line. (8)

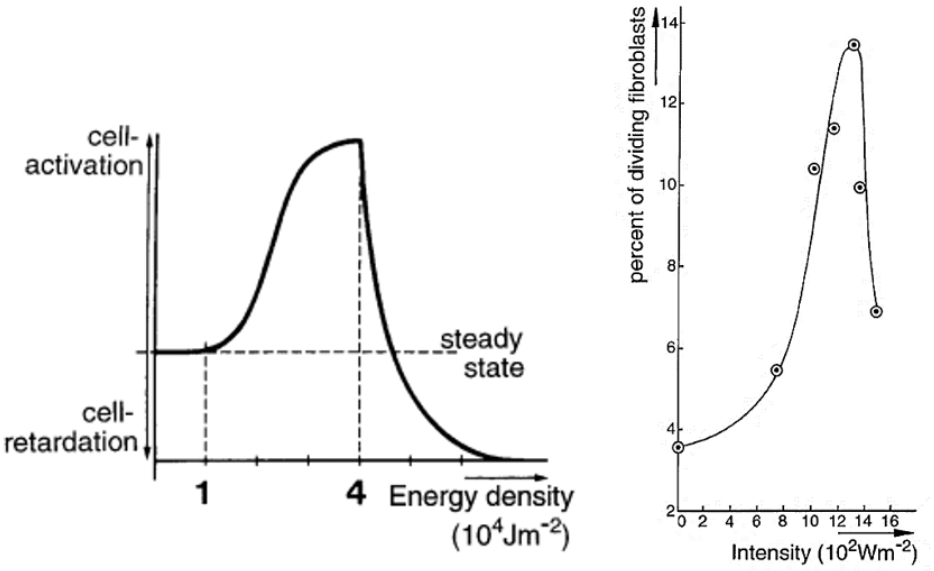

Figure 1 – Generic Arndt-Schulz curve (left) and experimental curve of the experimental curve of the percentage of dividing fibroblasts as a function of light intensity.

Source: SOMMER, A. P. *et al.* (9)

Thus, the determination of the lighting parameters is fundamental in PBMT. The fluence delivered usually ranges from 0.04 to 50 J/cm^2, with irradiance between 5 mW/cm^2 - 300 mW/cm^2, in the region of 600-700 nm and 780-1100 nm, depending on the application. In 2010, the World Association for Photobiomodulation published recommended guidelines regarding illumination parameters (10), which is shown in Figures 2 and 3. LEDs and lasers are used as continuous and pulsed light sources. However, it is not yet fully understood whether there are benefits of the laser due to its coherence and monochromatic nature in all photobiomodulation applications. (5)

Recommended treatment doses for Low Level Laser Therapy

Laser class 3B, 904 nm GaAs Lasers
(Peak pulse output >1 Watt, mean output >5 mW and power density > 5mW/cm2)
Irradiation times should range between 30 and 600 seconds

Diagnoses	**Min. area/points**	**Min. total dose**	
Carpal-tunnel	2-3	4	Minimum 2 Joules per point
Lateral epicondylitis	2-3	2	Maximum 100mW/cm2
Biceps humeri cap.long.	2-3	2	
Supraspinatus	2-3	4	Minimum 2 Joules per point
Infraspinatus	2-3	4	Minimum 2 Joules per point
Trochanter major	2-3	2	
Patellartendon	2-3	2	
Tract. Iliotibialis	2-3	2	Maximum 100mW/cm2
Achilles tendon	2-3	2	Maximum 100mW/cm2
Plantar fasciitis	2-3	4	Minimum 2 Joules per point
Arthritis	**Points or cm2**	**Joules 904nm**	
Finger PIP or MCP	1-2	1	
Wrist	2-3	2	
Humeroradial joint	2-3	2	
Elbow	2-3	2	
Glenohumeral joint	2-3	2	Minimum 1 Joules per point
Acromioclavicular	2-3	2	
Temporomandibular	2-3	2	
Cervical spine	4	4	Minimum 1 Joules per point
Lumbar spine	4	4	Minimum 1 Joules per point
Hip	2	4	Minimum 2 Joules per point
Knee anteromedial	4-6	4	Minmum 1 Joules per point
Ankle	2-4	2	

Daily treatment for 2 weeks or treatment every other day for 3-4 weeks is recommended
Irradiation should cover most of the pathological tissue in the tendon/synovia.

Start with energy dose in table, then reduce by 30% when inflammation is under control
Therapeutic dose windows typically range from +/- 50% of given values, and doses outside these windows are inappropriate and should not be considered as Low Level Laser Therapy.
Recommended doses are for white/caucasian skin types based on results from clinical trials or extrapolation of study results with similar pathology and ultrasonographic tissue measurements.

Disclaimer
The list may be subject to change at any time when more research trials are being published.
World Association of Laser Therapy is not responsible for the application of laser therapy in patients, which should be performed at the sole discretion and responsibility of the therapist.

Revised April 2010

Figure 2 – WALT recommended guidelines for 904 nm PBMT dosage

Source: WORLD ASSOCIATION OF PHOTOBIOMODULATION THERAPY (10)

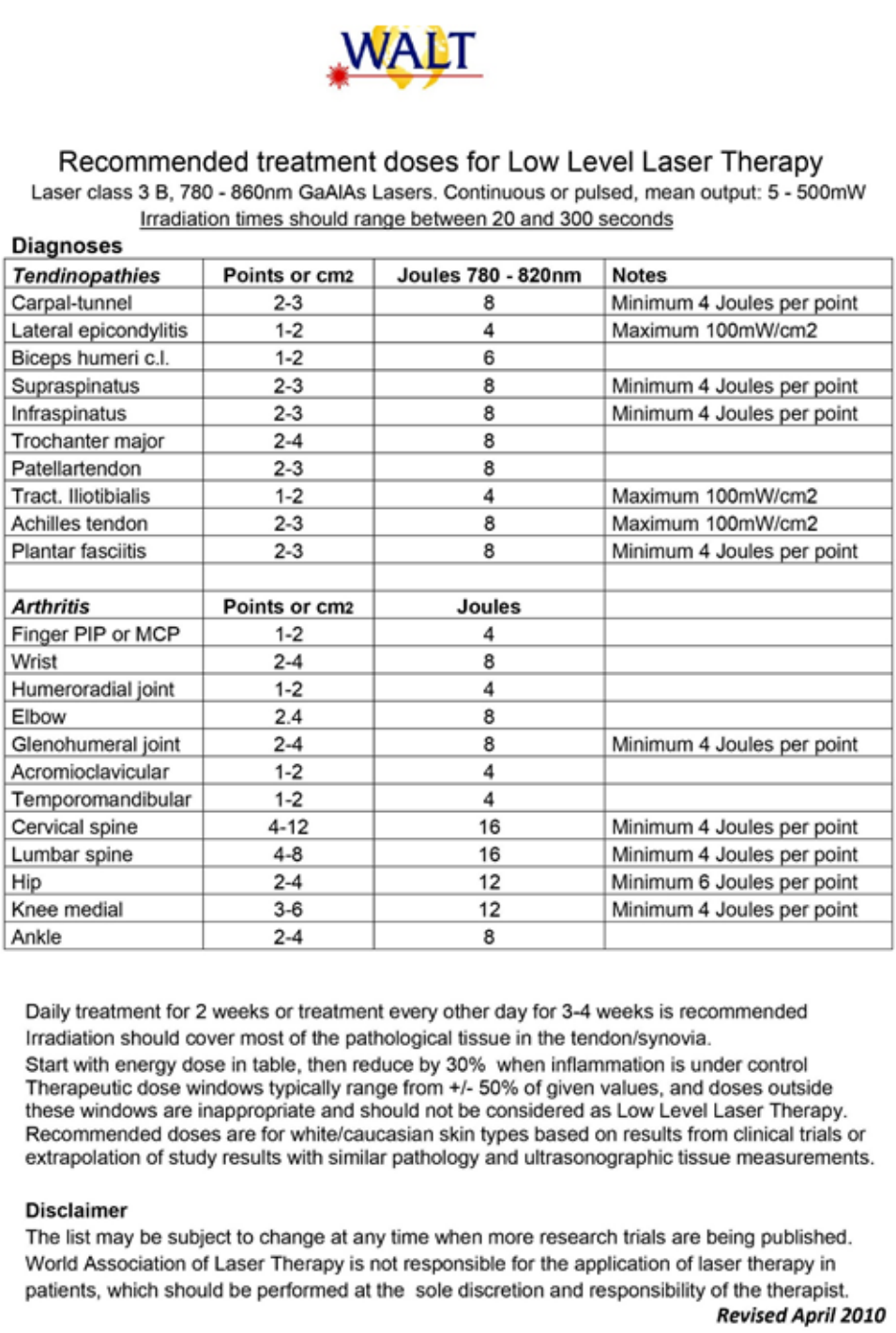

WALT

Recommended treatment doses for Low Level Laser Therapy

Laser class 3 B, 780 - 860nm GaAlAs Lasers. Continuous or pulsed, mean output: 5 - 500mW

Irradiation times should range between 20 and 300 seconds

Diagnoses

Tendinopathies	**Points or cm2**	**Joules 780 - 820nm**	**Notes**
Carpal-tunnel	2-3	8	Minimum 4 Joules per point
Lateral epicondylitis	1-2	4	Maximum 100mW/cm2
Biceps humeri c.l.	1-2	6	
Supraspinatus	2-3	8	Minimum 4 Joules per point
Infraspinatus	2-3	8	Minimum 4 Joules per point
Trochanter major	2-4	8	
Patellartendon	2-3	8	
Tract. Iliotibialis	1-2	4	Maximum 100mW/cm2
Achilles tendon	2-3	8	Maximum 100mW/cm2
Plantar fasciitis	2-3	8	Minimum 4 Joules per point
Arthritis	**Points or cm2**	**Joules**	
Finger PIP or MCP	1-2	4	
Wrist	2-4	8	
Humeroradial joint	1-2	4	
Elbow	2.4	8	
Glenohumeral joint	2-4	8	Minimum 4 Joules per point
Acromioclavicular	1-2	4	
Temporomandibular	1-2	4	
Cervical spine	4-12	16	Minimum 4 Joules per point
Lumbar spine	4-8	16	Minimum 4 Joules per point
Hip	2-4	12	Minimum 6 Joules per point
Knee medial	3-6	12	Minimum 4 Joules per point
Ankle	2-4	8	

Daily treatment for 2 weeks or treatment every other day for 3-4 weeks is recommended
Irradiation should cover most of the pathological tissue in the tendon/synovia.
Start with energy dose in table, then reduce by 30% when inflammation is under control
Therapeutic dose windows typically range from +/- 50% of given values, and doses outside these windows are inappropriate and should not be considered as Low Level Laser Therapy.
Recommended doses are for white/caucasian skin types based on results from clinical trials or extrapolation of study results with similar pathology and ultrasonographic tissue measurements.

Disclaimer

The list may be subject to change at any time when more research trials are being published.
World Association of Laser Therapy is not responsible for the application of laser therapy in patients, which should be performed at the sole discretion and responsibility of the therapist.

Revised April 2010

Figure 3 – WALT recommended guidelines for 780-860 nm PBMT dosage.
Source: WORLD ASSOCIATION OF PHOTOBIOMODULATION THERAPY (10)

1.2 PBMT and Cancer

As previously stated, current photobiomodulation therapy applications vary from musculoskeletal disorders and osteoarthritis to Alzheimer's disease. (11, 12) One of its

most prominent uses is in supportive cancer care for patients undergoing chemotherapy and radiation therapy to prevent and reduce morbidities in normal tissue, such as oral mucositis and radiodermatitis. (13–17) PBMT, following recommended guidelines, is considered safe in normal tissue applications. (18) but its use in oncology is still restrict due to the medical community concern regarding the effects of illuminating tumors. In normal tissue, especially in wound healing, its cascade of events may lead to increased proliferation. (5) Due to that, efforts have been made to determine whether it increases tumor volume and metastatic potential in cancer and determine its safety in tumors. Several in vitro studies demonstrated inhibitory effects of PBM. Sroka et al. studied the mitosis rate of different human cell lines after illumination (410, 488, 630, 635, 640, 805, and 1,064 nm and broad band white light). (19) A slight decrease in the mitosis rate of the cancer cell lines MCF7, U373MG, and ZMK1 was observed with the increase in the irradiation energy for all wavelengths. Nevertheless the urothelial carcinoma cells (J82) presented a slight increase at 410, 635 and 805 nm at fluences 2-20 J/cm^2. Schartinger et al. investigated the effect of PBM (660 nm) on human SCC-25 cells (oral squamous cell carcinoma) in comparison with human normal cells in regard to cell proliferation, cell cycle and apoptosis. (20) They revealed that PBM significantly decreased cell proliferation and the percentage of G1-phase cells and significantly increased the percentage of S-phase cells when compared to controls. Moreover, a proapoptotic effect was observed on SCC25 after PBM. Takemoto et al. studied the effect of LED-based PBM with different energy densities (3, 6,9,12, 24, 36 J/cm^2, 660 nm) on the progression of malignant invasion of human SCC cell lines (CAL27) seeded over normal stromal of gingival fibroblasts. (21) They found that after 72h of treatment (36 J/cm^2), PBM inhibited the expansion of CAL27 colonies and observed a general advantage of the stromal fibroblasts over cancer cells regarding cell viability, apoptosis, and death assays. In the study of Shirazian et al. on the effects of PBM on the proliferation and invasion of SCC cells originated from the tongue (TSCC-1), authors reported that illumination (660 nm with 80 mW and 810 nm with 200 mW) at 4 J/cm^2 can have an inhibitory effect on the proliferation of OSCC. (22) Additionally, 810 nm groups (100 and 200 mW), presented higher percentages of cyclin D1 and MMP-9, and a significant decrease in VEGF marker at the power of 200 mW. Cyclin D1 is a cell cycle protein that regulates the transition from phase G1 to phase S while MMP-9 increase is associated with tumor aggressiveness, poor differentiation, proliferation, invasion, and metastasis. With 660 nm (40 and 80 mW), higher levels of E-cadherin and -catenin were observed. These markers are present in the cell membrane and are among the molecules that influence cell adhesion and migration, their increase means cell adhesion strengthening which has a negative impact on the migration of malignant cells. No differences were observed among groups for the Ki67 marker, which is an antigen that indicated increase in cell proliferation since it is expression with cell cycle progression. On the other hand, the study of Sperandio et al. suggests opposite effects using 660 nm and 780 nm (40 mW,

and fluences of 2.05, 3.07, or 6.15 J/cm^2 for each) regarding the aggressiveness of oral dysplastic cells (DOK) and oral cancer cells (SCC9 and SCC25). Protein analysis by Western blot and immunofluorescence revealed that PBM significantly modified the expression of progression- and invasion-related proteins by modulating the Akt/mTOR/CyclinD1 signaling pathway. Gomes Henriques et al. also studied the effect of PBM on the protein expression analysis of human SCC of the tongue (SCC25) using a 660 nm laser with two energy densities (0.5 and 1.0 J/cm^2). They observed similar results, where 1.0 J/cm^2-PBM resulted in a significant increase in the expressionof cyclin D1 and nuclear-catenin, and promotion of invasion through the reduction o fE-cadherin and induction of MMP-9 expression. Other study have demonstrated 660 nm-PBM undesirable outcomes and stimulating effect on the proliferation of malignant cells, as well, with 150 and 1050 J/cm^2 in melanoma cells (B16F10) in vivo and in vitro. (23) The authors observed did not observe significant difference among groups, except for a stimulatory effect of PBM in vivo with 1050 J/cm^2 resulting in an increase in tumor volume, blood vessels, and cell abnormalities. Nevertheless, the fluences used are much higher than the recommended for the usual recommendations of photobiomodulation therapy. (10) There is a controversy in PBMT results in vivo, as well. Myakishev-Rempel et al. studied the effects of full body PBMT in a protocol of 2.5 J/cm^2 at 670 nm, twice daily for 37 days, in SKH mouse non-melanoma UV-induced skin cancer. (24) Photographic measurements did not reveal a significant effect of PBMT on tumor growth. Ottaviani et al. investigated three protocols of PBMT (660, 800 and 900 nm) on cultured cells and on oral carcinogenic-induced tumor models in mice using 4-NQO. (25) They observed a reduction of tumor progression associated with the secretion of type I interferons from T-lymphocytes and dendritic cells, as well as a decrease in the tumoral angiogenic macrophages with vessel normalization promotion. In contrast, de C Monteiro et al. observed a significant progression of the severity of oral carcinogenic-induced tumors in a protocol of 660 nm PBMT (56.4J/cm^2) on a hamster model. (26) Moreover, Rhee et al. reported an increase in the aggressiveness of orthotopic anaplastic thyroid tumors with a single dose of PBMT (650 nm, 15 and 30 J/cm^2). (27) The authors assessed tumor volume, histology, over proliferated cancer cells, p-Akt, VEGF, and transforming growth factor 1 (TGF-1). They found that PBM caused an elevation of HIF-1 and p-Akt, and a decrease in TGF-1 expression that led to loss of cell cycle regulation. It was concluded that these effects may cause an over-proliferation and angiogenesis of cancer cells and PBM may cause aggressiveness of cancer through TGF-1 and Akt/HIF-1 cascades. There are some reviews on the subject of PBMT in cancer that have reported the inconsistency of results presented here. (6,28–31) Their conclusions are that the conflicting results of in vitro studies on a diverse range of cell lines may be due to the diversity of illumination parameters used. They also observe that in vivo studies and clinical trials present indications that PBMT is safe for tumor growth. In the light of that, it is clear the importance of investigating the effects of PBMT, since it has the

potential of enhancing cancer treatment by reducing adverse side effects and, in some conditions, it also seems to sensitize tumor cells to the treatment. Therefore, this study investigates the effects of PBMT on carcinoma cells, in comparison to a normal cell line, and its potential to enhance photodynamic therapy and radiotherapy.

2 PBM EFFECTS ON CANCER METABOLISM

To be published in Biomedical Optics Express:

Title:	Effects of photobiomodulation on the redox state of healthy and cancer cells
Authors:	Clara de Faria,Heloisa Ciol,Vanderlei Bagnato,Sebastião Pratavieira
Accepted:	29 April 21
Posted	29 April 21
DOI:	https://doi.org/10.1364/BOE.421302

Effects of photobiomodulation on the redox state of healthy and cancer cells

Clara Maria Gonçalves de Faria,[1,*] Heloisa Ciol,[1] Vanderlei Salvador Bagnato,[1,2] and Sebastião Pratavieira [1]

[1] *São Carlos Institute of Physics - University of São Paulo, São Carlos, SP, Brazil*
[2] *Faculty Fellow at the Hagler Institute for Advanced Study and Visiting Professor at the Department of Biomedical Engineering - Texas A&M University, College Station Texas - USA*
[*] *claramgf@ifsc.usp.br*

Abstract: Photobiomodulation therapy (PBMT) uses light to stimulate cells. The molecular basis of the effects of PBMT is being unveiled, but it is stated that the cytochrome-c oxidase enzyme in mitochondria, a photon acceptor of PBMT, contributes to an increase in ATP production and modulates the reduction and oxidation of electron carriers NADH and FAD. Since its effects are not fully understood, PBMT is not used on tumors. Thus, it is interesting to investigate if its effects correlate to mitochondrial metabolism and if so, how it could be linked to the optical redox ratio (ORR), defined as the ratio of FAD/(NADH + FAD) fluorescences. To that end, fibroblasts (HDFn cell line) and oral squamous cell carcinoma (SCC-25 cell line) were irradiated with a light source of 780 nm and a total dose of 5 J/cm^2, and imaged by optical microscopy. PBMT down-regulated the SCC-25 ORR by 10%. Furthermore, PBMT led to an increase in ROS and ATP production in carcinoma cells after 4 h, while fibroblasts only had a modest ATP increase 6 h after irradiation. Cell lines did not show distinct cell cycle profiles, as both had an increase in G2/M cells. This study indicates that PBMT decreases the redox state of oral cancer by possibly increasing glycolysis and affects normal and tumor cells through distinct pathways. To our knowledge, this is the first study that investigated the effects of PBMT on mitochondrial metabolism from the initiation of the cascade to DNA replication. This is an essential step in the investigation of the mechanism of action of PBMT in an effort to avoid misinterpretations of a variety of combined protocols.

1. Introduction

Photobiomodulation therapy (PBMT) has been used for decades for wound healing, tissue regeneration, analgesia, inflammation reduction, osteoarthritis, reducing edema on lymph nodes, and muscle relaxation, among others [1,2]. However, it is a developing field which results in partial acceptance and recognition from authorities in biomedical science, professionals and scholarly journals [3]. It encompasses a variety of reactions caused by non-ionizing and non-thermal light absorption in tissues and cells, resulting in a physiological response according to tissue stimulation. However, its effects are still unclear, particularly on premalignant and malignant cells. One of PBMT most popular applications, due to its effectiveness, is the prevention and management of oral mucositis in head and neck squamous cell carcinoma (HNSCC) patients [4,5]. Still, a recent systematic review, including 13 papers, demonstrated that the data does not support a definite conclusion of photobiomodulation (PBM) impact on HNSCC cells, despite many studies on the topic [4]. Among the challenges are the wide variety of study designs, PBMT protocols and the limited type of assays performed, where cell proliferation and viability are the primary ones.

Evidence indicates that the PBM cascade of events begins with cytochrome c oxidase (COX), the fourth protein complex in the mitochondrial electron transport chain and primary photoreceptor of red and near-infrared light [6–8]. The energy absorbed by COX changes the mitochondrial

potential and leads to up or downregulation of reactive oxygen species (ROS), adenosine triphosphate (ATP) [9], [3] and calcium (Ca^{2+}) [1]. These molecules trigger the activation of transcription factors (e.g., NF-κB, Nrf2 and activator protein-1[AP-1]) [10], changes in protein expression and release of cytokines and growth factors [11]. The exact effects that follows are hard to predict: it includes altered mitochondrial activity [12], gene expression [1, 13, 14], promotion of anti-inflammatory response [3] and cell proliferation [15]. ROS, for example, leads to apoptosis, if found in great amounts, and may also increase proliferation at lower levels. Therefore, investigating the modulation of these molecules activity by PBM and its connection with changes in metabolism and physiological effects, within the same conditions of illumination and cell type, is fundamental.

Glucose is the primary fuel of cellular respiration; its catabolism reduces the electron carriers by transferring electrons to FAD molecules, producing $FADH_2$ and NAD coenzymes, providing NADH [16]. The NADH and $FADH_2$ are oxidized, respectively, to NAD^+ and FAD at complexes I and II of the electron transport chain, producing an electrical potential that results in a donation of electrons to molecular oxygen and phosphorylation of adenosine diphosphate (ADP) by the ATP synthase enzyme [17]. Generally, lower oxygen concentrations shift the glucose catabolism to anaerobic glycolysis, which converts glucose to lactate instead of pyruvate, supplying enough energy for the maintenance of cellular processes [18]. The glycolytic pathway takes place at the cytosol resulting in ATP generation and oxidation of phosphoenolpyruvate to pyruvate.

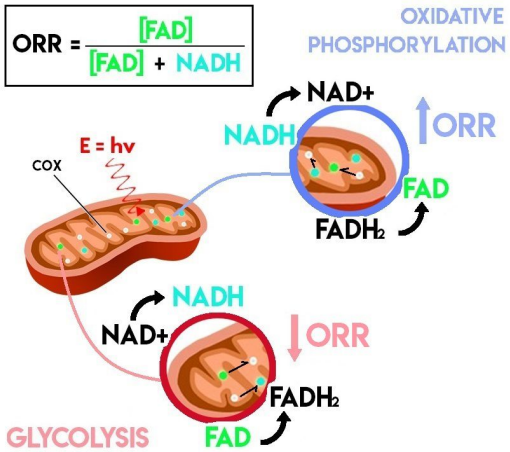

Fig. 1. Schematics of the optical redox ratio (ORR) in mitochondria, following light absorption by cytochrome c oxidase (COX), and its correlation to the ATP generation pathway. Normal cells produce ATP by oxidative phosphorylation (OXPHOS) in normoxic conditions. Within the mitochondria, NADH and $FADH_2$ are oxidized, respectively, to NAD^+ and FAD, increasing RR. In hypoxic conditions, cells use the glycolysis pathway to supply ATP. Glycolysis reduces the electron carriers NAD^+ and FAD to NADH and $FADH_2$, respectively, lowering the ORR.

In non-cancer cells, this pathway can either provide enough energy to cells under hypoxic conditions or supply the citric acid cycle with pyruvate to produce mitochondrial ATP by oxidative phosphorylation (OXPHOS) [19]. The formed NADH and FAD of these coenzymes present an intrinsic fluorescence, which allows the redox ratio (RR) of the cell to be calculated optically by FAD/ [NADH + FAD] fluorescence intensities [17, 20, 21]. The optical redox ratio (ORR) is proportional to the balance of oxidative phosphorylation/glycolysis and can be used to monitor living tissues and cells (Figure 1) [22]. Several conditions change cellular metabolism and alter this balance, such as hypoxia, high carbon demands, increased proliferation rate, and fatty acid

synthesis [21]. The ORR is also used to investigate cancer mechanisms since different types of tumors, and cancer cells favor glycolysis over OXPHOS, even in the presence of oxygen, a phenomenon called "Warburg effect" or aerobic glycolysis [23]. Choosing aerobic glycolysis could benefit cancer cells by supplying ATP faster than oxidative phosphorylation [24] and by going through an energetic pathway that produces lower concentrations of ROS [17]. It must be stated that cancer cells can favor oxidative metabolism over aerobic glycolysis, for reasons not fully elucidated. Highly invasive tumor cells, for example, have shown modulation of the glucose metabolic pathway depending on the site of metastasis [25–27]. Oral cancer is one of them, and its location is convenient to make optical measurements and an ORR analysis. Previous studies have shown that it is possible to differentiate healthy tissue, hyperplasia, and dysplasia with this technique *in vivo*, which shows its potential to monitor metabolism changes in the tumor [28].

Therefore, in order to increase PBMT acceptance, it is fundamental to investigate its effects on the metabolism of cancer cells, since it is a modality clinically used to treat and prevent side effects, such as mucositis, in cancer patients undergoing radio and chemotherapy. To do so, PBMT mechanisms on oral cancer and normal tissue must be known. Despite studies on the activation of a few pathways and the regulation of important molecules alone do exist, the overall PBMT effect on metabolism or the existing correlations among them have not been clearly identified or understood [21]. Thus, the aims of this study were to explore PBM effects on ORR and its correlation with the cell cycle, ATP levels, and ROS production, and to elucidate PBM effects related to the activation of biochemical carriers and the overall impact on the metabolism of oral cancer cells and fibroblasts, which play an important role in normal tissue regeneration, including mucositis regeneration.

2. Material and Methods

2.1. Cell Culture

Human dermal fibroblasts neonatal (HDFn) and squamous carcinoma SCC-25 (American Type Culture Collection - ATCC), Wesel, Germany), were cultivated at 37°C in humidified 5% CO_2 atmosphere in Dulbecco's modified Eagle medium (DMEM) and DMEM/Ham's (Cultilab), respectively. Media were supplemented with 10% (v/v) Fetal Bovine Serum (Cultilab, Brazil) and to DMEM/Ham's hydrocortisone was added (Sigma-Aldrich, USA) at a concentration of 400 ng/ml. Cells were used at maximum passage of 20 and tested negatice for mycoplasma prior the experiments.

2.2. Illumination protocol

PBMT groups were illuminated using a custom-made LED array device (Figure S1) emitting at 780 nm with an irradiance of 30 mW/cm^2 and a total fluence rate of 5 J/cm^2, given in 2 min and 53 s at room temperature. [29] The control groups were sham treated. A flow chart of all analysis performed after PBM is shown in Figure S2.

2.3. Optical Redox Ratio Imaging

Cells were plated on a 35 mm glass bottom dish (Greiner Bio-One, Germany) at a density of 5 x 10^5 cells and let in a heated chamber (37°C, 5%, CO_2) overnight. Four hours after PBMT, cells were washed twice in PBS and maintained in the buffer for image acquisition, perfomed on an inverted fluorescence confocal microscope (Zeiss - LSM780, Zeiss, Germany) equipped with a Ti:Sapphire tunable laser source (Chameleon Vision II, Coherent Inc., USA), using the multiphoton modality of two-photon absorption induced fluorescence. The laser excitation source was tuned to 755 nm (NADH excitation, 300 mW at the sample) or 860 nm (FAD excitation, 600 mW at the sample), and images were acquired in the channel mode of the microscope with 440 - 480 nm (NADH fluorescence) or 500 - 550 nm (FAD fluorescence) wavelength range,

respectively (1.58 μs dwell time, 2 line/frame averaging). Images (1024 x 1024 pixels; 8-bit depth; 425 μm x 425 μm) were acquired using a 20x objective (NA = 0.8). For each condition, two plates were prepared and 10 fields were imaged for each one. Three independent experiments were performed (n=3). To calculate cell-to-cell ORR heterogeneity, a region of interest (ROI) was selected and used to create a mask to compute the mean ORR of a single cell. The mask was created manually from the FAD image. Three cells of each field were analyzed, resulting in the analysis of 120 cells per group, from three independent dishes (n=3). To ensure that the same dish would yield the same result, two dishes were calculated twice, using different cells from the field. Then, the 'heterogeneity', defined as the ratio of standard deviation/mean ORR, was calculated for each dish. Therefore, the error bar of this parameter represents the standard deviation of the heterogeneity value of three dishes. All images were acquired using Zen 2010 software (Zeiss, Germany). Laser power was checked daily to ensure its value was approximately the same at all experimnt-days. Additionally, a control plate was imaged as the standard, in order to compare its value among the different days and account for daily system fluctuations. Image analysis was performed using MATLAB (MathWorks, USA), thresholding was performed by removing pixels with NAD+FAD < 0.4 to eliminate saturated pixels, background and contribution from other chromophores, such as keratin. The latter results in pixels with a high intensity in one channel but a low one on the other. This approach was validated by analysing the isolated contributions from the removed pixels for all conditions, and concluding that their contribution was minor and uniform along the groups. Redox images and their mean values were created by computing pixel-wise ratios of FAD/(NADH + FAD) fluorescence. For statistical analysis and bar plot presentation, the average redox ratios of each group were calculated by separately computing the means from their respective images.

2.4. Glycolysis assay

Glycolysis was assessed with a fluorescent kit (Abcam ab197244, Abcam, USA) following manufacturer protocols. $2x10^4$ cells/well were seeded in 96-well opaque black walls 24 h prior illumination, in 6 replicates per group. Then, 1h after PBMT, CO_2 was removed from the incubator and at 4h after PBMT wells were washed twice with Respiration Buffer and 15 μl of Glycolysis assay reagent in 100 μl of Buffer was added to each well. Fluorescence (ex/em: 380/615 nm) was measured with a SpectraMax M5 Multi-Mode Microplate Reader (Molecular Devices, USA) for 2h in 1.5 min intervals. The means correspond to two independent experiments (n=2).

2.5. Metabolic activity assessment by MTT assay

Metabolic activity was assessed at 4h and 24h after PBMT. Cells were seeded in triplicate for each condition in 24-wells plates at a density of $1x10^5$ per well (500 μl) and illuminated in culture medium the following day according to the parameters mentioned above. After 4h or 24h, medium was replaced by 250 μl of new media with 3-(4,5-dimethylthiazol-2-yl)-2,5-diphenyltetrazolium bromide (MTT) (5 μg/ml) and incubated for 3h, until 1 ml of DMSO was added and absorbance was measured at 570 nm in a microplate reader (Multiskan™ FC Microplate Photometer – ThermoFisher Scientific, USA). Each experiment was performed three independent times (n=3). To confirm whether the results from MTT resulted proliferation and viability, a trypan blue exclusion assay was performed in quadruplicate, in the same conditions.

2.6. ROS Assay

Quantification of ROS after PBMT was performed by flow cytometry assessment using DCFH-DA. For the assay, a 1×10^6 cells per ml suspension was made in phenol and FBS free medium. Triplicates of 250 μl of the cell suspension were illuminated in a 24-wells plate with a dose of 5 J/cm^2 at 780 nm in a black 24-wells plate with clear bottom. Samples were immediately

incubated with 250 μl of DCFDA solution, resulting in a concentration of 25 μM, for 30 minutes at room temperature in the dark and assessed by flow cytometry (BD, C6 Accuri Plus, USA) at an excitation/emission of 492–495 nm/517–527 nm.

2.7. ATP Assay

Cells were seeded in 96-well plates at a $2x10^4$ cells/well density and incubated at 37°C, 5% CO_2 for 24h prior the ATP assay, performed with the ATP bioluminescent assay kit (Sigma–Aldrich, USA). Plates were illuminated or sham-illuminated in medium and at a specific time after that ranged from 1-24h supernatant was removed, wells were washed twice with PBS and 100 μl of Releasing Reagent were added. The working solution was prepared as indicated (10% of ATP Mix Working Solution in ATP Mix Dilution Buffer). Immediately prior to the bioluminescent reading, 100 μl was added to the wells with a multi-channel pipette to ensure all wells were incubated simultaneously and only 6 wells were read at a time. The luminescence was measured with a SpectraMax M5 Multi-Mode Microplate Reader (Molecular Devices, USA). Experiments were repeated three times with 6 replicates per group (n=3).

2.8. Cell cycle assessment

Cell cycle evaluation was performed by flow cytometry analysis using propidium iodide (PI). Cells were seeded in 24-wells plate and illuminated in culture medium as described previously, in triplicate. Then, at 0h, 8h and 24h after illumination, cells were collected and fixed in ice-cold 70 % ethanol at -20°C for at least 24 h, then washed with PBS and stained with PI (50 μg PI/ml in PBS, BD Biosciences) containing 0.1 mg/ml RNase (Sigma–Aldrich, USA) for 40 min. Samples were analyzed in an Accuri C6 flow cytometer (BD Biosciences, USA) in triplicate and cell cycle was determined using FlowJo software univariate analysis (BD Biosciences, USA). Two independent experiments were performed (n=2). Representative histograms of each group, showing the estimated areas of the cell cycle stages, are shown in Figure S3.

2.9. Statistical analysis

The data were plotted using boxplot with a whisker of 1-99 or represented as means ± standard deviation and were analyzed using the commercially available software Origin 2018 (Origin Lab., USA). One-way analysis of variance (ANOVA) was used among the categories “HDFn” and “SCC-25” cells and “Control” and “PBM” for the ORR measurements. For experiments that we compared only “PBM” and “Control” independently for the same cell line, a single ANOVA test was performed. Differences were considered as statistically significant at $p<0.05$. Asterisks placed above bars indicate statistical significance.

3. Results

3.1. Optical Redox Ratio Imaging

For imaging, two-photons excitation fluorescence (TPEF) microscopy allowed the acquisition of high resolution images of depth sectioning without the need for a confocal pinhole, since TPEF is a non-linear light process limited to the focal plane, which also spares any damage to surrounding tissue or cells [21, 30]. Figure 2 shows the NADH (blue) and FAD (green) fluorescence by TPEF microscopy and the merged image (red) indicating the ORR of the SCC-25 cells (Figure 2a-c) and HDFn (Figure 2d-f).

From the results shown in Figure **??**g, it is evident that HDFn fibroblasts present a higher ORR than SCC-25 carcinoma cells. This is rational since normal cells favor oxidative phosphorylation (↑FAD/(↑FAD+↓NADH)) over glycolysis (↓FAD/(↓FAD+↑NADH)) and is consistent with previous observations [17, 21]. Regarding PBMT, illumination did not show a significant effect on HFDn ORR value, however, it decreased the ratio of SCC-25 cells by 10%, indicating increased

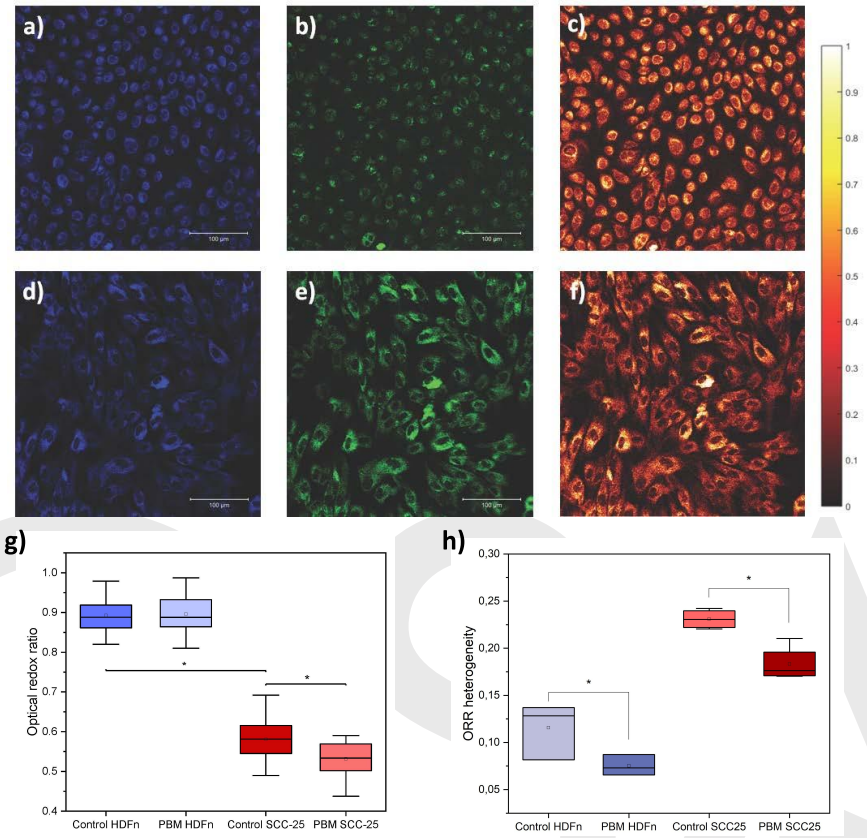

Fig. 2. Fluorescence microscopy of SCC-25 (a-c) and HDFn (d-f) cells. The false color blue images (a and d) correspond to NADH fluorescence, false color green (b and e) correspond to FAD fluorescence and the false color red (c and f) are the calculated optical redox ratio image. (g) Mean optical redox ratio of HDFn and SCC-25 cells, control and PBM groups (n=3, * indicates $p < 0.01$). (h) Cell-to-cell relative heterogeneity in the redox ratio for SCC-25 and HDFn cells, control and PBM (n=3, * indicates $p < 0.05$).

glucose catabolism. Additionally, cell-to-cell ORR heterogeneity was calculated using a region of interest (ROI) mask to compute the mean redox ratio of a single cell. It is noticeable that the heterogeneity shown is greater for SCC-25 cells than for healthy HDFn cells. This is consistent with the fact that some tumor cells, presenting a more metastatic potential, contradict the Warburg effect, [17] which consists in the preferential metabolism of glucose to lactate, independent of oxygen presence, by cancer cells [31]. Another interesting observation is that PBM reduced the heterogeneity in both cell lines (**??**f), despite not causing a difference in the ORR mean of HDFn cells. This means that the balance of oxidative phosphorylation/glycolysis among the population became more homogeneous after illumination. If we combine this result with the decrease in the mean of SCC-25 ORR, it is possible to raise the hypothesis that PBM induces an upregulation of glucose catabolism compared to OXPHOS. For HDFn cells, the decrease in heterogeneity could be related to PBM producing slightly different effects according to the state of a cell, upregulating OXPHOS in cells presenting a lower redox state and decreasing glycolysis

in the ones that favored it instead of OXPHOS.

3.2. Glycolysis

Glycolysis results after 4 hr of PBMT are shown in Figure 3. It is seen in Figure 3a that fibroblasts present a lower baseline for glycolysis than the tumor cell line, as expected due to the Warburg effect observed in cancer cells. The PBMT caused an increase in this parameter in both cell lines (Fig 3b and 3c), in a similar proportion. As HDFn cells did not present a difference in ORR after PBMT we conclude that OXPHOS increased as well, and the balance was not altered. The SCC-25 cells showed a decrease in ORR and an increase in glycolysis, making it possible to infer that OXPHOS had either a smaller increase than glycolysis, was not affected, or had a slight decrease.

3.3. MTT assay

Cell viability was assessed by the Metabolic activity assessment by 3-(4,5-dimethylthiazol-2-yl)-2,5-diphenyltetrazolium bromide (MTT) assay 4 h and 24 h after PBMT and is shown in Figure 4. Since this assay is used to measure cell viability based on cell metabolism, cell counting was performed to confirm the results from MTT and showed a good correlation (see SI). Thus, the first time point was chosen to investigate metabolic changes only, while 24 h allows the visualization of viability and different cell numbers as well. Earlier times were not investigated since PBM effects take a few hours to result in metabolic alterations. In the results, it is possible to observe a difference in cell viability 4 h after PBMT in both cell lines alongside similar cell counting, which indicates a change in metabolism in both cells. Mitochondrial activity was increased in fibroblasts (Fig. 4a) and decreased in SCC-25 cells (Fig. 4b). At 24 h, it was observed that PBM induced proliferation in fibroblasts, as both MTT and cell counting increased. However, there was no significant change in the tumor population.

3.4. ROS and ATP Assay

The ROS quantification after PBMT was performed by flow cytometry to investigate if its production correlated to illumination (Figure 5). Figure 5a shows the ratio of mean intensities between PBMT and the control of each cell line. In fibroblasts, no significant ($p > 0.05$) changes were found among the samples. In SCC-25, however, a statistically significant ($p < 0.05$) increase of about 30% was observed after PBMT. This suggests that ROS could play an important role in mediating PBM effects in tumor cells but not in normal fibroblasts. One common consequence of several pathways initiated by ROS is increased ATP production. As seen in Figure 5b, endogenous ATP increased within the 24 h-after PBMT period evaluated for SCC-25 and HDFn cells, even though kinetics differed among the cell lines. SCC-25 cells presented a peak of 1.25 units compared to the control at 4 h after PBMT while fibroblasts modestly increased ATP by 7 % 6 h after PBMT. Interestingly, both cells showed a decrease immediately after its ATP peaks, indicating consumption by energy demanding processes.

3.5. Cell cycle assessment

Cell cycle was evaluated by flow cytometry 8 h and 24 h after PBMT or sham treatment. The proportion of cells in G2/M after PBMT relative to the control is shown in Figure 6. Cells in G0/G1 and S phase were not statistically different. It was observed that both fibroblast and tumor cells increased mitosis in a linear manner and at the same rate, reaching a 20 % increase in 24 h.

4. Discussion

Photobiomodulation is the use of light, mainly in the red and near-infrared regions, for a variety of purposes. It is promising since it is a non-invasive and an affordable technique already used to

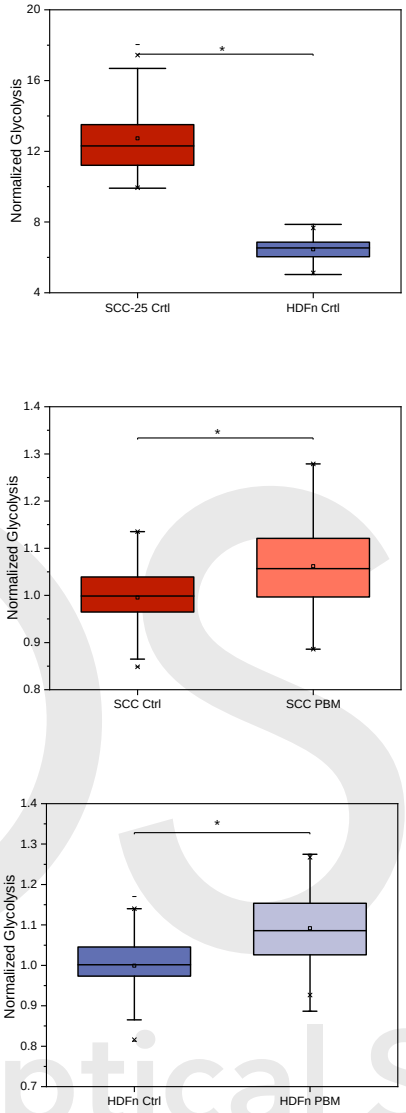

Fig. 3. Glycolysis experiment assay. (a) Baseline of glycolysis for SCC-25 and HDFn cell line showing that the tumor cell line (SCC-25) has a greater baseline for glycolysis when compared to HDFn cells. This result was expected and could be related to the Warburg effect. (b) Glycolysis quantification after PBMT for SCC-25 cell line and (c) for HDFn cell line. Results show that PBM did not influence the glycolysis rate of normal cells but increased the rate of tumor cells. $^{*}p < 0.05$

reduce inflammatory conditions [3], in the treatment of arthritis [32] and wound healing [33], among others, resulting in pain relief and modulation of expression of genes related to the inflammatory response [6,34,35]. The PBMT encompasses such a broad spectrum of illumination protocols, parameters, and uses; its mechanism of action is not fully understood. This causes

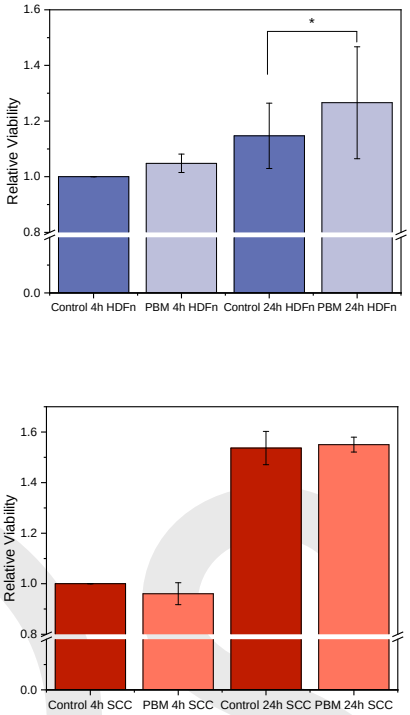

Fig. 4. Metabolic activity by MTT assay 4 h and 24 h after PBMT. (a) shows the HDFn cell line viability of control samples and illuminated samples, indicating that PBM induced cell proliferation in fibroblasts after 24 h. (b) Cell viability assay for SCC-25 cells. When compared to control, no cell proliferation was observed in tumor line 24 h after illumination.

skepticism from the medical community and limits its impact. As stated by Stephen Sonis [36], until we obtain enough data we cannot answer whether we should avoid PBMT in head and neck cancer tumors or not. So it is fundamental to understand these effects to ensure the safety of this technique and explore its potential in enhancing cancer treatment.

In this study, we investigated the effects of PBM on the metabolism of healthy (HDFn) and cancer cells (SCC-25) *in vitro* and revealed that their pathways are different. It was also established that ORR evaluation by TPEF is a technique that is sensitive enough to significantly detect slight changes caused by PBM. Thus, it is a powerful tool to investigate metabolism modulation in both cancer and normal cells. The PBMT illumination protocol was based on previous mucositis studies [37, 38] and the results are summarized in Figure 7. In fibroblasts cells, no changes in the redox state were observed 4 h after illumination despite increased glycolysis displayed by a different method. Therefore, both forms of respiration might have increased at the same rate in these cells, maintaining the ratio constant. In SCC-25 cells, a lower ORR after PBM indicates a possible increase of glycolysis compared to OXPHOS. Nevertheless, there are other process that affect the redox state of the cells, such as glutaminolysis, fatty acid oxidation/synthesis and apoptosis, so further studies are needed to confirm this hypothesis [39, 40].

Previous work by Heymann and colleagues reported a PBM-induced decrease in the redox ratio, measured by the extracellular flux assay, along with increased proliferation in HeLa cells,

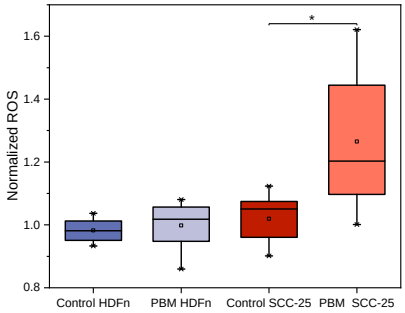

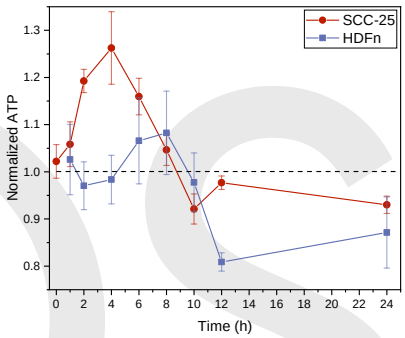

Fig. 5. ROS and ATP assay. (a) The ROS production assay indicating that PBM induced ROS production in the SCC-25 cell line ($p < 0.05$), but not in fibroblasts. (b) The ATP production of both cell lines, indicating that SCC-25 (red-dot) cells increased a peak of 1.25 units 4 h after PBMT, as fibroblasts modestly increased 7 % after 6 h (grey-square).

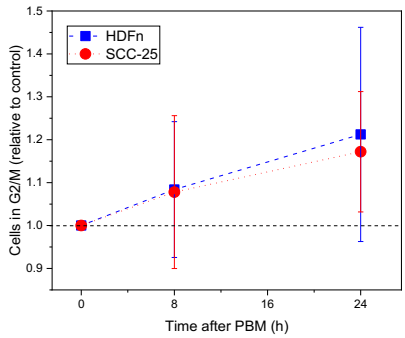

Fig. 6. Cell cycle assessment by flow cytometry. Illuminated samples of HDFn (blue-square line) and SCC-25 (red-dot line) linearly increased the mitosis rate up to 20% after 24 h when compared to controls.

using 670 nm and 12 J/cm^2 [41]. Since the illumination protocol and cell type were different, but

the effect similar, it might be a common effect of PBM in tumors. Its consequences in cancer cells need to be investigated since it may correlate to the Warburg effect and its therapeutic implications, such as tumor aggressiveness shown by Li et. al. [42].

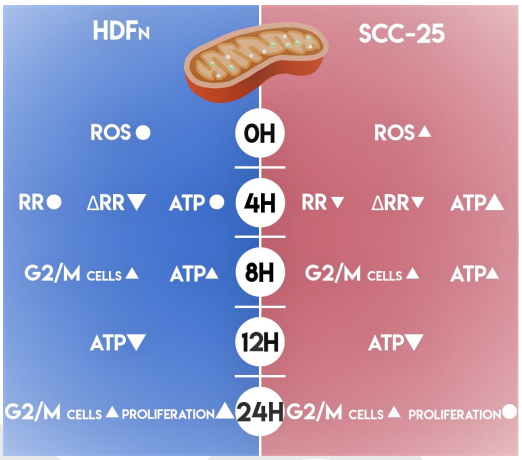

Fig. 7. Summary of HDFn and SCC-25 modulations caused by PBM indicating increase, decrease or no change in reactive oxygen species (ROS), redox ratio (RR), redox ratio heterogeneity (ΔRR), adenosine triphosphate (ATP), number of cells in G2/M and proliferation, compared to its respective controls.

Additional evidence that arose from the ORR analysis is that PBM may have different effects and mechanism of action depending on the previous redox state of the cells. This was shown by decreased heterogeneity in ORR values 4 h after illumination, in both cell lines, caused by a decrease in the highest and an increase in the lowest values of ORR. It suggests that PBM acts differently according to the cells. In this instance, it may be more effective to the ones that differ from the mean redox state of the population.

Beyond the differences in ORR, fibroblasts and SCC-25 cells, these seem to have distinguished pathways that initiate the cascade of events that characterize PBM. ROS is known to be an important biomarker that induces apoptosis if found in high concentrations, and modulates pro-survival and proliferation effects at low concentrations [43]. In this study, ROS concentration increased only in SCC-25 cells, indicating that PBM acts by a different pathway in fibroblasts. Engel and colleagues showed increased catalase in fibroblasts after PBM scavenged ROS. Therefore, they suggested that lineage-specific differences maintain homeostatic redox status within each cell type [43]. Lunova et al have stressed how PBM mechanisms are complex by showing that blue and red light cause opposite changes in the mitochondrial potential by exciting different structures in COX [44]. Lynnyk et al have demonstrated that different doses of laser irradiation result in distinct biochemical signaling, which may be initiated by different intracellular ROS compartmentalization [45].

Nevertheless, ATP levels were increased in both cell lines after PBMT. Chen et. al. showed in fibroblasts, that ATP increase after PBM is not altered with the addition of antioxidants. Despite showing an increase in ROS that was not seen in our study, both results suggest that ATP synthesis after PBMT is not dependent on ROS signaling [46]. ATP kinetics after PBMT, however, have not been investigated yet. Such an investigation is important because end-point measurements can lead to false conclusions. For example, ATP increase in fibroblasts was only seen 8 h after PBMT while its peak for SCC-25 cells was seen at 4 h. At 12 h, ATP levels were lower when compared to the non-illuminated groups for both cells lines. This indicates higher ATP demands from processes induced by PBM, such as protein synthesis and DNA replication involved in

proliferation, or a mechanism of feedback that tends to suppress the effects caused by light.

In fact, we observed an increase in G2/M fraction for both cells at 8 and 12 h after PBMT. However, it did not result in increased proliferation in the tumor cell line but did in HDFn cells. This is an encouraging result that supports the evidence that PBM does not affect tumor growth [47]. Schartinger et al. reported similar results using 660 nm, an increase in fibroblasts but a decrease in SCC-25 cells [48]. This indicates regarding proliferation, that PBM effects are similar for multiple wavelengths. Regarding cell cycle, they observed an increase fraction in cell cycle G1 and S phases, but did not report the time after PBMT in which the measurement was performed. In contrast, Sperandio et al. observed increased proliferation in SCC-25 cells for both 660 and 780 nm, at 24 h (780 nm, 6.15 J/cm^2) and 48 h (660 and 780 nm, 3.07 J/cm^2) after illumination [49]. Certainly, further studies need to be conducted to understand if PBM stimulates proliferation in tumors, and under what conditions, in order to advance the reliability and security of its applications in cancer.

Therefore, it was demonstrated that PBMT with 5 J/cm^2 at 780 nm alters the metabolism of fibroblasts and HNSCC cells, but in different pathways and kinetics. Its mechanism of action needs to be further investigated to improve the understanding of these differences. For that, studies in more complex models, 3D cell cultures and *in vivo*, need to be conducted. So the influence of the extracellular matrix, spatial fluence distribution, surrounding tissues, immune and vascular response, among others, can be evaluated. Then, it may be possible to explore PBM mechanisms to improve cancer treatments, or avoid applications involving tumors to prevent negative effects. Additionally, TPEF was depicted as a powerful tool to evaluate redox state after PBMT. It is a sensitive technique that allows the assessment of small redox ratio differences and heterogeneity among cells. It is also nondestructive, so the sample can be used after measurements, and it can be combined with other fluorescent markers.

Funding. Content in the funding section will be generated entirely from details submitted to Prism. Authors may add placeholder text in the manuscript to assess length, but any text added to this section in the manuscript will be replaced during production and will display official funder names along with any grant numbers provided. If additional details about a funder are required, they may be added to the Acknowledgments, even if this duplicates information in the funding section. See the example below in Acknowledgements.

Acknowledgments. The authors thank Camila Bramorski and André Longo for the support with the figures and acknowledge the support provided by Brazilian Funding Agencies: Coordenação de Aperfeiçoamento de Pessoal de Nível Superior - Brasil (CAPES) - Finance Code 001; CNPq (465360/2014-9 and 306919/2019-2) and São Paulo Research Foundation (FAPESP) grants: 2009/54035-4 (EMU); 2013/07276-1 (CePOF); 2014/50857-8 (INCT); 2017/14182-4 (CMGF scholarship).

Disclosures. The authors declare no conflicts of interest.

Data Availability Statement. Data underlying the results presented in this paper are available in Dataset 1

References

1. L. F. de Freitas and M. R. Hamblin, "Proposed Mechanisms of Photobiomodulation or Low-Level Light Therapy," IEEE J. Sel. Top. Quantum Electron. **22**, 348–364 (2016).
2. T. Karu, "Is it time to consider photobiomodulation as a drug equivalent?" Photomed. Laser Surg. **31**, 189–191 (2013).
3. M. R. Hamblin, "Mechanisms and applications of the anti-inflammatory effects of photobiomodulation," AIMS biophysics **4**, 337–361 (2017).
4. F. M. Silveira, M. d. P. Paglioni, M. M. Marques, A. R. Santos-Silva, C. A. Migliorati, P. Arany, and M. D. Martins, "Examining tumor modulating effects of photobiomodulation therapy on head and neck squamous cell carcinomas," Photochem. & Photobiol. Sci. Off. J. Eur. Photochem. Assoc. Eur. Soc. for Photobiol. **18**, 1621–1637 (2019).
5. Y. Zadik, P. R. Arany, E. R. Fregnani, P. Bossi, H. S. Antunes, R.-J. Bensadoun, L. A. Gueiros, A. Majorana, R. G. Nair, V. Ranna, W. J. E. Tissing, A. Vaddi, R. Lubart, C. A. Migliorati, R. V. Lalla, K. K. F. Cheng, S. Elad, and On behalf of The Mucositis Study Group of the Multinational Association of Supportive Care in Cancer/International

Society of Oral Oncology (MASCC/ISOO), "Systematic review of photobiomodulation for the management of oral mucositis in cancer patients and clinical practice guidelines," Support. Care Cancer **27**, 3969–3983 (2019).
6. A. C.-H. Chen, P. R. Arany, Y.-Y. Huang, E. M. Tomkinson, S. K. Sharma, G. B. Kharkwal, T. Saleem, D. Mooney, F. E. Yull, T. S. Blackwell, and M. R. Hamblin, "Low-Level Laser Therapy Activates NF-kB via Generation of Reactive Oxygen Species in Mouse Embryonic Fibroblasts," PLoS ONE **6** (2011).
7. T. Karu, "Mitochondrial Mechanisms of Photobiomodulation in Context of New Data About Multiple Roles of ATP," Photomed. Laser Surg. **28**, 159–160 (2010).
8. D. Pastore, M. Greco, and S. Passarella, "Specific helium-neon laser sensitivity of the purified cytochrome c oxidase," Int. J. Radiat. Biol. **76**, 863–870 (2000).
9. C. Ferraresi, B. Kaippert, P. Avci, Y.-Y. Huang, M. V. P. de Sousa, V. S. Bagnato, N. A. Parizotto, and M. R. Hamblin, "Low-level laser (light) therapy increases mitochondrial membrane potential and ATP synthesis in C2c12 myotubes with a peak response at 3-6 hours," Photochem. photobiology **91**, 411–416 (2015).
10. P. R. Arany, A. Cho, T. D. Hunt, G. Sidhu, K. Shin, E. Hahm, G. X. Huang, J. Weaver, A. C.-H. Chen, B. L. Padwa, M. R. Hamblin, M. H. Barcellos-Hoff, A. B. Kulkarni, and D. J Mooney, "Photoactivation of endogenous latent transforming growth factor-β1 directs dental stem cell differentiation for regeneration," Sci. Transl. Medicine **6**, 238ra69 (2014).
11. J. T. Eells, M. M. Henry, P. Summerfelt, M. T. T. Wong-Riley, E. V. Buchmann, M. Kane, N. T. Whelan, and H. T. Whelan, "Therapeutic photobiomodulation for methanol-induced retinal toxicity," Proc. Natl. Acad. Sci. United States Am. **100**, 3439–3444 (2003).
12. T. I. Karu, "Multiple roles of cytochrome c oxidase in mammalian cells under action of red and IR-A radiation," IUBMB Life **62**, 607–610 (2010).
13. K. R. Byrnes, X. Wu, R. W. Waynant, I. K. Ilev, and J. J. Anders, "Low power laser irradiation alters gene expression of olfactory ensheathing cells in vitro," Lasers Surg. Medicine **37**, 161–171 (2005).
14. Y. Zhang, S. Song, C.-C. Fong, C.-H. Tsang, Z. Yang, and M. Yang, "cDNA microarray analysis of gene expression profiles in human fibroblast cells irradiated with red light," The J. Investig. Dermatol. **120**, 849–857 (2003).
15. F. Ginani, D. M. Soares, M. P. E. V. Barreto, and C. A. G. Barboza, "Effect of low-level laser therapy on mesenchymal stem cell proliferation: a systematic review," Lasers Med. Sci. **30**, 2189–2194 (2015).
16. D. F. Wilson, "Oxidative phosphorylation: regulation and role in cellular and tissue metabolism," The J. Physiol. **595**, 7023–7038 (2017).
17. K. Alhallak, L. G. Rebello, T. J. Muldoon, K. P. Quinn, and N. Rajaram, "Optical redox ratio identifies metastatic potential-dependent changes in breast cancer cell metabolism," Biomed. Opt. Express **7**, 4364–4374 (2016).
18. W. Jones and K. Bianchi, "Aerobic Glycolysis: Beyond Proliferation," Front. Immunol. **6** (2015).
19. S. Papa, P. L. Martino, G. Capitanio, A. Gaballo, D. De Rasmo, A. Signorile, and V. Petruzzella, "The Oxidative Phosphorylation System in Mammalian Mitochondria," in *Advances in Mitochondrial Medicine,* vol. 942 R. Scatena, P. Bottoni, and B. Giardina, eds. (Springer Netherlands, Dordrecht, 2012), pp. 3–37.
20. Z. Liu, D. Pouli, C. A. Alonzo, A. Varone, S. Karaliota, K. P. Quinn, K. Münger, K. P. Karalis, and I. Georgakoudi, "Mapping metabolic changes by noninvasive, multiparametric, high-resolution imaging using endogenous contrast," Sci. Adv. **4** (2018).
21. O. I. Kolenc and K. P. Quinn, "Evaluating Cell Metabolism Through Autofluorescence Imaging of NAD(P)H and FAD," Antioxidants & Redox Signal. (2018).
22. C. Stringari, L. Abdeladim, G. Malkinson, P. Mahou, X. Solinas, I. Lamarre, S. Brizion, J.-B. Galey, W. Supatto, R. Legouis, A.-M. Pena, and E. Beaurepaire, "Multicolor two-photon imaging of endogenous fluorophores in living tissues by wavelength mixing," Sci. Reports **7** (2017).
23. M. Potter, E. Newport, and K. J. Morten, "The Warburg effect: 80 years on," Biochem. Soc. Transactions **44**, 1499–1505 (2016).
24. M. V. Liberti and J. W. Locasale, "The Warburg Effect: How Does it Benefit Cancer Cells?" Trends Biochem. Sci. **41**, 211–218 (2016).
25. V. S. LeBleu, J. T. O'Connell, K. N. Gonzalez Herrera, H. Wikman, K. Pantel, M. C. Haigis, F. M. de Carvalho, A. Damascena, L. T. Domingos Chinen, R. M. Rocha, J. M. Asara, and R. Kalluri, "PGC-1α mediates mitochondrial biogenesis and oxidative phosphorylation in cancer cells to promote metastasis," Nat. Cell Biol. **16**, 992–1003, 1–15 (2014).
26. X. Lu, B. Bennet, E. Mu, J. Rabinowitz, and Y. Kang, "Metabolomic changes accompanying transformation and acquisition of metastatic potential in a syngeneic mouse mammary tumor model," The J. Biol. Chem. **285**, 9317–9321 (2010).
27. P. E. Porporato, V. L. Payen, J. Pérez-Escuredo, C. J. De Saedeleer, P. Danhier, T. Copetti, S. Dhup, M. Tardy, T. Vazeille, C. Bouzin, O. Feron, C. Michiels, B. Gallez, and P. Sonveaux, "A mitochondrial switch promotes tumor metastasis," Cell Reports **8**, 754–766 (2014).
28. R. Sethupathi, K. Gurushankar, and N. Krishnakumar, "Optical redox ratio differentiates early tissue transformations in DMBA-induced hamster oral carcinogenesis based on autofluorescence spectroscopy coupled with multivariate analysis," Laser Phys. **26**, 116202 (2016).
29. E. C. Lins, C. F. Oliveira, O. C. Guimarães, C. A. d. S. Costa, C. Kurachi, and V. S. Bagnato, "A novel 785-nm laser diode-based system for standardization of cell culture irradiation," Photomed. Laser Surg. **31**, 466–473 (2013). PMID: 24102164.

30. W. Denk, J. H. Strickler, and W. W. Webb, "Two-photon laser scanning fluorescence microscopy," Sci. (New York, N.Y.) **248**, 73–76 (1990).
31. O. Warburg, "The Metabolism of Carcinoma Cells," The J. Cancer Res. **9**, 148–163 (1925).
32. M. Yamaura, M. Yao, I. Yaroslavsky, R. Cohen, M. Smotrich, and I. E. Kochevar, "Low level light effects on inflammatory cytokine production by rheumatoid arthritis synoviocytes," Lasers Surg. Medicine **41**, 282–290 (2009).
33. M. E. de Abreu Chaves, A. R. de Araújo, A. C. C. Piancastelli, and M. Pinotti, "Effects of low-power light therapy on wound healing: LASER x LED," Anais Brasileiros de Dermatol. **89**, 616–623 (2014).
34. S. George, M. R. Hamblin, and H. Abrahamse, "Effect of red light and near infrared laser on the generation of reactive oxygen species in primary dermal fibroblasts," J. Photochem. Photobiol. B: Biol. **188**, 60–68 (2018).
35. T. I. Karu, L. V. Pyatibrat, and N. I. Afanasyeva, "Cellular effects of low power laser therapy can be mediated by nitric oxide," Lasers Surg. Medicine **36**, 307–314 (2005).
36. S. Sonis, "Could the impact of photobiomodulation on tumor response to radiation be effected by tumor heterogeneity?" Support. Care Cancer (2019).
37. M. M. Schubert, F. P. Eduardo, K. A. Guthrie, J.-C. Franquin, R.-J. J. Bensadoun, C. A. Migliorati, C. M. E. Lloid, C. P. Eduardo, N.-F. Walter, M. M. Marques, and M. Hamdi, "A phase iii randomized double-blind placebo-controlled clinical trial to determine the efficacy of low level laser therapy for the prevention of oral mucositis in patients undergoing hematopoietic cell transplantation," Support. Care Cancer **15**, 1145–1154 (2007).
38. G. Jaguar, J. Prado, I. Nishimoto, M. Pinheiro, D. De Castro Jr, D. Da Cruz Perez, and F. Alves, "Low-energy laser therapy for prevention of oral mucositis in hematopoietic stem cell transplantation," Oral Dis. **13**, 538–543 (2007).
39. L. Hu, N. Wang, E. Cardona, and A. J. Walsh, "Fluorescence intensity and lifetime redox ratios detect metabolic perturbations in t cells," Biomed. Opt. Express **11**, 5674–5688 (2020).
40. J. M. Levitt, A. Baldwin, A. Papadakis, S. Puri, J. Xylas, K. Münger, and I. Georgakoudi, "Intrinsic fluorescence and redox changes associated with apoptosis of primary human epithelial cells," J. Biomed. Opt. **11**, 1 – 6 (2006).
41. P. G. B. Heymann, K. S. E. Henkenius, T. Ziebart, A. Braun, K. Hirthammer, F. Halling, A. Neff, and R. Mandic, "Modulation of Tumor Cell Metabolism by Laser Photochemotherapy with Cisplatin or Zoledronic Acid In Vitro," Anticancer. Res. **38**, 1291–1301 (2018).
42. L. Z. Li, R. Zhou, H. N. Xu, L. Moon, T. Zhong, E. J. Kim, H. Qiao, R. Reddy, D. Leeper, B. Chance, and J. D. Glickson, "Quantitative magnetic resonance and optical imaging biomarkers of melanoma metastatic potential," Proc. Natl. Acad. Sci. **106**, 6608–6613 (2009).
43. K. W. Engel, I. Khan, and P. R. Arany, "Cell lineage responses to photobiomodulation therapy," J. Biophotonics **9**, 1148–1156 (2016).
44. M. Lunova, B. Smolková, M. Uzhytchak, K. Ž. Janoušková, M. Jirsa, D. Egorova, A. Kulikov, Š. Kubinová, A. Dejneka, and O. Lunov, "Light-induced modulation of the mitochondrial respiratory chain activity: possibilities and limitations," Cell. Mol. Life Sci. **77**, 2815–2838 (2020).
45. A. Lynnyk, M. Lunova, M. Jirsa, D. Egorova, A. Kulikov, Šárka Kubinová, O. Lunov, and A. Dejneka, "Manipulating the mitochondria activity in human hepatic cell line huh7 by low-power laser irradiation," Biomed. Opt. Express **9**, 1283–1300 (2018).
46. A. C.-H. Chen, P. R. Arany, Y.-Y. Huang, E. M. Tomkinson, S. K. Sharma, G. B. Kharkwal, T. Saleem, D. Mooney, F. E. Yull, T. S. Blackwell, and M. R. Hamblin, "Low-level laser therapy activates nf-kb via generation of reactive oxygen species in mouse embryonic fibroblasts," PLOS ONE **6**, 1–8 (2011).
47. M. R. Hamblin, S. T. Nelson, and J. R. Strahan, "Photobiomodulation and Cancer: What Is the Truth?" Photomed. Laser Surg. **36**, 241–245 (2018).
48. R. D. Volker Hans Schartinger, Oliver GalvanHerbert, "Differential responses of fibroblasts, non-neoplastic epithelial cells, and oral carcinoma cells to low-level laser therapy," Support. Care Cancer **20**, 523–529 (2012).
49. F. F. Sperandio, F. S. Giudice, L. Corrêa, D. S. P. Jr., M. R. Hamblin, and S. C. de Sousa, "Low-level laser therapy can produce increased aggressiveness of dysplastic and oral cancer cell lines by modulation of akt/mtor signaling pathway," J. Biophotonics **6**, 839–847 (2013).

Supplemental document accompanying submission to *Biomedical Optics Express*

Title: Effects of photobiomodulation on the redox state of healthy and cancer cells

Authors: Clara de Faria, Heloisa Ciol, Vanderlei Bagnato, Sebastião Pratavieira

Submitted: 1/29/2021 3:49:32 PM

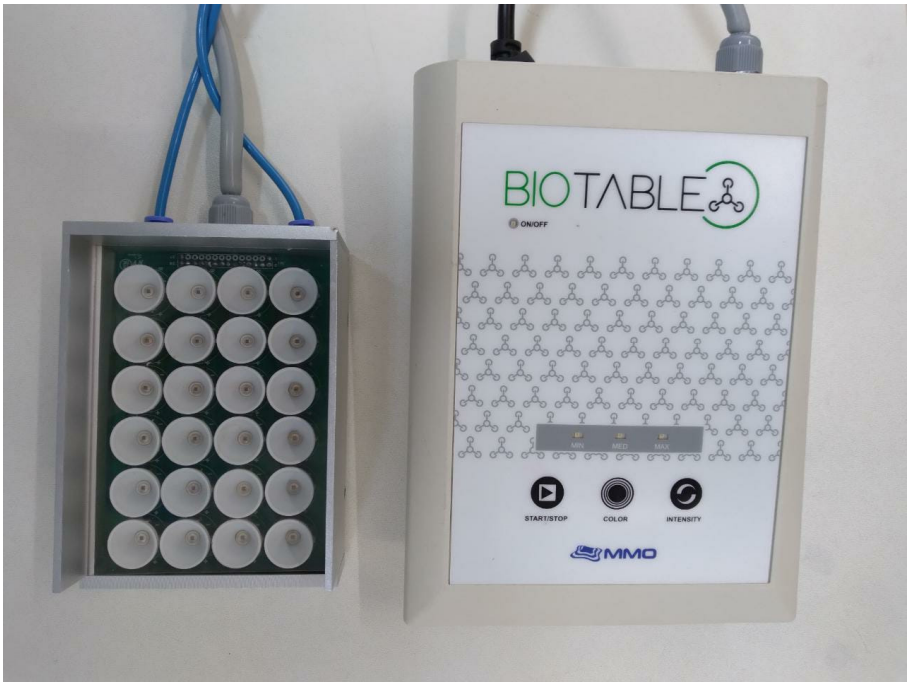

Figure S1: Illumination device used for PBMT, composed of 24 LEDs of 780 nm.

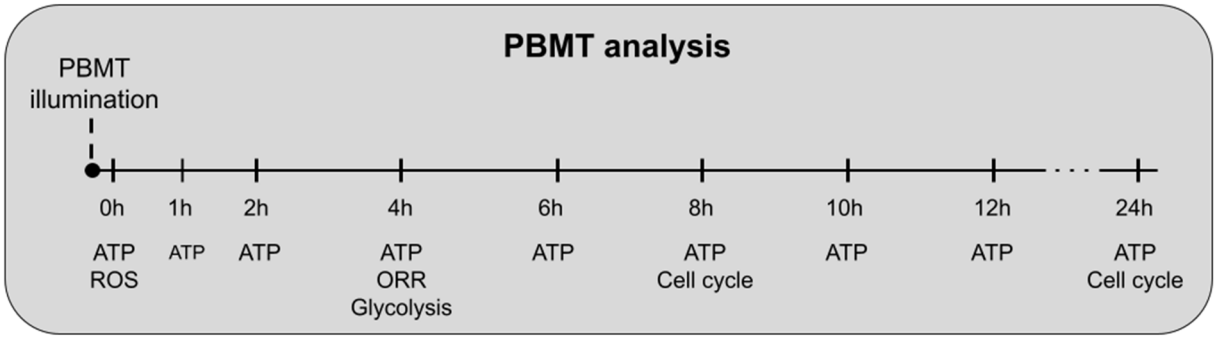

Figure S2:Flow chart indicating the experiments performed after PBMT.

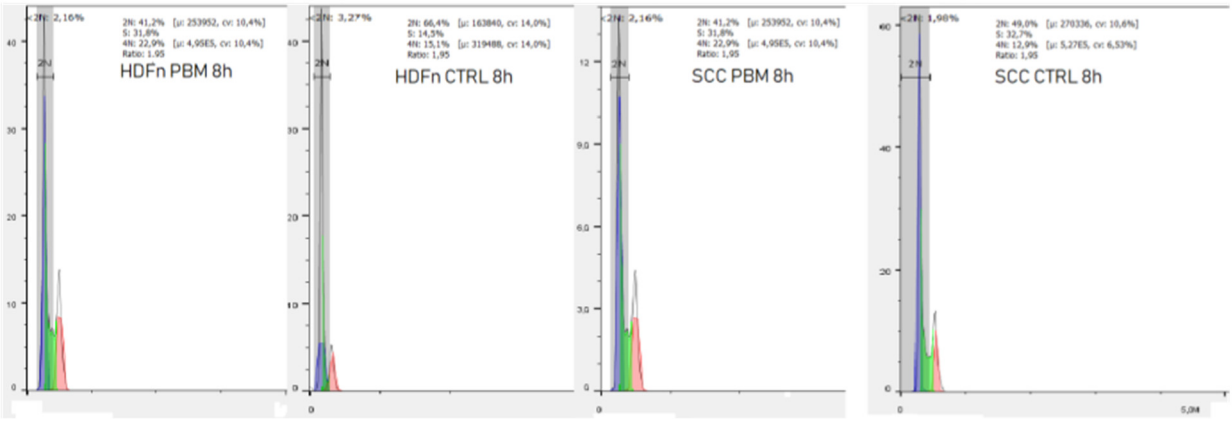

Figure S3: Cell cycle representative histograms from all groups.

3 PHOTOBIOMODULATION IN PHOTODYNAMIC THERAPY

Journal of Photochemistry & Photobiology, B: Biology 217 (2021) 112170

Contents lists available at ScienceDirect

Journal of Photochemistry & Photobiology, B: Biology

journal homepage: www.elsevier.com/locate/jphotobiol

Photobiomodulation effects on photodynamic therapy in HNSCC cell lines

Clara M.G. de Faria *, Camilla S. Costa, Vanderlei S. Bagnato

University of São Paulo, São Carlos Institute of Physics, Brazil

ARTICLE INFO

Keywords:
Photobiomodulation
Photodynamic therapy
Head and neck cancer

ABSTRACT

A combination of metabolic modifications by light stimulus and photodynamic action is very attractive. Photobiomodulation therapy (PBMT) comprehends a vast range of applications and has been shown to be suitable to ease morbidities caused by chemotherapy and radiation, such as mucositis and dermatitis. The current study investigates the effects of near-infrared PBMT combined with porphyrin-based photodynamic therapy (PDT) in squamous cell carcinoma cell lines SCC-25 and SCC-4. The aim is to evaluate the potential of this combination to improve PDT outcome by increasing cell toxicity. Many techniques were used to verify the combined effect. Photobiomodulation (PBM) enhanced PDT action in SCC-25 cells by increasing photosensitizer (PS) uptake and production of reactive oxygen species (ROS). The equivalent was not seen in SCC-4 cells compared to the PDT only group. We believe these effects are strongly related to the interval of application between PBMT, PS incubation and PDT. Additionally, the effect of ascorbic acid on preventing PBM effects in PDT shows that ROS play an important role in the early mechanisms of PBM-PDT. Therefore, we believe PBM-PDT combination is worth exploring, for its benefit-cost ratio and simple protocols, along with the possibility of improvement in treatment resuts.

1. Introduction

Photobiomodulation therapy (PBMT), formerly called Low-Level Light/Laser Therapy, is the application of light to modify the expression or activity of endogenous enzyme photoreceptors, initiating cell signaling pathways that modulate cellular and tissue metabolisms, proliferation and inflammatory response [1,2]. The applications of this technique include tissue repair, analgesia, inflammation reduction, pain relief in the treatment of wounds, mucositis, muscle regeneration, among others [3,4]. The light source usually consists in a low power laser (below 500 mW) or LED in the red and near infrared (NIR) wavelength region (600–850 nm), which presents effective penetration, lack of carcinogenic or mutagenic effects and minimal thermal effects [4]. Increased levels of reactive oxygen species (ROS) are involved in photobiomodulation (PBM), but in small amounts that act as mediators and initiate a cascade of cellular processes [5]. Other molecules that play a role in the early mechanisms of PBM are ATP, Ca2+, and NO [6]. The redox potential changes induced by PBM activate redox-sensitive transcription factors, such as necrosis factor-Kb, resulting in fibroblast proliferation, migration, collagen synthesis, modulation of inflammatory and antioxidant responses, increased angiogenesis, oxygenation and tissue repair [7].

On the other hand, Photodynamic Therapy (PDT) is a treatment based on the interaction of a photosensitizer (PS) with light and oxygen, producing toxic amounts of ROS in the target tissue. It is well known for its oncological use, but it is also explored in anti-microbial, dermatological and ophthalmological applications [8]. Many PDT procedures are approved and routinely used in several countries, including for the treatment of head and neck cancer (HNC) [9–12]. However, most cases are diagnosed at advanced stages, so treatment is less effective and surgery results in organ mutilation and impairment of speech, swallowing, aesthetic and self-perception [13]. In this scenario, PDT is a good alternative, since its advantages encompass effective tumor eradication along with tissue sparing and great cosmetic outcome [14,15]. Yet, there are some challenges in PDT that reduce treatment efficacy, such as low PS specificity and accumulation in the tumor and low light penetration. Efforts are being conducted in developing novel photosensitizers as well as illumination devices and protocols. In this scenario, strategies that could improve the protocols that have already been tested are also interesting.

In this study, we propose the investigation of the use of PBMT combined to PDT to improve the outcome results. PBMT alone is not suitable for an anti-tumor approach, however, its role in improving the overall outcome in cancer research as a treatment of the morbidities

* Corresponding author.
E-mail address: claramgf@ifsc.usp.br (C.M.G. de Faria).

https://doi.org/10.1016/j.jphotobiol.2021.112170
Received 2 October 2020; Received in revised form 13 January 2021; Accepted 24 February 2021
Available online 27 February 2021

caused by chemotherapy and radiation – mucositis and dermatitis, for example – is well known [16–19]. Combination of techniques with PDT has also been investigated, for instance, chemotherapy, radiotherapy and surgery, and additive and synergistic effects were observed [20–25]. For mucositis, Pinheiro et al. have studied PBM and PBM-PDT treatments and obtained positive results such as acceleration of healing time [26,27]. PBMT and PDT combined have also been studied as treatment for other oral conditions, in particular palatal ulcers and oral graft-*versus*-host disease [28,29]. The combination of PBMT and PDT in oncological applications has only been described in two [30,31], where both observed promising results when applying NIR light a few hours before PDT. Interestingly, the protocols had little in common as they differed in cell type, PBMT wavelength, photosensitizer and its incubation time. Nevertheless, they observed similar PBM effects in the PDT outcome that related to increased PS uptake. Tsai and Negri hypothesized that the PDT enhancement effect caused by PBMT was mediated by increased metabolism and ATP production, which resulted in higher PS uptake and energy supply to undergo apoptosis. In fact, several studies in different cells and conditions indicate that PBM increases ATP synthesis and metabolism [32]. Because modifications caused by PBM act on metabolism that can improve PDT efficiency either by increasing uptake or oxygenation in the reaction site, it is a very promising combination.

Therefore, in this study we investigated the effects of PBMT, employing a NIR light source, combined with porphyrin-based PDT in squamous cell carcinomas originated from the oral cavity, a common HNC. We aim to evaluate the potential of this combination to improve PDT results by increasing toxicity in tumor cells *in vitro*.

2. Materials and Methods

Two squamous carcinoma cell lines were used, SCC-25 (ATCC® CRL-1628™) and SCC-4 (ATCC® CRL-1624™), which were grown by adhesion in Dulbecco's Modified Eagle's Medium (DMEM)/ Ham's Nutrient Mixture F12, supplemented with 10% (*v*/v) fetal bovine serum (FBS), antibiotics and hydrocortisone (400 ng/mL). Cells were maintained at a density of $2x10^6$cells per culture flask, in an incubator at 37 °C under a humidified atmosphere of 5% CO_2. Cell medium was changed three times a week and cells were subcultured following standard protocol with 0.25% trypsin and 0.53 mM EDTA. Subculturing was performed whenever cells reached between 80% and 95% confluence, and the subculture ratio was maintained between 1:3 and 1:10.

2.1. Photobiomodulation Therapy - PBMT

Regarding PBMT, two experimental conditions were settled: control (cells not exposed to modulating radiation); and PBM, cells illuminated at 780 nm, 5 J/cm^2. PBMT parameters were determined based on studies that showed some photobiomodulatory effect in this range [33].

2.2. Photodynamic Therapy - PDT

For each PBM condition, two groups were established: control for PDT (0 J/cm^2) and illuminated PDT (630 nm, 15 J/cm^2), totaling six experimental groups. For PDT groups, the Photogem® PS was used at 5 μg/mL in DMEM/Ham's 1% FBS and without phenol red. PS was immediately incubated after PBM, during 4 h. Then, cells were washed twice with phosphate solution (PBS) at a pH of 7,2, fresh medium (DMEM/Ham's, 1% FBS, no phenol) was added and cells were exposed to 630 nm and 15 J/cm^2 fluence rate.

2.3. Cell Counting

PBMT effects on cell proliferation were analyzed 24 h after PBMT illumination. Cells were inoculated in 24-well plates at a 5×10^4 cells/ well density 24 h before PBMT illumination. PBMT was performed (780 nm, 5 J/cm^2), and plates were kept in an incubator for another 24 h. Cells were washed with PBS, detached with trypsin and filtered to remove cell clusters. Then, cells were counted by flow cytometry (488 nm excitation, 695/40 nm detection, BD Accuri C6 Plus, BD Biosciences). Two independent experiments were performed in triplicate for each group ($N = 6$).

2.4. Cell Viability and Morphology

Cell morphology was assessed by phase contrast microscopy (Axio Observer.Z1, Carl Zeiss) with 10× and 20× magnification 20 h after PDT. Cell viability was analyzed by the MTT assay (3-(4,5-dimethylthiazol-2yl) -2,5-diphenyltetrazolium bromide), which consists of a colorimetric method to quantify cell viability based on MTT conversion into purple formazan crystals due to cell metabolic action. Cells were inoculated in 96-well plates at a density of 1×10^4 cells/well 24 h before experiments. Cells with MTT at 0,5 mg/mL in DMEM 1% FBS without phenol were incubated 21 h after PDT irradiation during 3 h. Then, formazan crystals were diluted in DMSO and the absorbance was read at a microplate reader (570 nm and 690 nm), resulting in a measurement 24 h after PDT. For viability, three independent experiments were performed in three rows of 5 wells for each group ($N = 45$).

2.5. PS Uptake

Cellular PS uptake was also analyzed. Cells were inoculated in 24-well plates at a density of 5×10^4 cells/ well 24 h before PS incubation. PBMT 780 nm was performed, and immediately after illumination, PS was incubated for 4 h. Then, cells were washed twice with PBS, detached from wells with trypsin and PS fluorescence was measured by flow cytometry (488 nm excitation, 695/40 nm detection, BD Accuri C6 Plus, BD Biosciences). The experiment was performed in triplicate and repeated twice ($N = 6$).

2.6. DCFH-DA

DCFH-DA (2,7-dichlorofluorescin diacetate) is an oxidative stress marker related to reactive oxygen and nitrogen (RNS) species in cells. This probe penetrates the cell membrane and can be oxidized by ROS and RNS to DCF (2,7-dichlorofluorescin), a fluorescent compound [34]. Cells were inoculated in 24-well plates at a density of 5×10^4 cells/ well 24 h before DCFH-DA incubation. They were submitted to the PBMT 780 nm protocol, then PS was incubated for 4 h, as mentioned previously. After incubation and PBS washings, cells were detached from plates with trypsin, and DCFDA at 25 μM in DMEM Ham's without phenol red was added to the wells. PDT illumination was performed, and cells were incubated for another 20 min at 37 °C until DCF fluorescence was measured by flow cytometry at 488 excitation and 533/30 emission (BD Accuri C6 Plus, BD Biosciences). Two independent experiments were performed in triplicate ($N = 6$).

2.7. Ascorbic Acid

Ascorbic Acid (AA) is an antioxidant capable of scavenging ROS free radicals, preventing cellular damage caused by these species [35]. In this assay, AA was dissolved in PBS to a stock solution of 10 mM. Fresh stock solutions were prepared for each experiment. Then, it was diluted to DMEM Ham's 5% FBS without phenol red at a concentration of 100 μM, which was added to cells 2 h before PBM-PDT experiments. Afterward, the medium was changed to a new one, and PBM-PDT protocol proceeded as previously described. Three independent experiments were performed for this analysis, with a total $N = 45$.

2.8. Statistical Analysis

All quantitative data were described as means ± SD deviation.

Statistical analyses were performed with Origin software (version 2018, Originlab, USA). ANOVA followed by the Tukey test was applied to estimate the differences between two means for normal distributed data, and the Kruskal-Wallis ANOVA test was used when the results rejected normality. A value of $P < 0.05$ was considered to be statistically significant.

3. Results

3.1. Photobiomodulation and Photodynamic Therapy

Cell counting was performed 24 h after PBMT to investigate the effects of illumination protocol on proliferation (Fig. 1). PBMT and PDT viability results are shown in Figs. 2 and 3. The PBM effect on viability alone was statistically different from the controls, despite not being very expressive. SCC-25 presented a slight increase in it after PBM, of about 8%, as opposed to SCC-4, which had a 4% decrease compared to its control. Since viability was measured indirectly through MTT metabolic activity assay, these results may be due to differences in metabolism, instead of cell number or proliferation, since cell counting 24 h after PBMT did not indicate a statistically significant difference between groups.

The photodynamic treatment alone resulted in a reduction of 64% in cell viability in SCC-25 and of 32% in SCC-4 cells. Therefore, we see that SCC-25 cells are more sensitive to PDT than the latter. In regard to the PBM effect on PDT, we observed an enhancement in cell death for SCC-25 cells with a statistically significant difference. PBM-PDT viability on these cells is about 70% of the PDT group and represent an additional 10% reduction in viability compared to the control. Regarding SCC-4 cells, the PBM effect on PDT is not statistically significant.

3.2. Morphological Changes by PDT

Bright field microscopy of SCC-25 and SCC-4 cells 20 h after PDT is shown in Fig. 4. All groups present characteristic marks of damage and some clear signs of cell death, such as detached cells, apoptotic bodies and vacuolation. Comparatively, in SCC-25 cells differences are observed between the groups. In the PBM-PDT images it is seen an increase in cell detachment, apoptotic bodies and cells with large and numerous vacuoles. These indicate that PBM increases irreversible damage caused by PDT in those cells. Further tests are needed to quantify the processes of cell death and study if all are increased in the same manner or if any of them are more sensitive to the effects of PBM.

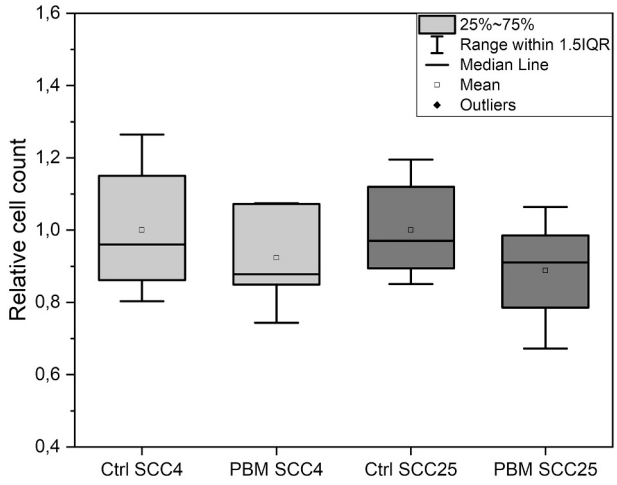

Fig. 1. Cell count 24 h after PBMT relative to its corresponding control group. No statistical difference is observed among groups.

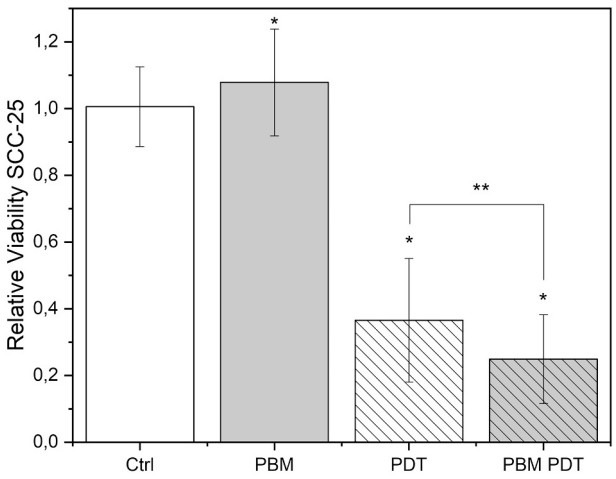

Fig. 2. Relative Viability of PBM-PDT in SCC-25 cells. Statistical significance from control ($p < 0.05$) is shown by (*) and by (**) when between other groups.

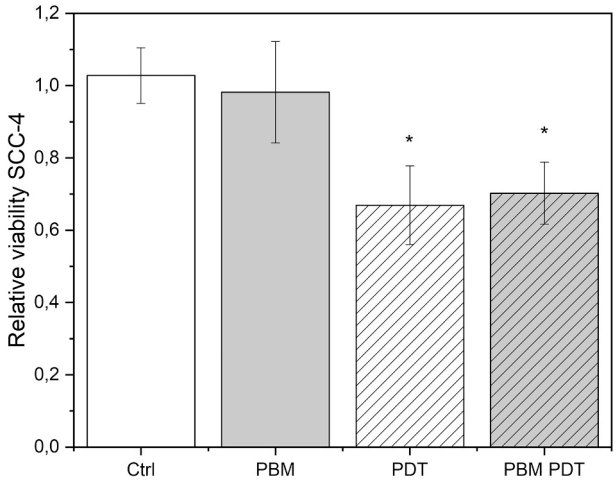

Fig. 3. Relative Viability of PBM-PDT in SCC-4 cells. Statistical significance from control ($p < 0.05$) is shown by (*).

3.3. PS Uptake

Photogem uptake after PBMT is shown in Fig. 5. We observe that PBM induced an increase of 5% in uptake in SCC25 cells, but the same protocol appears to decrease PS concentration in SCC4 cells at the same rate. The difference induced by PBMT in both cells is not very expressive, despite being statistically significant for SCC-25.

3.4. DCFDA

The relative production of ROS by PDT can be indicated by the DCFDA fluorescence intensity. Oxidized DCFDA is one of the most widely used methods for directly measuring the redox state of a cell [36]. Despite being unspecific, it can be used to track changes in ROS after PDT, since the treatment created several reactive species. Therefore, DCF fluorescence of PDT and PBM-PDT groups, compared to sham illuminated controls, was measured by flow cytometry and is shown in Fig. 6. PBM induced an increase of more than 20% in the SCC25 cells. Results from SCC4 cells displayed a tendency of decrease, but no significant difference could be seen.

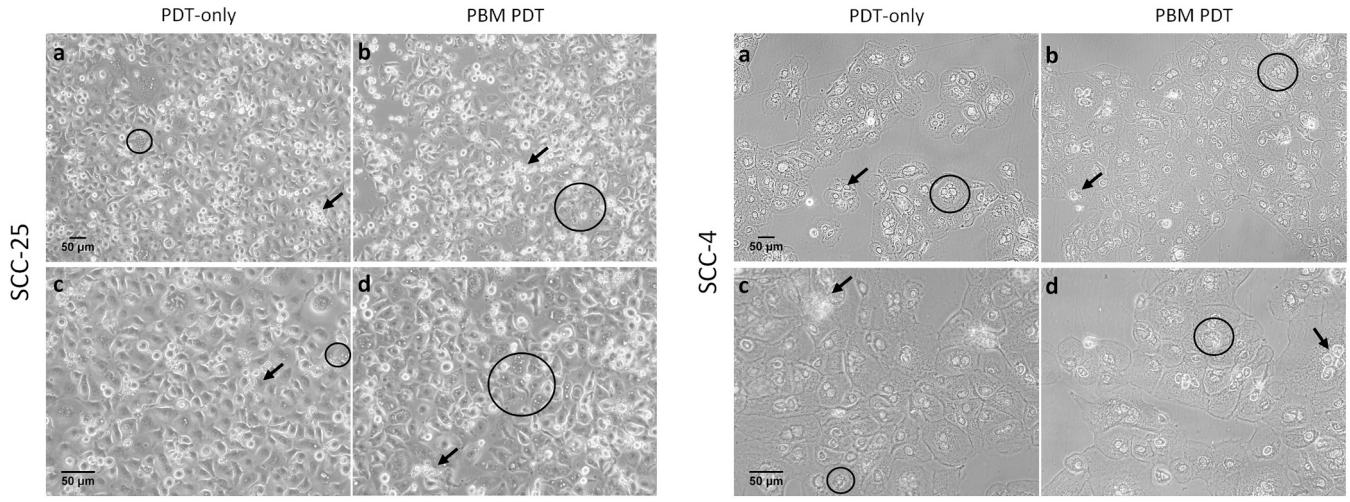

Fig. 4. Morphology of SCC cells 20 h after PBM-PDT. Bottom images of each cell line, (c) and (d), correspond to greater magnification of top images (a) and (b), respectively. Examples of damage are marked on the images: vacuolation is shown by dark circles, and arrows indicate apoptotic bodies and detached cells.

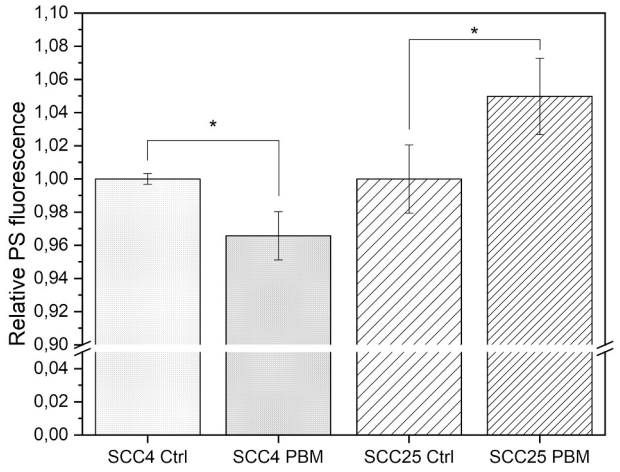

Fig. 5. Relative PS fluorescence after 4 h incubation, measured by flow cytometry. PBM groups were illuminated immediately before incubation. Statistical significance ($p < 0.05$) is shown by (*).

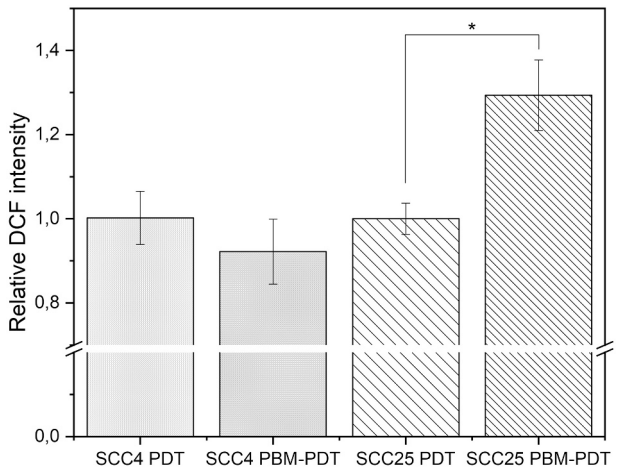

Fig. 6. DCFDA fluorescence intensity relative to control immediately after PDT, measured by flow cytometry. Statistical significance ($p < 0.05$) is shown by (*).

3.5. Ascorbic Acid

Ascorbic acid, an efficient antioxidant, was incubated for 2 h prior to PBMT illumination or sham-illumination, in the case of controls, then PBMT and PDT protocols were performed as described. Results are shown in Fig. 7. This compound had no significant effect in controls and PDT only groups (Sup Mat2), however, for SCC-25 it prevented the effects of PBM on PDT toxicity. PBMT viability was the same as in control, and PBM-PDT had no significant difference from PDT only. For SCC-4 we observed that AA did not completely revert PBM effect compared to control; it is still reduced, but PBM-PDT remained comparable to the PDT only group.

4. Discussion

There are several studies on PDT using SCC-4 and SCC-25 cell lines focused on enhancing PDT efficiency by different methods. [37–40]. D.-F. Yang et al. studied calcipotriol and methotrexate associated with ALA-PDT protocol in SCC-4 cells. Concerning SCC-25, Bhuvaneswari et al. evaluated the anti-angiogenic potential of nimotuzumab and cetuximab in Chlorin e6-PDT. Besides, Kelley et al. showed an increase in Photofrin-PDT effect by the pro-oxidant property of iron and ascorbate. Although these articles share similarities with the current study, regarding PDT, cell line and PS (Kelley, particularly), none of them correlates PDT and PBM. In fact, there are only few studies approaching this combination in any setting of cell line and protocol.

A great number of studies reported that PBM modulates intracellular processes as well as systemic effects. Primary human skin fibroblasts irradiated by Infrared A (IRA) revealed a change in gene transcription: there have been identified 599 IRA-regulated transcripts related to the extracellular matrix, calcium homeostasis, stress signaling, and apoptosis [41]. It is proposed that PBM upregulates ROS (primary superoxide anion $O2^{\bullet-}$, often converted to hydrogen peroxide H_2O_2), ATP and Ca^{2+} mainly by light activation of cytochrome *c* oxidase (CCO), which is the final mitochondrial respiratory chain enzyme [42,43]. These effects are related to the cell response to PDT, so the aim of this study was to evaluate the impact of PBM to PDT in oral cancer cell lines.

PBM effects on viability, shown by the MTT assay, are seen in both cell lines and are very modest, with a difference of 8% and 4% compared to the respective controls. Comparing it to the results of cell counting, where no difference is observed among groups, we can conclude that the tendency demonstrated by MTT must be solely due to differences in metabolism. Interestingly, the results observed are opposite from one another as PBMT increases metabolic activity in SCC-25 while reducing

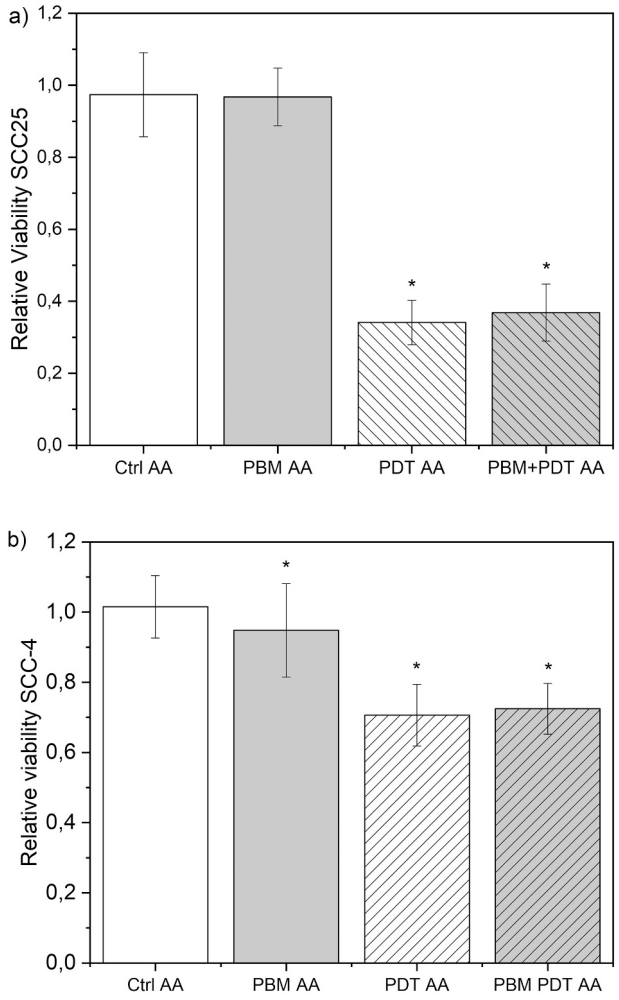

Fig. 7. Ascorbic Acid effect on PDT and PBM-PDT viability of (a) SCC-25 and (b) SCC-4 cell lines, showing that PBM effects on PDT in SCC-25 cells are ROS-mediated. Statistical significance ($p < 0.05$) from control is shown by (*).

it in SCC-4. These results endorse the evidence that indicates the safety of using PBMT in cancer cells [44]. Currently, illumination of the tumor area is avoided in clinical application of PBMT in supportive cancer treatment, such as prevention and reduction of chemo-radiotherapy morbidities in HNSCC patients, especially mucositis. Nevertheless, the concern among oncology professionals and researchers regarding PBM on tumors is still valid, since we know that PBMT can alter metabolism and that tumors from the same site may respond differently. Therefore, it is important to perform preclinical studies addressing PBM effects and mechanisms in tumor cells, and then clinical trials. Distinct PBM effects on the cell lines tested are the first indication of the differences between them. Next, we observe that they also differ from each other regarding PDT sensitivity, since cell death induced by the treatment in SCC-25 is two times the one observed for SCC-4. Finally, PBM induces an increment in cell death in SCC-25 that is not observed in the other cell line.

We acquired microscope images of the cells after PDT to confirm the previous results, and the differences in response were also observed in the morphological evaluation by bright field microscopy performed 20 h after the treatment, where we were able to see characteristic signs of damage and cell death, namely cell detachment, formation of apoptotic bodies and numerous intracellular vacuoles. For SCC-4, following the viability result, we did not observe differences between the groups. Similar amounts of cell damage were seen in the images of PDT and PBM-PDT. For SCC-25, however, all signs of it are increased for the group that received PBMT before PDT.

Detached cells are observed with various photosensitizers, including the Photogem analogue, Photofrin, in a concentration and fluence-dependent [45]. Hong et al. showed that the loss of cell attachment was related to an increase in Ca2+ concentration, which initiates apoptosis at high levels. Moreover, it is known that cells generally detach from the ones in their surroundings and lose contact with the extracellular matrix in the early stages of apoptosis [46]. Therefore, the number of detached cells is likely to be proportional to the amount of photodamage and also an indication of initiated apoptosis. In contrast, a clear sign of apoptosis is the presence of apoptotic bodies, which is the result of the dead cell fragmentation into smaller parts that can easily be consumed by phagocytes. The last indication of cell damage seen in Fig. 4 is vacuolation, a feature of two main types of cell death: autophagy and paraptosis. Autophagy is frequently a pro-survival mechanism characterized by the formation of double membrane vacuoles, denominated autophagosomes, that remove and recycle cellular components that are dysfunctional or no longer necessary [47]. This process is known to repair photodamaged cellular components, such as organelles. However, in situations of irreversible damage, autophagy leads to cell death. In PDT, authors have identified the predominance of autophagy where apoptosis is unavailable, for instance, the absence of BAX and BAK proteins, but also in apoptosis competent cells [48,49]. It is still a difficult process x to measure, so its causes and consequences are unclear. A process that is similar to autophagy is paraptosis, which has recently been described as a potential type of death in PDT [50]. It is associated with ER mediated stress response, accumulation of misfolded protein and proteotoxicity [51]. While there is no biochemical assay to identify it, a recognizable morphological feature is the formation of multiple cytoplasmic vacuoles that differ from autophagosomes by having single membranes [52]. Therefore, techniques such as electron microscopy are necessary to allow the visualization of the vacuole membranes, and to distinguish between autophagy and paraptosis. Despite not being done in this study, we consider it an important step to understand the mechanisms of PDT in general and the effects of the PBMT combination with it, since these two types of death have different implications and may be involved in the explanation for the differences observed in SCC-25.

Therefore, bright field microscopy results were important in the visualization of the death promoted by PDT and enhanced by PBM, for SCC-25 cells. We propose the use of confocal microscopy with specific markers in further studies, as well as electron microscopy, to confirm the indications seen in bright field images.

Photogem uptake after PBMT is significantly increased by 5% in SCC-25 cells, while the same protocol appears to decrease PS concentration in SCC-4 cells at the same rate, despite not being statistically significant. This result does not completely explain the impact of PBM on PDT viability, since it only accounts for a fraction of it. We hypothesized that, in addition to uptake, PBM may change PS subcellular localization to more sensitive sites. It is known that Photofrin®, a Photogem analog, is a hydrophobic photosensitizer, often localized in plasma and intracellular membranes [40]. Since ROS are highly reactive, presenting a short half-life, the most sensitive sites are those close to ROS generation sites, *i.e.*, PS subcellular localization [53]. Another hypothesis is that PBM could modulate cell permeability to PS. Sommer et al. concluded that 670 nm laser light is capable of changing the density and viscosity of nanoscopic interfacial water layers contained between hydrophilic surfaces, promoting a transmembrane convection effect, forcing HeLa cells to internalize cytostatic drugs in a high rate.

The relative production of ROS by PDT, compared to sham illuminated controls, was measured by flow cytometry and contributed to the elucidation of the mechanisms of PBM effect in PDT. We observed an increase of more than 20% in the SCC-25 cells. PBM-PDT results from SCC-4 cells displayed a tendency of decrease, but with no statistically significance. This result is certainly correlated with PS uptake, since it is directly dependent on its concentration inside the cells. Nevertheless, on SCC-25 cells, the increase of ROS (20%) is higher than the PS increment

(5%). This difference may also be due to changes in PS subcellular localization, since some sites are more sensitive to damage than others.

The effect of ascorbic acid incubation was evaluated due to its potential to prevent PBM effects on PDT. The photobiomodulation cascade of events is believed to start by the absorption of energy by cytochrome *c* oxidase and then concentration changes of a few mediators, including ROS. Its increase after PBMT is reported by several groups [5,54–59]. Therefore, if the presence of a scavenger reduces or suppresses the effect of PBMT, one can conclude that ROS are fundamental to the initiation of the pathways that lead to the effects observed [56,60]. Zhang et al. reported that PBM activation of Src tyrosine kinases is mediated by ROS and that the presence of AA decreased the concentrations of it nearly to the basal level [59]. Chen et al. observed that the presence of AA, in the same concentration and incubation time used in our study, abrogated the ROS increase and NF-kB activation by PBM but not the increase in ATP [5]. In our results, it is seen that AA eliminated the effects of PBMT in all its groups of SCC-25 cells, resulting in values that are similar to the groups with no PBM. Therefore, we can conclude that ROS play an important role in the early mechanisms of the PBM effect on PDT. In SCC-4 cells, however, AA did not alter the effect of PBMT alone, which means a tendency of decrease in cell viability, nor did it have any effect on PBM-PDT that remained comparable to PDT only. We hypothesized that the PBM pathways in SCC-4 and SCC-25 may be different, yielding the distinct results observed in this study.

Finally, we highlight the agreement of our results with the ones from Tsai and Negri, despite studying three distinct PBMT and PDT protocols and different cell lines, with similar mechanisms of increased PS uptake (Tsai 2015, Negri 2019). This indicates that PBM effects on PDT are not specific and its window of action may consist in a wide range of wavelengths, fluences, photosensitizers and tumor types. Additionally, it is important to state that the results observed are limited to cellular effects of PBMT. They don't account for extracellular matrix interactions or systemic response. It is known that PBM can increase tissue oxygenation and modulate inflammatory responses. Therefore, studies in 3D tumor models and *in vivo* should be conducted.

5. Conclusions

The results presented demonstrate the effect of combining PBMT illumination before PDT in oral cancer cells. Despite the evidence indicating that PBM induces cell metabolism in a way that enhances the photodynamic action (increasing uptake and ROS production), we observed distinct effects between the cell lines. It is important to note, however, that PBMT did not reduce the PDT effect in either of them, which indicates the safety of the combination. Nevertheless, further experiments are fundamental to confirm it, including the investigation of other tumor types and treatment protocols, using *in vitro* and *in vivo* models that would allow the design of clinical trials. Therefore, we believe PBM-PDT combination potential is worth exploring, since it may be a safe, low-cost technique with simple protocols that may result in significant improvement in treatment outcome. The tendency of decrease in PS uptake and ROS production for SCC-4, nevertheless, must be further investigated along with understanding which PBM mechanisms modulate these results.

Declaration of Competing Interest

All authors (Clara M G de Faria, Camilla S Costa and Vanderlei S Bagnato) certify that they have NO affiliations with or involvement in any organization or entity with any financial interest (such as honoraria; educational grants; participation in speakers' bureaus; membership, employment, consultancies, stock ownership, or other equity interest; and expert testimony or patent-licensing arrangements), or non-financial interest (such as personal or professional relationships, affiliations, knowledge or beliefs) in the subject matter or materials discussed in this manuscript.

Acknowledgements

This work is supported by FAPESP (Fundação de Amparo à Pesquisa do Estado de São Paulo) grants 2013/07276-1 (CEPOF); 2014/50857-8 (INCT); 2017/14182-4 (de Faria scholarship); and CNPq (Conselho Nacional de Desenvolvimento Científico e Tecnológico) for Costa scholarship.

Appendix A. Supplementary data

Supplementary data to this article can be found online at https://doi.org/10.1016/j.jphotobiol.2021.112170.

References

[1] R.O. Poyton, K.A. Ball, Therapeutic photobiomodulation: nitric oxide and a novel function of mitochondrial cytochrome c oxidase, Discov. Med. 57 (2011).
[2] J.J. Anders, R.J. Lanzafame, P.R. Arany, Low-level light/laser therapy versus Photobiomodulation therapy, Photomed. Laser Surg. 33 (2015) 183–184, https://doi.org/10.1089/pho.2015.9848.
[3] H. Chung, T. Dai, S.K. Sharma, Y.-Y. Huang, J.D. Carroll, M.R. Hamblin, The nuts and bolts of low-level laser (light) therapy, Ann. Biomed. Eng. 40 (2012) 516–533, https://doi.org/10.1007/s10439-011-0454-7.
[4] L.F. de Freitas, M.R. Hamblin, Proposed mechanisms of photobiomodulation or low-level light therapy, IEEE J. Selected Top. Quantum Elect. 22 (2016) 348–364, https://doi.org/10.1109/JSTQE.2016.2561201.
[5] A.C.-H. Chen, P.R. Arany, Y.-Y. Huang, E.M. Tomkinson, S.K. Sharma, G. B. Kharkwal, T. Saleem, D. Mooney, F.E. Yull, T.S. Blackwell, M.R. Hamblin, Low-level laser therapy activates NF-kB via generation of reactive oxygen species in mouse embryonic fibroblasts, PLoS One 6 (2011), e22453, https://doi.org/10.1371/journal.pone.0022453.
[6] R. Zein, W. Selting, M.R. Hamblin, Review of light parameters and photobiomodulation efficacy: dive into complexity, J. Biomed. Opt. 23 (2018) 1, https://doi.org/10.1117/1.JBO.23.12.120901.
[7] P. Pandeshwar, M.D. Roa, R. Das, S.P. Shastry, R. Kaul, M.B. Srinivasreddy, Photobiomodulation in oral medicine: a review, J. Investig. Clin. Dent. 7 (2016) 114–126, https://doi.org/10.1111/jicd.12148.
[8] A. Oniszczuk, K.A. Wojtunik-Kulesza, T. Oniszczuk, K. Kasprzak, The potential of photodynamic therapy (PDT)—experimental investigations and clinical use, Biomed. Pharmacother. 83 (2016) 912–929, https://doi.org/10.1016/j.biopha.2016.07.058.
[9] M.H. Abdel-kader, CHAPTER 1. The Journey of PDT Throughout History: PDT from Pharos to Present, Royal Society of Chemistry, 2016, pp. 1–21.
[10] H.R. Nava, S.S. Allamaneni, T.J. Dougherty, M.T. Cooper, W. Tan, G. Wilding, B. W. Henderson, Photodynamic therapy (PDT) using HPPH for the treatment of precancerous lesions associated with barrett's esophagus, Lasers Surg. Med. 43 (2011) 705–712, https://doi.org/10.1002/lsm.21112.
[11] M.A. Biel, Photodynamic therapy treatment of early Oral and laryngeal cancers, Photochem. Photobiol. 83 (2007) 1063–1068, https://doi.org/10.1111/j.1751-1097.2007.00153.x.
[12] S.A.H.J. de Visscher, P.U. Dijkstra, I.B. Tan, J.L.N. Roodenburg, M.J.H. Witjes, mTHPC mediated photodynamic therapy (PDT) of squamous cell carcinoma in the head and neck: a systematic review, Oral Oncol. 49 (2013) 192–210, https://doi.org/10.1016/j.oraloncology.2012.09.011.
[13] J. Wagenblast, M. Baghi, M. Helbig, C. Arnoldner, S. Bisdas, W. Gstöttner, M. Hambek, A. May, Craniofacial reconstructions with bone-anchored Epithesis in head and neck Cancer patients – a valid way Back to self-perception and social reintegration, Anticancer Res. 28 (2008) 2349–2352.
[14] P.-J. Lou, L. Jones, C. Hopper, Clinical outcomes of photodynamic therapy for head-and-neck Cancer, Technol. Cancer Res. Treat. 2 (2003) 311–317, https://doi.org/10.1177/153303460300200405.
[15] K.H. Nelke, W. Pawlak, J. Leszczyszyn, H. Gerber, Photodynamic therapy in head and neck cancer, Postępy Higieny i Medycyny Doświadczalnej. 68 (2014) 119–128, https://doi.org/10.5604/17322693.1088044.
[16] J.A.E.M. Zecha, J.E. Raber-Durlacher, R.G. Nair, J.B. Epstein, S. Elad, M. R. Hamblin, A. Barasch, C.A. Migliorati, D.M.J. Milstein, M.-T. Genot, L. Lansaat, R. van der Brink, J. Arnabat-Dominguez, L. van der Molen, I. Jacobi, J. van Diessen, J. de Lange, L.E. Smeele, M.M. Schubert, R.-J. Bensadoun, Low-level laser therapy/photobiomodulation in the management of side effects of chemoradiation therapy in head and neck cancer: part 2: proposed applications and treatment protocols, Support. Care Cancer 24 (2016) 2793–2805, https://doi.org/10.1007/s00520-016-3153-y.
[17] H.S. Antunes, D. Herchenhorn, I.A. Small, C.M.M. Araújo, C.M.P. Viégas, G. de Assis Ramos, F.L. Dias, C.G. Ferreira, Long-term survival of a randomized phase III trial of head and neck cancer patients receiving concurrent chemoradiation therapy with or without low-level laser therapy (LLLT) to prevent oral mucositis, Oral Oncol. 71 (2017) 11–15, https://doi.org/10.1016/j.oraloncology.2017.05.018.
[18] K.A.M. Kalhori, F. Vahdatinia, M.R. Jamalpour, P. Vescovi, C. Fornaini, E. Merigo, R. Fekrazad, Photobiomodulation in oral medicine, Photobiomodulat. Photomed. Laser Surg. 37 (2019) 837–861, https://doi.org/10.1089/photob.2019.4706.

[19] R.J. Chan, J. Webster, B. Chung, L. Marquart, M. Ahmed, S. Garantziotis, Prevention and treatment of acute radiation-induced skin reactions: a systematic review and meta-analysis of randomized controlled trials, BMC Cancer 14 (2014) 53, https://doi.org/10.1186/1471-2407-14-53.

[20] M.Y. Nahabedian, R.A. Cohen, M.F. Contino, T.M. Terem, W.H. Wright, M. W. Berns, A.G. Wile, Combination cytotoxic chemotherapy with cisplatin or doxorubicin and photodynamic therapy in murine Tumors1, JNCI J. Nat. Cancer Inst.. 80 (1988) 739–743, https://doi.org/10.1093/jnci/80.10.739.

[21] M.-F. Zuluaga, N. Lange, Combination of photodynamic therapy with anti-cancer agents, Curr. Med. Chem. 15 (2008) 1655–1673, https://doi.org/10.2174/092986708784872401.

[22] C.T. de Andrade, J.D. Vollet-Filho, L. Pires, J.F. Pavoni, O.B. Filho, H.M. Oliveira, L.F. Tirapelli, V.S. Bagnato, C. Kurachi, Synergic effect in combining photodynamic therapy and radiotherapy in Wistar rats skin model, Photodiagn. Photodyn. Ther. 12 (2015) 344, https://doi.org/10.1016/j.pdpdt.2015.07.077.

[23] C.T. de Andrade, M.S. Nogueira, S.C. Kanick, K. Marra, J. Gunn, J. Andreozzi, K. S. Samkoe, C. Kurachi, B.W. Pogue, Optical Spectroscopy of Radiotherapy and Photodynamic Therapy Responses in Normal Rat Skin shows Vascular Breakdown Products, 2016, p. 969410, https://doi.org/10.1117/12.2210988.

[24] G.D. Wang, H.T. Nguyen, H. Chen, P.B. Cox, L. Wang, K. Nagata, Z. Hao, A. Wang, Z. Li, J. Xie, X-ray induced photodynamic therapy: a combination of radiotherapy and photodynamic therapy, Theranostics. 6 (2016) 2295–2305, https://doi.org/10.7150/thno.16141.

[25] A. Fraix, S. Sortino, Combination of PDT photosensitizers with NO photodononors, Photochem. Photobiol. Sci. 17 (2018) 1709–1727, https://doi.org/10.1039/C8PP00272J.

[26] S.L. Pinheiro, A.C. Bonadiman, A.L. Dos A. Borges Lemos, B.M. Annicchino, B. Segatti, D.S. Pucca, P.T. Dutra, R.M. De Carvalho E. Silva, F. Leal, Photobiomodulation therapy in cancer patients with mucositis: a clinical evaluation, Photobiomodulat. Photomed. Laser Surg. 37 (2019) 142–150, https://doi.org/10.1089/photob.2018.4526.

[27] E.C. Pires Marques, F. Piccolo Lopes, I.C. Nascimento, J. Morelli, M.V. Pereira, V. M. Machado Meiken, S.L. Pinheiro, Photobiomodulation and photodynamic therapy for the treatment of oral mucositis in patients with cancer, Photodiagn. Photodyn. Ther. 29 (2020) 101621, https://doi.org/10.1016/j.pdpdt.2019.101621.

[28] L. Campos, S.B. Rezende, A. Simões, L.F. Palma, R.Y. Tateno, R.L. da Silva, M. C. Macedo, Photobiomodulation and photodynamic therapy for the management of oral graft-versus-host disease: a case report, Photodiagn. Photodyn. Ther. 30 (2020) 101776, https://doi.org/10.1016/j.pdpdt.2020.101776.

[29] R. Maya, L.L.C. Ladeira, J.E.P. Maya, L.M.G. Mail, S.K. Bussadori, M.A.B. Paschoal, The combination of antimicrobial photodynamic therapy and photobiomodulation therapy for the treatment of palatal ulcers: a case report, J. Lasers in Med. Sci. 11 (2020) 228–233, https://doi.org/10.34172/jlms.2020.38.

[30] S.-R. Tsai, R. Yin, Y.-Y. Huang, B.-C. Sheu, S.-C. Lee, M.R. Hamblin, Low-level light therapy potentiates NPe6-mediated photodynamic therapy in a human osteosarcoma cell line via increased ATP, Photodiagn. Photodyn. Ther. 12 (2015) 123–130, https://doi.org/10.1016/j.pdpdt.2014.10.009.

[31] L.B. Negri, T.J. Martins, R.S. da Silva, M.R. Hamblin, Photobiomodulation combined with photodynamic therapy using ruthenium phthalocyanine complexes in A375 melanoma cells: effects of nitric oxide generation and ATP production, J. Photochem. Photobiol. B Biol. 198 (2019) 111564, https://doi.org/10.1016/j.jphotobiol.2019.111564.

[32] Shirin Farivar, Talieh Malekshahabi, Reza Shiari, Biological effects of low level laser therapy, J. Las. Med. Sci. 5 (2) (2014) 58–62.

[33] K.M. AlGhamdi, A. Kumar, N.A. Moussa, Low-level laser therapy: a useful technique for enhancing the proliferation of various cultured cells, Lasers Med. Sci. 27 (2012) 237–249, https://doi.org/10.1007/s10103-011-0885-2.

[34] O. Myhre, J.M. Andersen, H. Aarnes, F. Fonnum, Evaluation of the probes 2′,7′-dichlorofluorescin diacetate, luminol, and lucigenin as indicators of reactive species formation, Biochem. Pharmacol. 65 (2003) 1575–1582, https://doi.org/10.1016/S0006-2952(03)00083-2.

[35] M.C. Putchala, P. Ramani, H.J. Sherlin, P. Premkumar, A. Natesan, Ascorbic acid and its pro-oxidant activity as a therapy for tumours of oral cavity – a systematic review, Arch. Oral Biol. 58 (2013) 563–574, https://doi.org/10.1016/j.archoralbio.2013.01.016.

[36] E. Eruslanov, S. Kusmartsev, Identification of ROS using oxidized DCFDA and flow-cytometry, in: D. Armstrong (Ed.), Advanced Protocols in Oxidative Stress II. Methods in Molecular Biology (Methods and Protocols) 594, Humana Press, Totowa, NJ, 2010, https://doi.org/10.1007/978-1-60761-411-1_4.

[37] D.-F. Yang, J.-H. Chen, C.-P. Chiang, Z. Huang, J.-W. Lee, C.-J. Liu, J.-L. Chang, Y.-C. Hsu, Improve efficacy of topical ALA-PDT by calcipotriol through up-regulation of coproporphyrinogen oxidase, Photodiagn. Photodyn. Ther. 11 (2014) 331–341, https://doi.org/10.1016/j.pdpdt.2014.05.001.

[38] D.-F. Yang, J.-W. Lee, H.-M. Chen, Z. Huang, Y.-C. Hsu, Methotrexate enhances 5-aminolevulinic acid-mediated photodynamic therapy-induced killing of human SCC4 cells by upregulation of coproporphyrinogen oxidase, J. Formos. Med. Assoc. 113 (2014) 88–93, https://doi.org/10.1016/j.jfma.2013.12.005.

[39] R. Bhuvaneswari, Q.F. Ng, P.S.P. Thong, K.-C. Soo, Nimotuzumab increases the anti-tumor effect of photodynamic therapy in an oral tumor model, Oncotarget 6 (2015) 13487–13505, https://doi.org/10.18632/oncotarget.3622.

[40] E.E. Kelley, F.E. Domann, G.R. Buettner, L.W. Oberley, C.P. Burns, Increased efficacy of in vitro Photofrin® photosensitization of human oral squamous cell carcinoma by iron and ascorbate, J. Photochem. Photobiol. B Biol. 40 (1997) 273–277, https://doi.org/10.1016/S1011-1344(97)00068-7.

[41] C. Calles, M. Schneider, F. Macaluso, T. Benesova, J. Krutmann, P. Schroeder, Infrared a radiation influences the skin fibroblast transcriptome: mechanisms and consequences, J. Investig. Dermatol. 130 (2010) 1524–1536, https://doi.org/10.1038/jid.2010.9.

[42] S. Passarella, T. Karu, Absorption of monochromatic and narrow band radiation in the visible and near IR by both mitochondrial and non-mitochondrial photoacceptors results in photobiomodulation, J. Photochem. Photobiol. B Biol. 140 (2014) 344–358, https://doi.org/10.1016/j.jphotobiol.2014.07.021.

[43] T.I. Karu, Mitochondrial signaling in mammalian cells activated by red and near-IR radiation, Photochem. Photobiol. 84 (2008) 1091–1099, https://doi.org/10.1111/j.1751-1097.2008.00394.x.

[44] T.D. Schalch, M.H. Fernandes, M.F.S. Destro Rodrigues, et al., Photobiomodulation is associated with a decrease in cell viability and migration in oral squamous cell carcinoma, Lasers Med. Sci. 34 (2019) 629–636, https://doi.org/10.1007/s10103-018-2640-4.

[45] X. Hong, F. Jiang, S.N. Kalkanis, Z.G. Zhang, X. Zhang, X. Zheng, H. Jiang, M. Chopp, Intracellular free calcium mediates glioma cell detachment and cytotoxicity after photodynamic therapy, Lasers Med. Sci. 24 (2009) 777–786, https://doi.org/10.1007/s10103-008-0640-5.

[46] R.C. Taylor, S.P. Cullen, S.J. Martin, Apoptosis: controlled demolition at the cellular level, Nat. Rev. Mol. Cell Biol. 9 (2008) 231–241, https://doi.org/10.1038/nrm2312.

[47] N. Mizushima, M. Komatsu, Autophagy: renovation of cells and tissues, Cell. 147 (2011) 728–741, https://doi.org/10.1016/j.cell.2011.10.026.

[48] E. Buytaert, G. Callewaert, N. Hendrickx, L. Scorrano, D. Hartmann, L. Missiaen, J. R. Vandenheede, I. Heirman, J. Grooten, P. Agostinis, Role of endoplasmic reticulum depletion and multidomain proapoptotic BAX and BAK proteins in shaping cell death after hypericin-mediated photodynamic therapy, FASEB J. 20 (2006) 756–758, https://doi.org/10.1096/fj.05-4305fje.

[49] L. Xue, S. Chiu, K. Azizuddin, S. Joseph, N.L. Oleinick, The death of human Cancer cells following photodynamic therapy: apoptosis competence is necessary for Bcl-2 protection but not for induction of autophagy, Photochem. Photobiol. 83 (2007) 1016–1023, https://doi.org/10.1111/j.1751-1097.2007.00159.x.

[50] V. Pierroz, R. Rubbiani, C. Gentili, M. Patra, C. Mari, G. Gasser, S. Ferrari, Dual mode of cell death upon the photo-irradiation of a Ru ^{II} polypyridyl complex in interphase or mitosis, Chem. Sci. 7 (2016) 6115–6124, https://doi.org/10.1039/C6SC00387G.

[51] D. Lee, I.Y. Kim, S. Saha, K.S. Choi, Paraptosis in the anti-cancer arsenal of natural products, Pharmacol. Ther. 162 (2016) 120–133, https://doi.org/10.1016/j.pharmthera.2016.01.003.

[52] D. Kessel, Apoptosis, Paraptosis and autophagy: death and survival pathways associated with photodynamic therapy, Photochem. Photobiol. 95 (2019) 119–125, https://doi.org/10.1111/php.12952.

[53] C.A. Robertson, D.H. Evans, H. Abrahamse, Photodynamic therapy (PDT): a short review on cellular mechanisms and cancer research applications for PDT, J. Photochem. Photobiol. B Biol. 96 (2009) 1–8, https://doi.org/10.1016/j.jphotobiol.2009.04.001.

[54] R. Lubart, M. Eichler, R. Lavi, H. Friedman, A. Shainberg, Low-energy laser irradiation promotes cellular redox activity, Photomed. Laser Surg. 23 (2005) 3–9, https://doi.org/10.1089/pho.2005.23.3.

[55] G.A. Callaghan, C. Riordan, W.S. Gilmore, I.A. McIntyre, J.M. Allen, B. M. Hannigan, Reactive oxygen species inducible by low-intensity laser irradiation alter DNA synthesis in the haemopoietic cell line U937, Lasers Surg. Med. 19 (1996) 201–206, https://doi.org/10.1002/(SICI)1096-9101(1996)19:2<201::AID-LSM12>3.0.CO;2-9.

[56] N. Grossman, N. Schneid, H. Reuveni, S. Halevy, R. Lubart, 780 nm low power diode laser irradiation stimulates proliferation of keratinocyte cultures: involvement of reactive oxygen species, Lasers Surg. Med. 22 (1998) 212–218, https://doi.org/10.1002/(SICI)1096-9101(1998)22:4<212::AID-LSM5>3.0.CO;2-S.

[57] R. Lavi, A. Shainberg, H. Friedmann, V. Shneyvays, O. Rickover, M. Eichler, D. Kaplan, R. Lubart, Low energy visible light induces reactive oxygen species generation and stimulates an increase of intracellular calcium concentration in cardiac cells, J. Biol. Chem. 278 (2003) 40917–40922, https://doi.org/10.1074/jbc.M303034200.

[58] W. Yu, J.O. Naim, M. McGowan, K. Ippolito, R.J. Lanzafame, Photomodulation of oxidative metabolism and Electron chain enzymes in rat liver mitochondria, Photochem. Photobiol. 66 (1997) 866–871, https://doi.org/10.1111/j.1751-1097.1997.tb03239.x.

[59] J. Zhang, D. Xing, X. Gao, Low-power laser irradiation activates Src tyrosine kinase through reactive oxygen species-mediated signaling pathway, J. Cell. Physiol. 217 (2008) 518–528, https://doi.org/10.1002/jcp.21529.

[60] T.I. Karu, L.V. Pyatibrat, G.S. Kalendo, Cell attachment modulation by radiation from a pulsed light diode (λ = 820 nm) and various chemicals, Lasers Surg. Med. 28 (2001) 227–236, https://doi.org/10.1002/lsm.1043.

4 TUMOR RADIOSENSITAZION BY PHOTOBIOMODULATION THERAPY

4.1 Introduction

As mentioned before, PBMT results in oral mucositis and other oral diseases such as dermatitis and radiation fibrosis syndrome are promisingand its use in normal tissue is considered safe. Still, the medical community remains reluctant to incorporate the technique as a routine procedure due to safety concerns regarding the illumination of tumors. In PBMT, the upregulation of reactive oxygen species (ROS), Ca2+, nitric oxide (NO) and adenosine triphosphate (ATP) is involved in initiating the cascade of events that lead to tissue repair, reduced inflammation, analgesia, and increased proliferation. Owing to these effects, especially the latter, efforts have been made to determine whether it increases tumor volume and metastatic potential in cancer. If proven safe, PBMT can improve tumor eradication and the patient's quality of life by reducing acute side effects on normal tissue due to radiation and chemotherapy, which is the major cause of treatment interruption. In vitro studies have indicated that PBMT induces a radiosensitizing effect on tumors. (32–36) Nevertheless, the number of these studies, parameters tested, and conclusions that can be made from in vitro results are very limited. Only two studies address this combination in vivo. Barasch et al, using 660-nm light, recently reported no difference between the radiation combined with photobiomodulation therapy (PBMT-RT and radiation only (RT) groups. (35) Silva et al. later reported positive results with the same wavelength, in three illumination protocols, on triple-negative breast cancer (TNBC)-bearing mice. (36) They reported that PBMT arrested tumor growth, improved the clinical condition, prevented hemolytic anemia, and, despite resulting in a high neutrophil:lymphocyte ratio (NLR), decreased the number of lung metastases and enhanced mouse survival. In a clinical trial of head and neck cancer patients receiving chemoradiation with the same wavelength, there was strong evidence that PBMT can improve the treatment and response of chemoradiotherapy patients. (37) The illumination protocol excluded the tumor area, so it is not possible to conclude whether these effects were due to the effects of PBMT on cancer cells. In this chapter, we propose an in vitro and in vivo investigation of the radiosensitizing potential of PBMT in tumor cells in vitro and in vivo. A 780 nm light source was chosen because of its common use in PBMT and its deeper penetration depth, making it suitable for the treatment of tumors beyond the superficial layers of tissue.

4.2 Materials and Methods

4.2.1 Cell line and culture conditions

The human epidermoid carcinoma cell line A431 (ATCC® 1555™, USA) was used and grown by adhesion in Dulbecco's Modified Eagle's Medium (DMEM) High Glucose (Cultilab, Brazil) with 10% (v/v) fetal bovine serum (FBS, Cultilab, Brazil). Cells were maintained at 37°C under a humidified atmosphere of 5% CO2.

4.2.2 Photobiomodulation Therapy

For in vitro PBMT, cells were illuminated using a LED array system (Biotable® 780 nm, MM OpticsLtda., Brazil) at 780nm, 30 mW/cm^2 at a total energy density of 5J/cm^2, delivered in 3 min and 53 s. For in vivo experiments, the same energy density of 5J/cm^2 was given using a GaAlAs diode laser system (Twin Flex Evolution MM Optics®, MM OpticsLtda., Brazil) at 780 nm, 20 mW/cm^2 and a spot area of 4.0 mm^2, which delivered the desired energy density in 10 s.

4.2.3 Radiotherapy

Irradiation was performed in an XRAD 225x X-ray cabinet (Precision X-ray Inc., USA) at 225 kV and 13.3 mA for all conditions. In vitro experiments were performed at 33 cm source-to-specimen distance (SSD) using a 2.0-mm aluminum filtration, yielding a dose rate of 4.0 Gy/min. In vivo irradiation was conducted at a dose rate of 1.7 Gy/min with a 0.3 mm copper filter, with a 40 cm SSD from the shelf and an offset of 1.5 cm to account for the tumor position in relation to the table, using a cylindrical lead collimator that conformed a 1.8 cm diameter field limited to the tumor area. Animals were irradiated in a prone position under inhalatory anesthesia. Groups that were not given ionizing radiation were sham irradiated in all experiments.

4.2.4 MTT proliferation assay

Cells were inoculated in 96-well plates at a density of 1x104 cells/well 24h before experiments. Cell viability 48h and 72h after PBMT was analyzed by the MTT assay (3-(4,5-dimethylthiazol-2yl) -2,5-diphenyltetrazolium bromide). Cells were incubated with MTT at 0.5 mg/mL in DMEM 1% FBS without phenol for 3h. Then, medium was removed and 100 l of dimethyl sulfoxide (DMSO) was added to dissolve the formazan crystals. Absorbance at 570 nm was read at a microplate reader (Multiskan™FC Microplate Photometer, ThermoFisher Scientific, USA) and corrected by absorbance at 690 nm. Two independent experiments were performed in quintuplicate for each group.

4.2.5 Cell cycle assessment

To perform the flow cytometric analysis of the cell cycle, PBMT was performed in duplicate as described in the MTT assay, but in 24 wells-plate (1x105 per well in 500 l). Cells were trypsinized 24h after illumination, washed with phosphate-buffered saline (PBS) and fixed with cold 70% ethanol and stored at -20 °C for at least 12h. Then, cells were collected via centrifugation (at 400 × g for 5 min, room temperature) and resuspended in staining buffer of 50 g/ml propidium iodide (BD Biosciences, USA) in PBS, 0.1 mg/ml RNase (Sigma–Aldrich, USA) for 40 min. Samples were analyzed in an Accuri C6 flow cytometer (BD Bio-411sciences, USA), and cell cycle was determined using FlowJo software univariate analysis (BD Biosciences, USA). The results shown are from 4 independent treatments (N=4).

4.2.6 Clonogenic assay

To evaluate cell survival after irradiation, cells were seeded at 250 cells/well in 24 wells plates, in quadruplicate, then incubated overnight. Then, illumination was performed and cells were then incubated for 24h until radiation therapy was given. Immediately after, the second session of PBMT was applied and cells were left in the incubator for 24h, until the second session of irradiation. Analogous to the first session of radiation, cells were then given the third session of PBMT, which was followed by the last irradiation, 24h later. Summarizing, the protocol consisted in 3 x (PBMT- 24h – RT). A schematic representation of the treatment regime is shown in Figure 4. To obtain a survival curve, the following doses were used: 3 x 33 cGy (1 Gy total); 3 x 80 cGy (2.4 Gy total); 3 x 150 cGy (4.5 Gy total). 7 days after the last irradiation colonies were fixed and stained (0.5% crystal violet, 20 % methanol, Sigma-Aldrich, USA) for 15 min at room temperature, then rinsed in tap water and let to air dry. Afterwards, the number of cell colonies per dish were counted and the relative survival fraction was calculated as the ratio between the number of colonies formed in each treated well and the mean number for the control group. Three independent experiments were performed to obtain the curves.

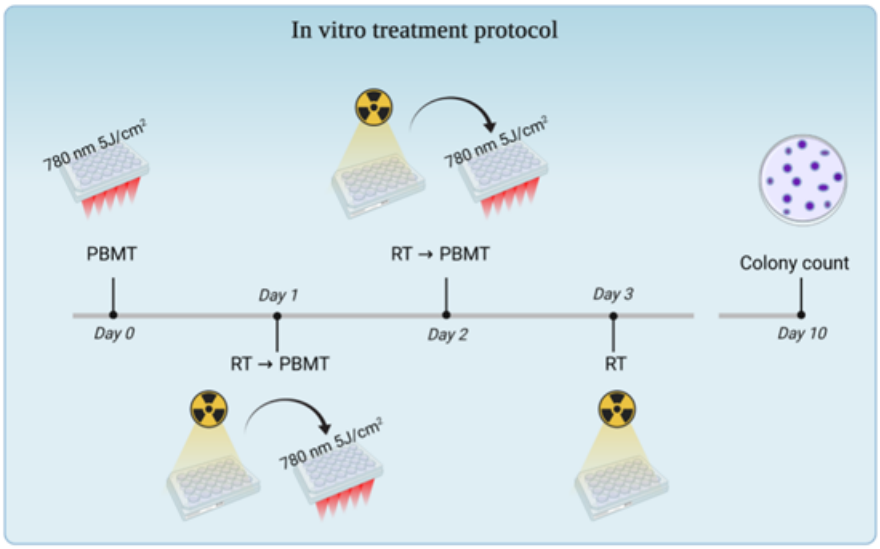

Figure 4 – Schematic representation of the treatment regimes in vitro.

Source: Elaborated by the author.

4.2.7 H2AX- assay immunolabeling

The number of radiation-induced foci (RIF) after fractionated treatment regime was evaluated with two protocols: (a) 1 h after the last session of a 3 x 0.8 Gy protocol; and (b) 0, 1 and 5 h after the last session of a 3 x 0.33 Gy protocol. For both, 200 cells per well were seeded in 96 black wells/clear bottom plate (Corning® CLS3603, Germany) and incubated overnight. The treatment regimen used was the same as described in the section "Clonogenic assay", consisting in 3x (PBMT - 24h - RT). Then, after the last irradiation, cells were stained with Alexa Fluor® 488 Mouse anti-H2AX (pS139) antibody (BD Pharmingen™, USA) as recommended by the manufacturer. Shortly, cells were fixed with 3.7% Formaldehyde in PBS for 10 min, then permeabilized with ice cold 90% methanol for 5 min and blocked with 3% FBS in PBS, all performed at room temperature. Additionally, wells were washed two to three times with PBS prior to each of these steps. H2AX-gamma antibody, 1:10 diluted, was incubated at a volume of 50 l per well for 1h in the dark. Imaging was performed with a fluorescence confocal microscope (Zeiss325- LSM780, Zeiss, Germany) at an excitation/emission wavelength of 488/519 nm at 400x magnification. Semi-automatic RIF detection and analysis was used with Python programming language. In it, a Gaussian bilateral filtering to reduce noise in the image was employed. Then a 41x41 kernel was used to select potential RIF based on local intensity (derived from the kernel) and global intensity (derived from the image's histogram) to create a preliminary mask. The original image was filtered with this mask and the resulting image was further refined, based on local average intensity, with a 15x15 kernel where pixels below this average value are discarded. Finally, connected-component analysis was performed (using 4-neighborhood) and regions smaller than a user-defined size

were discarded. The remaining regions were counted and their sizes recorded. For the 3 x 0.8 Gy protocol, two independent experiments were performed in triplicate for each one, with 10 microscopic images/well (N=2). For the RIF kinetics evaluation (3 x 0.33 Gy), three independent experiments were performed, with wells in duplicate and 6 microscopic images/well for each group (N=3).

4.2.8 Animals and tumor model

In vivo procedures were approved by the Animal Use Ethics Committee of the Sao Carlos Institute of Physics at the University of Sao Paulo (protocol number 3632181018). Xenograft tumor induction was performed as previously described (38), with the A431 cell line experiments. Intradermal injection containing 106 suspended cells in 30 L of PBS was given in the right flanks of the animal under inhalatory anesthesia with isoflurane. Tumor growth was assessed though volume, where a spherical volume was es-timated for each tumor from the average radius obtained from two diameter measurements, perpendicular to each other, and the diameter in depth, obtained using a vernier caliper. Mice were randomly assigned to each group in a total N=7 per sub-group. Sub-groups consisted of different intervals of the tumor's initial volume of treatment (sub-group 1: 30-40 mm3, sub-group 2: 40-55 mm3). The initial volume of treatment (V_{in}) was defined as the tumor volume on the day of the first irradiation. The survival endpoint for each animal was determined as the day the tumor reached six times its V_{in}, when animals were euthanized by isoflurane overdose and tumor biopsies were taken.

4.2.9 Kaplan-Meier survival analysis

Throughout the study period, tumor volumes were evaluated daily. Treatment protocols consisted in three sessions of (PBMT– 24 h – RT– 24 h). The first PBMT illumination, or sham, was given when tumors first reached a volume 30±3 mm3 for sub-group 1 and 40±4 mm3 for sub-group 2, at day 0. Then, after 24 h, irradiation was performed with a dose fraction of 5 Gy. Summarizing, the treatment protocol consisted in PBMT/sham given at days 0, 3 and 5 and RT/sham was given at days 2, 4 and 6. A schematic representation of the treatment regime is shown in Figure 5. Survival curves and median survival estimation was obtained through the Kaplan-Meier estimator (39), and statistical significance between the curves was evaluated using a log-rank test. (40) Animals lost in anesthesia or that did not reach the endpoint tumor volume are shown as censored.

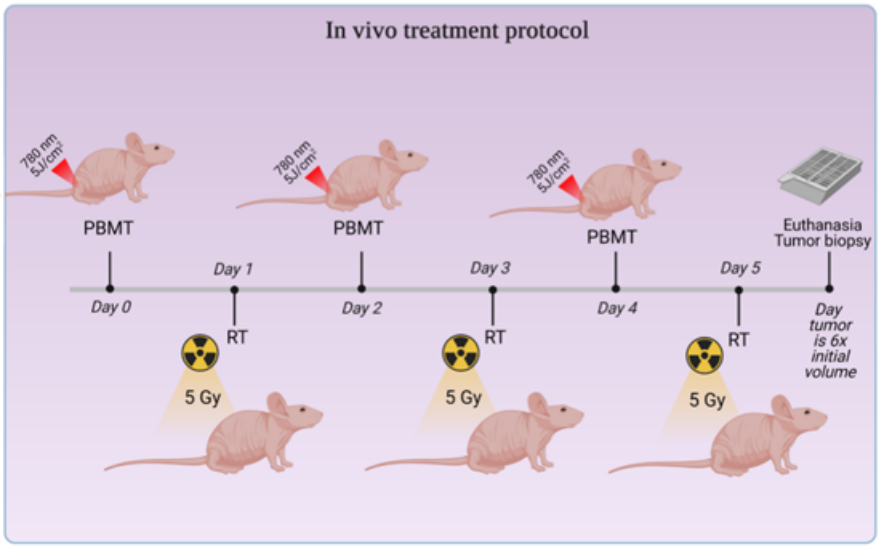

Figure 5 – Schematic representation of the treatment regimes in vivo

Source: Elaborated by the author.

4.2.10 Optical Coherence Tomography

The necrotic volume of the tumors was estimated from OCT volumetric images obtained from the day 5 of the study period until the animals were euthanized. The mean values for each group were initially obtained from 9 animals/group and, by the end (day 16), from at least 3 animals/group, since many were euthanized in the course of the analysis. For the acquisition of OCT images, animals were anesthetized, as previously described, in lateral recumbent position. A spectral domain OCT system (Telesto, Thorlabs, Germany, 1300 nm light source) was used to obtain the images from a region selected by the user (examples of selected regions with its correspondent images and 3D volumes are shown in Figure 6).

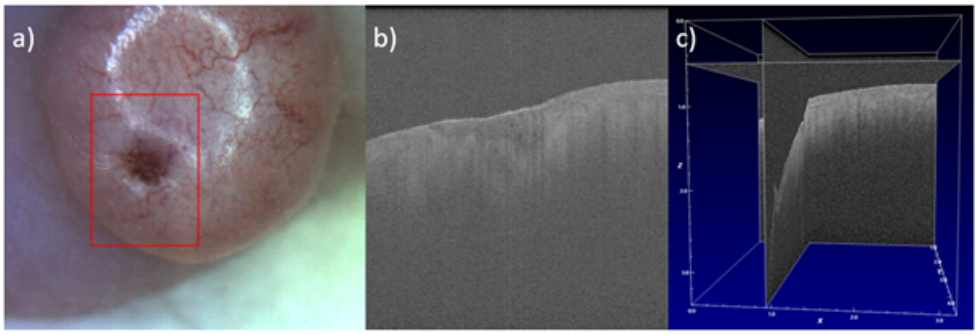

Figure 6 – Images of a PBM-RT tumor obtained on day 7 with the OCT equipment. a) Image from the CCD camera of the system, showing the selected scanned area. B) OCT 2D image from slice 136 of the xz plane. c) System software 3D reconstruction of the tumor from the OCT scan.

Source: Elaborated by the author.

The contour method (41) was implemented to identify the necrotic regions by differences in contrast of each 2D section of the OCT file (an example of the processing routine is shown in Figure 7). Once the section was identified, the 3D volume was constructed summing all 2D sections (300 slides in x, y axes and 1024 in z axis) using resolution and parameters obtained from the OCT files.

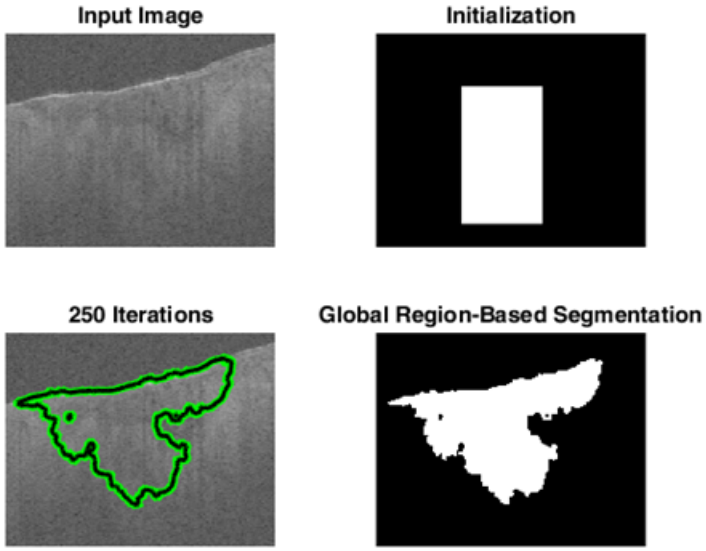

Figure 7 – Steps of the OCT image processing. Section identification from the routine computational tool used to identify the 2D section in the xz plane. The imput image corresponds to a PBM-RT tumor on day 7.

Source: Elaborated by the author.

4.2.11 Histological evaluation

Elliptic skin biopsy from the tumor area was removed from each animal and put in individual pre-identified recipients with 1% buffered formalin. After tissue fixation, tumor representative fragments were submitted to histological processing, consisted of dehydration in ethanol, clearing in xylem and embedding in paraffin. At least six serial histological sections (4m thick) were obtained per biopsy and distributed in two different slides, one for hematoxylin and eosin (HE) stain and other for Masson's trichrome. Then, slides were digitized on a histological slice scanner (Panoramic DESK, 3DHISTECH, Hungary). A total of 13 slides per group were used for each analysis, which were coded and blindly evaluated. A pathologist performed the assessment of differentiation grade and mitotic count, which were performed using an Olympus® BX51 microscope (Olympus, Japan), and supervised the quantification of mean vascular density (MVD) and necrotic area, performed with the Case Viewer Software® (3DHISTECH, Hungary). Differentiation grade was classified as undifferentiated (I), poorly (II), moderately (III) or well differentiated (IV). Mitotic activity was performed by counting the number of mitoses in 10 consecutive high-power fields (HPF), then the sum of mitoses per animal was used to calculate the

mean for each group. For the quantification of necrosis, necrotic areas of each tumor from HE stained slides were contoured, summed and divided by the total tumor area to obtain a relative parameter. MVP quantification was performed using Masson's trichrome stained slides. Five circular 40x field of view (FOV) circles were placed in different regions of the viable tumor (necrotic areas excluded), and vessels within them were quantified at 400x and divided by the total area of the circles to obtain the mean vascular density (MVP) of the tumor. Individual vessels were defined as single or grouped endothelial cells, with or without lumen.

4.2.12 Statistical analysis

All quantitative data were described as means ± SD deviation. ANOVA followed by the Tukey test was applied to estimate the differences between two means for normal distributed data, and the Kruskal-Wallis ANOVA test was used when the results rejected normality. A value of $P < 0.05$ was considered to be statistically significant.

4.3 Results

4.3.1 Impact of PBMT on G2/M fraction and proliferation

The cell cycle distribution was assessed 24 h after PBMT. As shown in Figure 8, there was a statistically significant increase of 27% in the G2/M fraction compared to the control. However, the increase in G2/M cells did not result in statistically significant variations in proliferation 48 h or 72 h after PBMT. Still, we observed a slight increasing trend at 48 h, and a decreasing trend at 72 h.

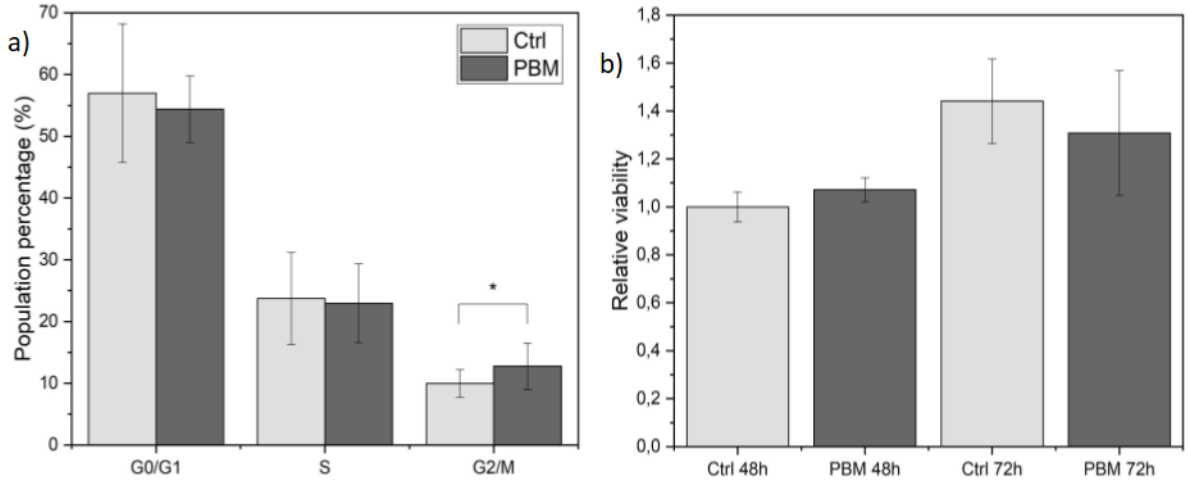

Figure 8 – Cell cycle and MTT assay results. (a) Cell cycle distribution for A431 cells 24 h after PBMT (5 J/cm^2) compared to the control (N=4); and (b) relative viability 48 h and 72 h after illumination (N=2). The symbol (*) indicates $p < 0.05$.

Source: Elaborated by the author.

4.3.2 PBMT impact on radiation effect of fractionated protocol

In a clonogenic assay, protocols of PBMT, radiation and the combination of them were tested, with a fluence rate of 5 J/cm^2 and 780 nm for the illumination, as a function of radiation dose (Figure 9). Radiation induces cell death and loss of integrity, which cause a clear reduction in the number of colonies in the irradiated groups. Additionally, at 2.4 Gy, PBMT enhanced this effect in comparison to radiation alone, with statistical significance ($p < 0.05$). Since the doses testes did not result in survival values lower than 1%, the curves could not be adjusted to a linear quadratic model.

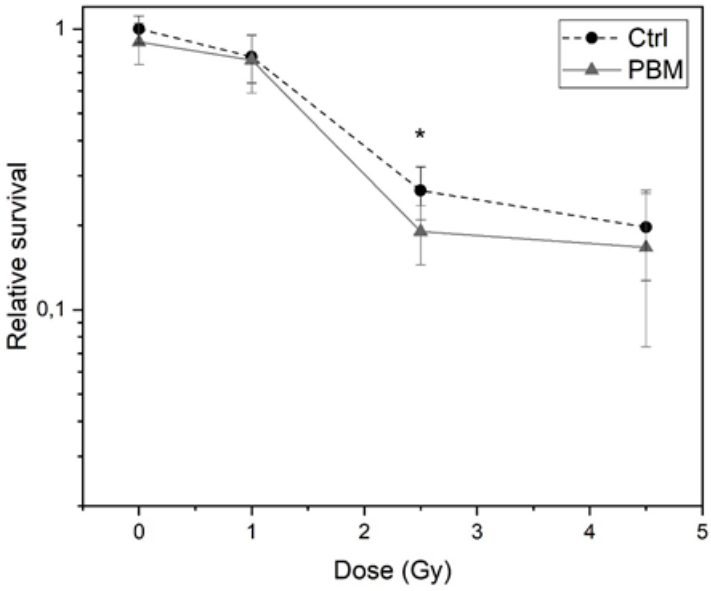

Figure 9 – Clonogenic assay as a function of total dose. The symbol (*) denotes $p < 0.05$ between PBMT and Ctrl groups of the same dose (N=3).

Source: Elaborated by the author.

With respect to DNA damage, double-strand breaks (DSBs) are the most relevant type since they lead to incorrect repair, the main cause of mitotic catastrophe and loss of viability. Therefore, it is important to quantify them when comparing the radiosensitizing effect of any strategy. One common and well accepted way to do so is through staining the first proteins that are recruted to repair DSBs. The fluorescent staining is shown in microscopic images as radiation induces foci (RIF). Here, were estimated RIF by H2AX-gamma foci after three-session protocols. Examples of microscope images from each protocol are shown in Figure 10. RIF assessed 1 h after the last fraction of a 3 x 0.8 Gy protocol, which corresponds to the point where PBMT-RT and RT are significant different (Figure 9), is shown in Figure 11.

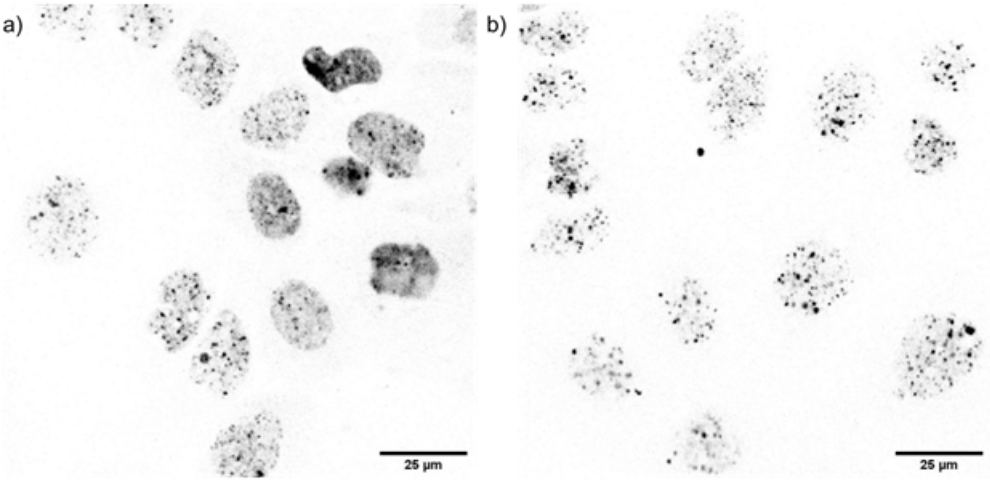

Figure 10 – Microscopic confocal images (400x magnification) from H2AX- fluorescent labeled cells. Irradiated cells from the (a) 3 x 0.33 Gy and (b) 3 x 0.8 Gy protocols.

Source: Elaborated by the author.

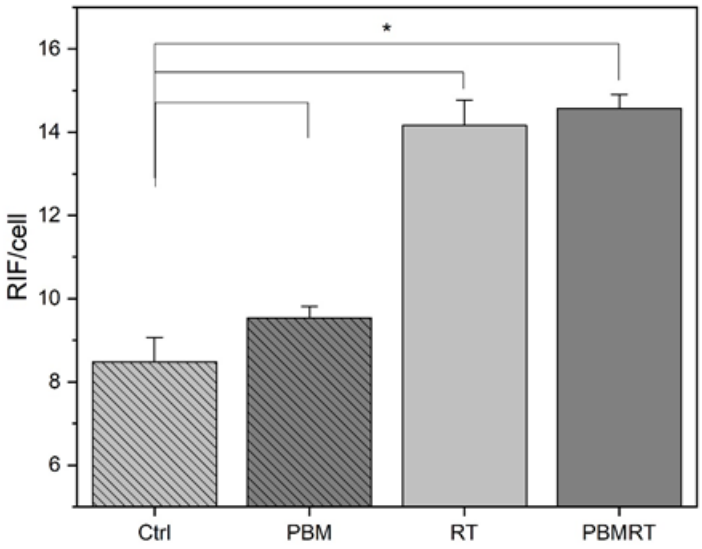

Figure 11 – RIF of all groups 45 min after a protocol of 3 x 0.8 Gy. The symbol (**) denotes $p < 0.01$ (N=3).

Source: Elaborated by the author.

PBMT, RT and PBMRT are all significant different than the control ($p < 0.05$). No difference is observed between RT and PBMRT. One aspect to consider, however, is clustering, which is when a single focus presents multiple strand breaks. (42) This happens when the assay resolution cannot distinguish between multiple breaks that happen too close to one another because they form a single large focus of repair proteins. It was found experimentally that clustering becomes relevant in vitro when doses reach 1 Gy, which

may be influencing the result in Figure 11, since the fraction dose is 0.8 Gy, but the total dose is 2.4 Gy. Therefore, we have performed an analysis with a total dose of 1 Gy (3x 0.33 Gy), shown in Figure 12, consisting in three time points after the last irradiation, to observe the kinetics of DNA damage and investigate the effect of PBMT on DNA damage and repair. The number of RIF/cell for the control group in this experiment was the same as the one for the 2.4 Gy protocol (not shown). Statistical difference shown as (*) refers to comparisons between RT and PBMT-RT regarding the time point. Compared to the radiation only group, PBMT presented a significantly higher number of foci at 0 h and 1 h ($p < 0.05$), but the difference is not seen at 5 h. This indicates that, although PBMT causes an increase in double-strand break (DSB), the mechanisms of repair were capable of reversing that effect. Still, incorrect DSB repair may lead to mitotic catastrophe in future generations of that cell, which should be investigated in future studies. When comparing the results from the 1 Gy and 2.4 Gy protocols (Figures 11 and 12), we confirm the effect of clustering at the higher dose, since there is a 2.4-fold between doses but only a 1.3-fold increase in RIF/cell for the RT group and 1.07-fold increase for PBMRT. This indicates that there is 46% of saturation for RT and 55% for PBMRT.

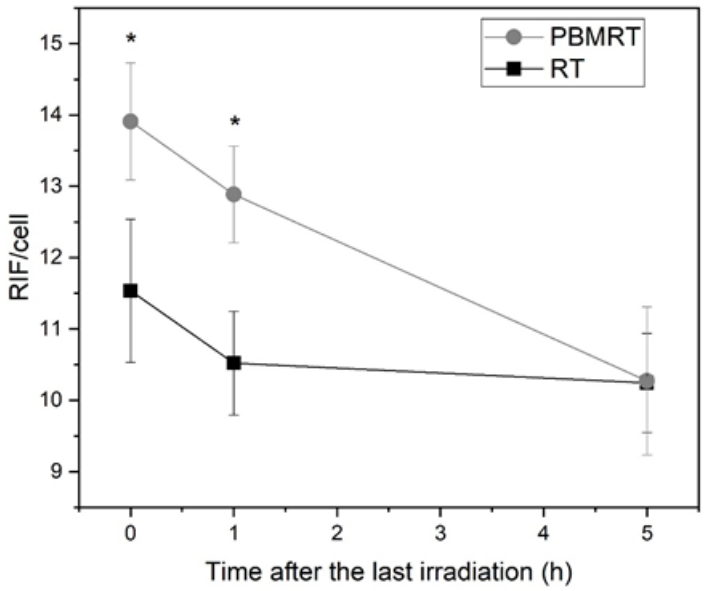

Figure 12 – RIF kinetics for a protocol of 3x0.33 Gy. No statistical difference was observed between RT and PBMT within the same time point (N=2).

Source: Elaborated by the author.

4.3.3 Impact of PBMT-RT on survival of tumor-bearing mice compared to radiation alone

Relative tumor volumes 10 days after treatment with radiation (15 Gy alone; 15 Gy with PBMT immediately before; 15 Gy with PBMT 24 h before) revealed no significant difference among them (Figure 13). However, due to differences in the final necrotic area

among groups, additional experiments were conducted to evaluate the protocols using the Kaplan–Meier survival curve.

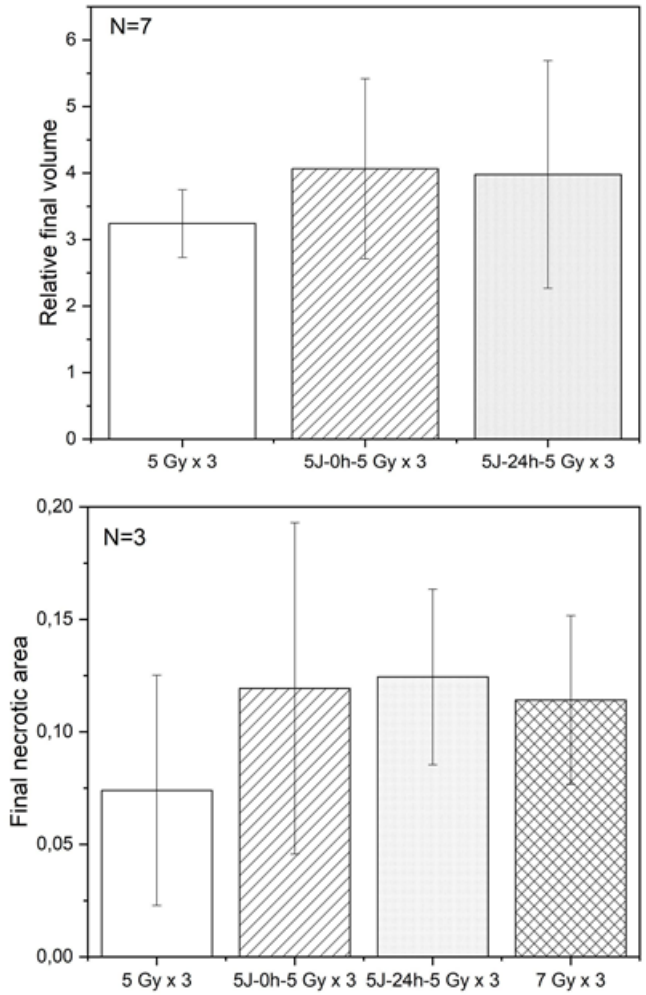

Figure 13 – Tumor volumes 10 days after three treatment sessions. No statistical difference was observed (N=7).

Source: Elaborated by the author.

Two sub-groups corresponding to different initial volumes of treatment, V_{in}, were studied for each treatment group. Results are shown in Figure 14. Overall, PBMT did not reduce survival in mice compared to the control, and both groups presented a median survival of approximately 10 days with no significant difference in the log-rank test. The hazard ratio, which measures the relative curve slope of two groups (in this case, PBMT over the control) was 1.004 (CI 95%: 0.485–2.080). As expected, radiation delayed tumor progression, but the combination of PBMT and radiation yielded the best outcome (log-rank p = 0.00784), with a median survival of 17 days compared to 13 days from the RT group and a hazard ratio of 0.417 (PBMT-RT compared to radiation alone, CI 95%: 0.173-1.006). In addition, the only animal that presented a consistent regression in tumor

volume was from the latter.

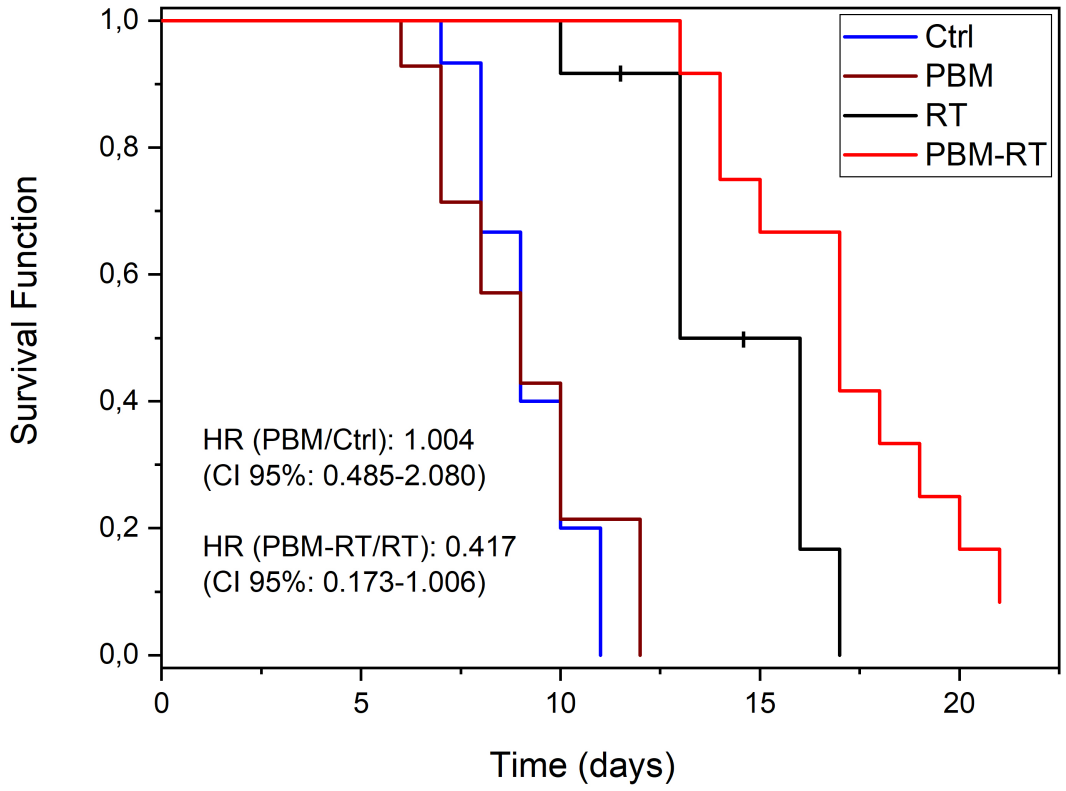

Figure 14 – Kaplan–Meier survival curves. The final point was defined as the day when the tumor reached six times its initial volume of treatment, (N=14).

Source: Elaborated by the author.

Regarding the sub-groups (Figure 15), we observed that the V_{in} had no impact on the curves, except for PBMT, in which subgroup 1, of the smaller initial tumors, corresponded to a statistically significant decrease in survival compared to the sub-groups in the control group.

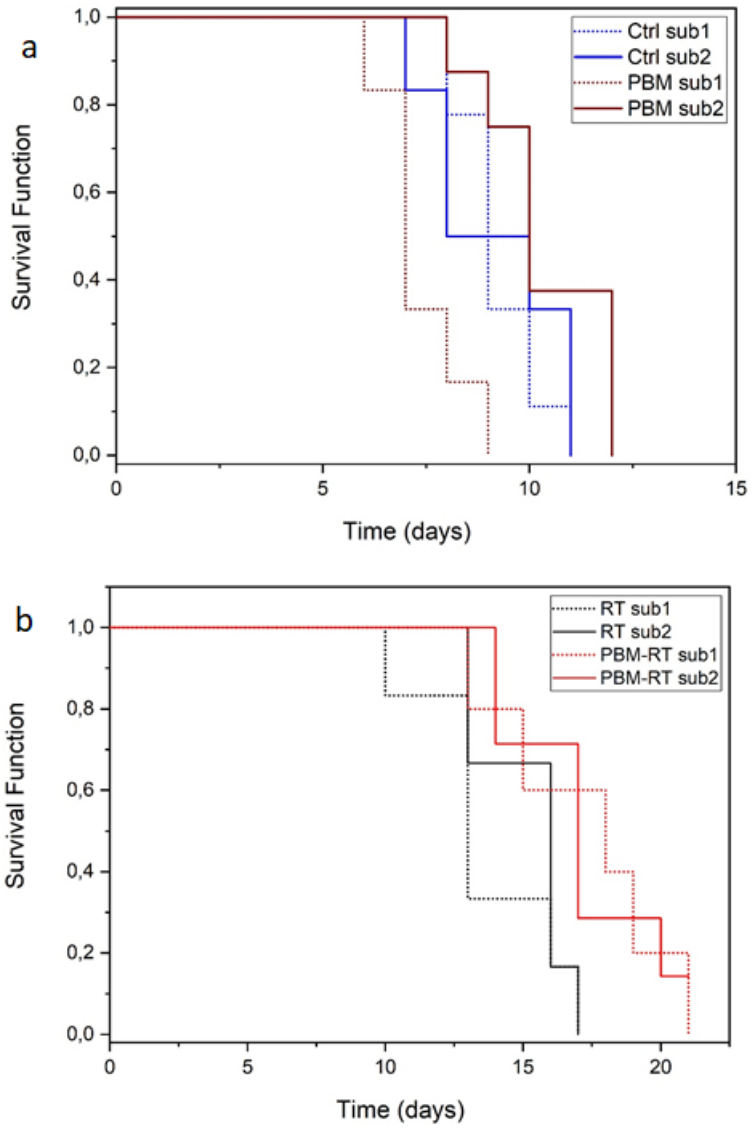

Figure 15 – Survival curves detailing the sub-groups' response to treatment regarding the V_{in}, showing no difference except for PBMT alone (N=7 for each sub-group).

Source: Elaborated by the author.

4.3.4 OCT and Histological evaluation

Optical coherence tomography was used to investigate in detail the progression of the damaged tissue from the superficial ulceration areas. A comparison of final OCT images and histological evaluation shows a correlation between tumor damage below the superficial ulceration area and regions with a lower refractive index in OCT images. Therefore, we quantified the volume of these regions from days 5 to 15 after treatment. Control tumors were followed until day 11 because of their lower survival of approximately 10 days (as seen in Figure 16). It is observed that both irradiated curves remained indistinguishable from the control until day 9, from which point PBMT-RT presented a significant increase, with statistical difference from the other groups.

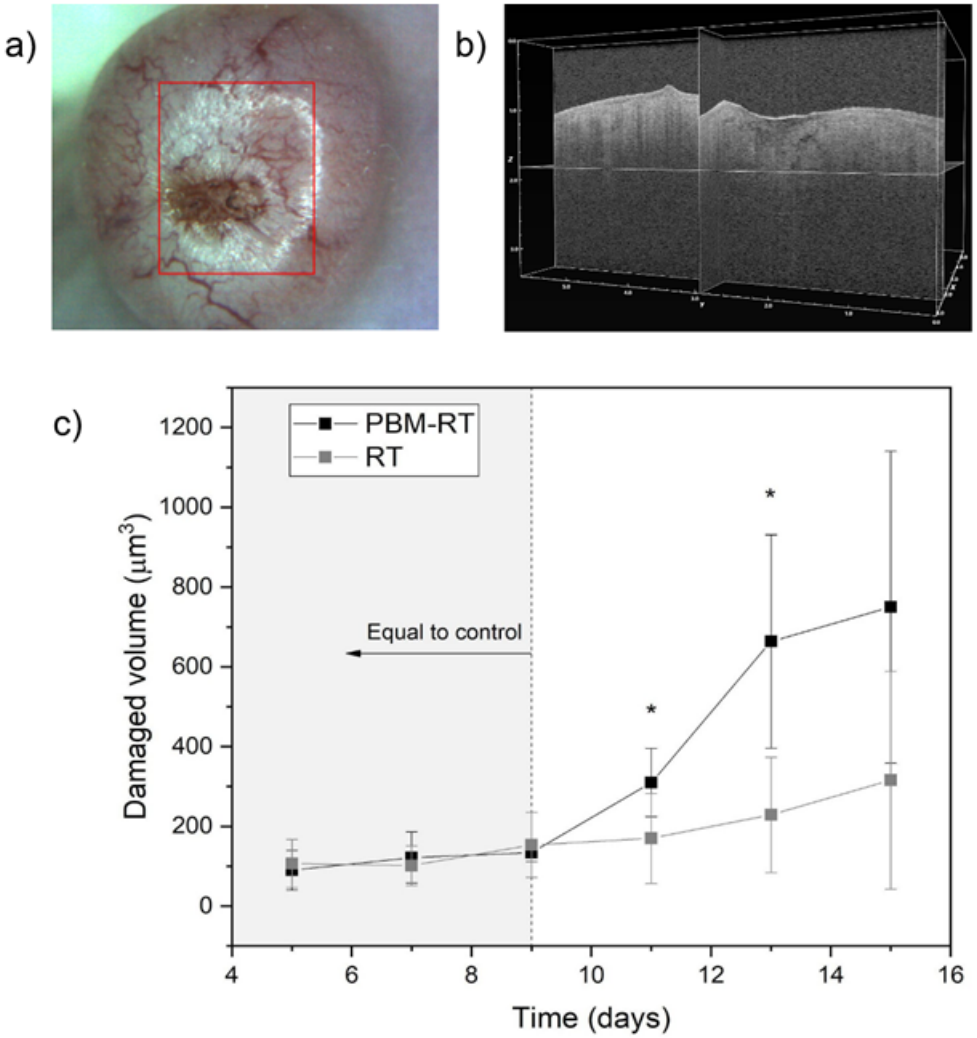

Figure 16 – OCT evaluation results for the necrotic volume on the tumoral superficial layers. (a) Top view from a tumor showing the delimitation of the OCT reconstruction volume, shown in (b); and in (c) the mean damaged volume from irradiated groups over time (N=9 initially and N=3 by the end, since many animals were euthanized before reaching 16 days).

Source: Elaborated by the author.

Histological evaluation with HE and Masson's trichrome staining was performed on tumors after reaching six times the initial treatment volume. Quantification of mitosis, differentiation grade, mean vascular density, and necrotic area are shown in Figure 17 (examples of histologic fields for each parameter is shown in Figure 18).

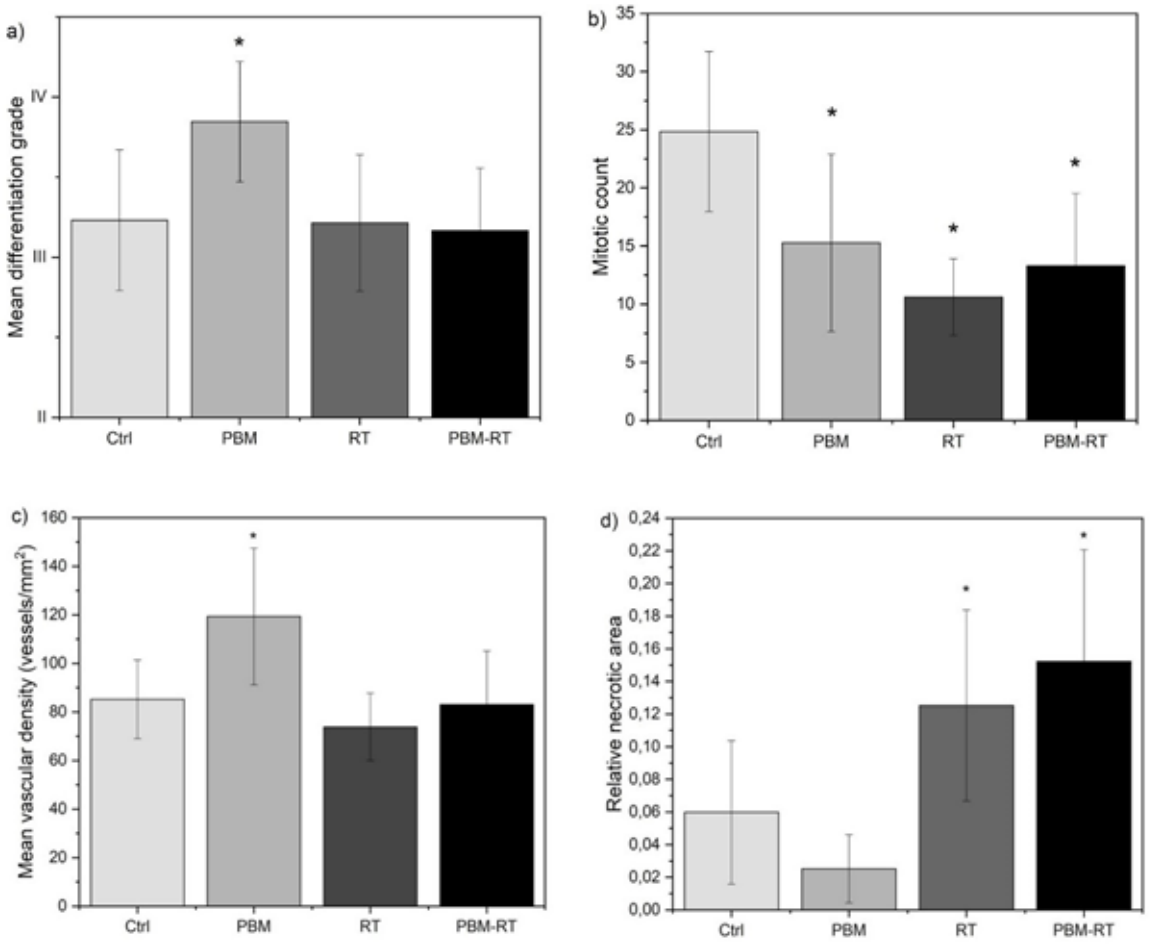

Figure 17 – Differentiation grade (a), mitotic count (b), mean vascular density (c), and relative necrotic area for all groups in vivo. The (*) symbol represents statistical significance ($p < 0.05$) from the control (N=13).

Source: Elaborated by the author.

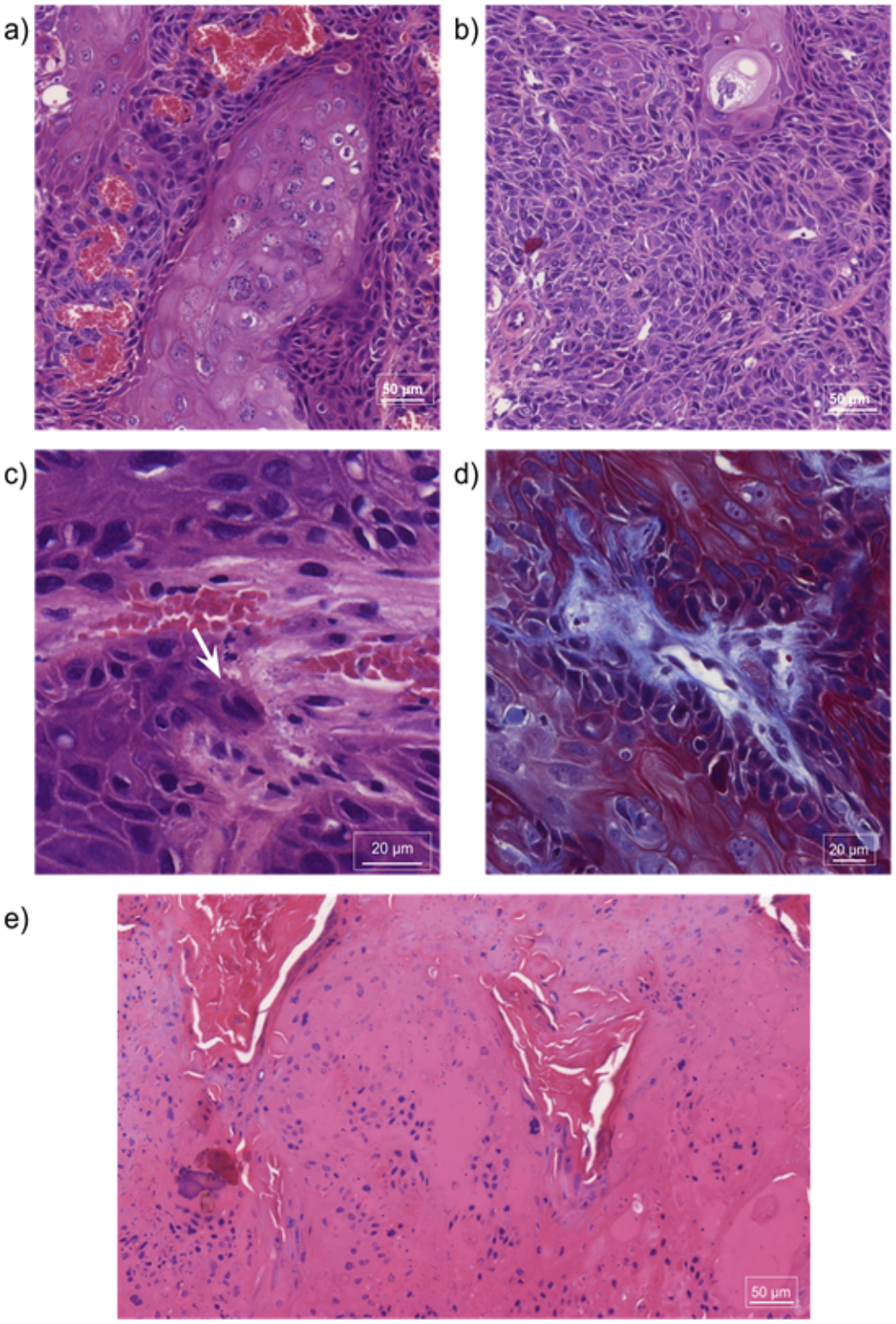

Figure 18 – Histologic images representing the parameters analysed in the study. All are stained with haematoxylin eosin staining except for (d) which is marked with Masson's trichrome. (a) Tumor showing well differenciated área - 200x, (b) Tumor showing poorly differenciated área - 200x, (c) Mitoses (arrow) - 400x, (d) Vessel's wall Masson's trichrome - 400x and (e) Tumoral necrosis - 200x.

Source: Elaborated by the author.

4.4 Discussion

PBMT in the supportive care of oncological patients has attracted increasing interest over the last few years owing to its low cost, effectiveness, and wide range of applications. Its safety on normal cells is well known, including wounds, inflammation and normal tissue sparing in radiotherapy patients. In a clinical trial by Antunes et al., in which PBMT was used as supportive care to prevent and treat mucositis, the authors reported an increase in the progression-free survival of PBMT patients compared to the placebo group and a better overall survival. (37) No adverse effects were observed in patients, and the protection of normal irradiated tissue alone improves radiotherapy outcomes; however, there remains a concern related to its effect on cancer cells. Three recent reviews have shown that the wide range of results is mostly due to a lack of standardization of illumination parameters. (6, 28, 29, 31) Bensadoun et al. stated that there are significant and growing indications in both in vivo and clinical trials that PBMT is safe and effective, and that it may even improve overall patient survival. In addition, a few studies have reported its potential to sensitize cells to radiation (6). In this study, we presented in vitro and in vivo evidence of its potential as a radiosensitizer in preclinical models, in addition to indications of its safe use on tumors, using a protocol of 780 nm at a fluence rate of 5 J/cm^2. Our in vitro results demonstrated no effect of PBMT on the proliferation of human skin cancer cells, A431 cell line. There is a modulation effect on the cell cycle after one session, with an increase in the G2/M fraction. However, it did not significantly alter proliferation, and there was a tendency to increase at 48 h, but, at 72 h, the MTT signal for PBMT cells was lower than that of the control. We believe the evidence from one session indicates a cumulative effect in the three-sessions treatment protocol. The clonogenic assay, for example, corroborates to the MTT results, as it showed a tendency for a decrease in the number of clones 7 days after the end of the protocol (comparison between control and PBMT for the 0 Gy point), but no significant difference between them. If we consider that this result is not limited to this cell line and illumination protocol, the different in vitro results observed in the literature may have resulted from the effect of PBMT over time. From the studies employing 780 nm in vitro, we see that the results reporting increased proliferation were analyzed 24 h after PBMT, and in the one that analyzed cancer cells at 24–72 h, the same behavior observed in this study was reported. (43) Additionally, Schalch et al. did not observe increased proliferation in SCC9 cells at any time after illumination. (44) Another evidence that corroborates to the hypothesis that the PBMT effects observed after one session are cumulative is the apparent relationship between the cell cycle modulation and the clonogenic assay. The increase observed in the G2/M fraction may be the cause of the enhancement of the radiation effect in A431 cells, as seen in Figure 2. Nevertheless, to confirm that, future experiments investigating PBMT effects throughout the treatment protocol are needed. To investigate whether PBMT could impact DNA damage after radiation, we have performed a RIF

quantification with H2AX-gamma labeling. In the 3 x 0.33 Gy protocol, we observed, at initial times (0h and 1h), a significant higher number of RIF/cell in the PBMRT group compared to RT. As previously stated, this result may be due to an increase in DNA damage, since a decrease in efficient repair is unlikely. Recently, Hoorelbeke et al. showed that Ca2+, ATP, ROS and NO act as propagators of DNA damage, increasing DSB in non-irradiated bystander cells. (45) Interestingly, these molecules are also upregulated after PBMT and act as mediators of their effects (5) Therefore, the propagation of DNA damage by these messengers may be enhanced by combining PBMT and radiation. Comparing both protocols, we were able to observe that clustering has a significant impact on the 3 x 0.8 Gy one. We propose future experiments with different time points and doses, as well as an analysis of repair mechanisms, to investigate this effect. Despite causing statistically significant enhancement of radiation, PBMT effects in vitro are modest. However, results in tumor xenografts indicate that the improvement of RT by PBMT is greatly enhanced in vivo, indicating that systemic effects are an important mechanism of the synergy. From the first experiments on mice, we hypothesized that the PBMT effect may appear later than the time point that was analyzed, so a Kaplan–Meier survival curve was constructed after treatment (Figures 14 and 15). From it, it is clear the enhancement of the radiation effect appears around day 12. It increased median survival in 30% and resulted in a hazard ratio of 0.417, within the confidence interval, indicating that PBMT decreased the death rate by 58.3% compared to RT. Additionally, in the PBMT-RT group there was an animal that presented not only a decrease in the growth rate, but a consistent tumor regression after treatment. Regarding PBMT alone, we observed that the initial tumor volume had impact on the curves, in which subgroup 1 (the smaller V_{in}) corresponded to a small but statistically significant decrease in survival compared to the sub-groups in the control group. Therefore, further studies should investigate the safety of PBMT alone in tumors of varied sizes. Using OCT, we could demonstrate the effects of the PBMT-RT combination over time, by quantifying superficial damage on the tumors after treatment. OCT is a non-destructive or invasive technique that has been shown to detect necrotic regions in tumors as lower refractive index regions. (46–48) PBMT-RT induced a significantly higher damage than the RT group, which was visible from day 11 to the end of the experiment. RT presented a mean damaged volume curve that was similar to that of the control for the days on which we had data from both. These observations agree with the survival results, as they indicate that the viable tumor fraction in PBMT-RT was lower than that in RT, which caused a decrease in tumor growth. From the histological analysis, we found evidence that help us understand the results from the survival curves and OCT measurements. Mitotic count, which is a measure of proliferation in vivo, was reduced in all groups compared to that in the control. This corroborates the fact that the illumination protocol used did not induce proliferation. Radiation is known to reduce the mitotic index, and we observed that irradiated groups did not behave differently with

respect to this parameter. (49) Moreover, PBMT alone increased differentiation and vascular formation, resulting in a tendency for a decrease in necrotic area compared to the control (Figure 18). Because the mean vascular density was defined from non-necrotic areas only, it is unlikely that the increase in MVP was a consequence of the larger viable tumor area in the PBMT group. In fact, we believe that the reduced necrosis may be a result of a higher and more efficient vascular system due to increased angiogenesis and differentiation, which decreases hypoxia. The decrease in hypoxia also contributes to increased radiation damage, as hypoxia is the main cause of tumor radioresistance. (50) As a result, this may have contributed to the longer survival in the PBMT group. Do Valle et al. recently published a study showing that PBMT induces an increase in blood flow and a vascular supply of illuminated wounds through the direct recruitment of pericytes to the injury site. (51) In future PBMT-RT combination studies, it would be interesting to investigate this mechanism along with the occurrence of metastasis, since increased vascularization may lead to migration of tumor cells. A431 tumor have a low metastatic potential, so it is not an adequate model for that analysis. (52) As expected, necrosis was significantly higher in the irradiated groups, with a tendency to increase in the animals receiving PBMT. Despite agreeing with the behavior observed in the OCT results, the differences were not as significant. One possible explanation for this is that the difference observed in the area becomes more relevant when integrated into a volume. Secondly, because the OCT maximum depth was about 1 mm, the measurements were limited to superficial necrosis, while histological analysis was based on the whole cross-sectional area of the tumors. Therefore, this difference may indicate that PBMT induced an increase in necrosis limited to the top portion of the tumor. If so, it would show that there is a fluence threshold for the effects that were observed because light is attenuated in the tissue, and the number of photons reaching the bottom part of the tumor is exponentially lower than at the surface. Hence, we reiterate the importance of understanding and standardizing the illumination protocols.

4.5 Conclusions

To date, there have been no studies on the impact of PBMT on tumor growth in vivo or on the radiomodulatory effect of 780-nm illumination on tumor cells, whether in vitro or in vivo. The results shown are promising, indicating that PBMT should be explored as an inexpensive, non-invasive technique that improves treatment outcomes by enhancing tumor eradication and reducing the adverse effects of radiation. With respect to PBMT alone on tumors, our results corroborate the safety of PBMT in the protocol presented, as there is no effect on proliferation, shown by two different assays. Nevertheless, future in vitro studies are encouraged, using different methods and cell lines, which should be analyzed over an extended period of time to investigate proliferation because there may be negative feedback after the initial effects of PBMT. Furthermore,

PBMT increased differentiation and vascular density, which, combined with radiation, was proven to be safe and beneficial to all initial tumor volumes, significantly increasing tumor damage and mouse survival. The combination was also positive in vitro, despite modest, increasing cell death and DSB by radiation through cell cycle modulation.

5 CONCLUSIONS

The aim of this study was to study the potential of PBMT in enhancing standard oncological treatments. For that, we initially investigated the molecular basis of PBM in cancer cells in order to understand its isolated effects. We showed that it can decrease the redox state of oral cancer as well as increase the fraction of dividing cells through distinct pathways than in normal cells. These metabolic modulation indicated PBMT potential in impacting the outcome of photodynamic therapy, since its target is the mitochondria. So we investigated that combination in oral cancer cells and observed that, for one cell line, PBMT increased the photosensitizer uptake and, consenquently, decreased survival. Additionally, as mentioned above, the experiments of PBMT alone showed that it modulates the cell cycle, which is one of the most important factor determining radiosensitivity. For that reason, combined with the knowledge that the most successful PBMT application is the prevention and reduction of morbidities in radiotherapy patients, we studied associating PBMT with ionizing radiation in an in vitro and in vivo model of squamous cell carcinoma. We demonstrated that this association increased DNA damage and death in cells and tumor regression in mice. Results indicate that the mechanism underlying these results is likely to be the modulation of the cell cycle and angiogenesis, causing an increase in necrosis when combined with radiation.

Thus, we have increased the amount of evidence suggesting that PBMT is a powerful tool to modulate biological processes in order to achieve specific biological effects. With that, it is possible to manipulate medical conditions and treatments in order to achieve better outcomes, such as sensitizing tumors to oncological therapies. Therefore, we believe that the field of PBMT is worth exploring, for its benefit-cost ratio and simple protocols, along with the possibility of improving cancer treatment.

REFERENCES

1 ARANY, P. R. Photobiomodulation: poised from the fringes. **Photomedicine and Laser Surgery**, v. 30, n. 9, p. 507–9, Sept 2012. ISSN 1557-8550.

2 ANDERS, J. J.; LANZAFAME, R. J.; ARANY, P. R. Low-level light/laser therapy versus photobiomodulation therapy. **Photomedicine and Laser Surgery**, v. 33, n. 4, p. 183–184, 2015. ISSN 15495418.

3 KARU, T. Mitochondrial mechanisms of photobiomodulation in context of new data about multiple roles of ATP. **Photomedicine and Laser Surgery**, v. 28, n. 2, p. 159–160, 2010. ISSN 15495418.

4 FARIVAR, S.; MALEKSHAHABI, T.; SHIARI, R. Biological effects of low level laser therapy. **Journal of Lasers in Medical Sciences**, v. 5, n. 2, p. 58–62, 2014. ISSN 22286721.

5 DE FREITAS, L. F.; HAMBLIN, M. R. Proposed mechanisms of photobiomodulation or low-Level light therapy. **IEEE Journal of Selected Topics in Quantum Electronics**, v. 22, n. 3, p. 348–364, 2016. ISSN 15584542.

6 BENSADOUN, R.-J.; EPSTEIN, J. B. Photobiomodulation safety in cancer patients: in vivo data. **Supportive Care in Cancer**, v. 28, n. 7, p. 3003–3006, 2020. ISSN 0941-4355.

7 HAMBLIN, M. R. *et al.* Biphasic dose response in low level light therapy - an update. **Dose-Response**, v. 9, n. 4, p. 602–618, 2011. ISSN 15593258.

8 ALGHAMDI, K. M.; KUMAR, A.; MOUSSA, N. A. Low-level laser therapy: a useful technique for enhancing the proliferation of various cultured cells. **Lasers in Medical Science**, v. 27, n. 1, p. 237–249, 2012. ISSN 02688921.

9 SOMMER, A. P. *et al.* Biostimulatory windows in low-intensity laser activation: Lasers, scanners, and NASA's light-emitting diode array system. **Journal of Clinical Laser Medicine and Surgery**, v. 19, n. 1, p. 29–33, 2001. ISSN 10445471.

10 WORLD ASSOCIATION FOR PHOTOBIOMODULATION THERAPY. **WALT Dosage recommendations**, Available from: https://waltza.co.za/documentation-links/recommendations/dosage-recommendations/. Accessible at: 19-05-2021.

11 GENDRON, D. J.; MÉNAGE, A. R. Photobiomodulation (PBM) with 20 W at 640 nm: pre-clinical results and propagation model. **Mechanisms of Photobiomodulation Therapy XII**, v. 10048, p. 100480K, 2017. ISSN 16057422.

12 ENENGL, J.; HAMBLIN, M. R.; DUNGEL, P. Photobiomodulation for Alzheimer's disease: translating basic research to clinical application. **Journal of Alzheimer's Disease**, v. 75, n. 4, p. 1405–1416, 2020. ISSN 18758908.

13 ANTUNES, H. S. *et al.* Cost-effectiveness of low-level laser therapy (LLLT) in head and neck cancer patients receiving concurrent chemoradiation. **Oral Oncology**, v. 52, p. 85–90, 2016. ISSN 18790593.

14 KALHORI, K. A. *et al.* Photobiomodulation in oral medicine. **Photobiomodulation, Photomedicine, and Laser Surgery**, v. 37, n. 12, p. 837–861, 2019. ISSN 25785478.

15 ZADIK, Y. *et al.* Systematic review of photobiomodulation for the management of oral mucositis in cancer patients and clinical practice guidelines. **Supportive Care in Cancer**, v. 27, n. 10, p. 3969–3983, 2019. ISSN 14337339.

16 ROBIJNS, J. *et al.* A narrative review on the use of photobiomodulation therapy for the prevention and management of acute radiodermatitis: proposed mechanisms, current clinical outcomes, and preliminary guidance for clinical studies. **Photobiomodulation, Photomedicine, and Laser Surgery**, v. 38, n. 6, p. 332–339, 2020. ISSN 25785478.

17 TAM, M. *et al.* Photobiomodulation therapy to mitigate radiation fibrosis syndrome. **Photobiomodulation, Photomedicine, and Laser Surgery**, v. 38, n. 6, p. 355–363, 2020. ISSN 25785478.

18 BENSADOUN, R. J. Photobiomodulation or low-level laser therapy in the management of cancer therapy-induced mucositis, dermatitis and lymphedema. **Current Opinion in Oncology**, v. 30, n. 4, p. 226–232, 2018. ISSN 1531703X.

19 SROKA, R. *et al.* Effects on the mitosis of normal and tumor cells induced by light treatment of different wavelengths. **Lasers in Surgery and Medicine**, v. 25, n. 3, p. 263–271, 1999. ISSN 01968092.

20 SCHARTINGER, V. H. *et al.* Differential responses of fibroblasts, non-neoplastic epithelial cells, and oral carcinoma cells to low-level laser therapy. **Supportive Care in Cancer**, v. 20, n. 3, p. 523–529, 2012. ISSN 09414355.

21 TAKEMOTO, M. M.; GARCEZ, A. S.; SPERANDIO, M. High energy density LED-based photobiomodulation inhibits squamous cell carcinoma progression in co-cultures in vitro. **Journal of Photochemistry and Photobiology B**: biology, v. 199, p. 111592, Oct. 2019. ISSN 18732682.

22 SHIRAZIAN, S. *et al.* Effects of 660 nm and 810 nm low-power diode laser on proliferation and invasion of oral cancer cells in cell culture media. **Photochemistry and Photobiology**, v. 97, n. 3, p. 168, 2020. ISSN 17511097.

23 FRIGO, L. *et al.* The effect of low-level laser irradiation (in-ga-al-asp - 660 nm) on melanoma in vitro and in vivo. **BMC Cancer**, v. 9, p. 404, Nov. 2009. ISSN 1471-2407.

24 MYAKISHEV-REMPEL, M. *et al.* A preliminary study of the safety of red light phototherapy of tissues harboring cancer. **Photomedicine and Laser Surgery**, v. 30, n. 9, p. 551–558, Sept 2012. ISSN 1549-5418.

25 OTTAVIANI, G. *et al.* Laser therapy inhibits tumor growth in mice by promoting immune surveillance and vessel normalization. **EBioMedicine**, v. 11, p. 165–172, Sept 2016. ISSN 23523964.

26 MONTEIRO, J. S. de C. *et al.* Influence of laser phototherapy (λ660 nm) on the outcome of oral chemical carcinogenesis on the hamster cheek pouch model: histological study. **Photomedicine and Laser Surgery**, v. 29, n. 11, p. 741–745, Nov. 2011. ISSN 1557-8550.

27 RHEE, Y.-H. *et al.* Low-level laser therapy promoted aggressive proliferation and angiogenesis through decreasing of transforming growth factor-β1 and increasing of akt/hypoxia inducible factor-1α in anaplastic thyroid cancer. **Photomedicine and Laser Surgery**, v. 34, n. 6, p. 229–235, June 2016. ISSN 1549-5418.

28 SILVEIRA, F. M. *et al.* Examining tumor modulating effects of photobiomodulation therapy on head and neck squamous cell carcinomas. **Photochemical and Photobiological Sciences**, v. 18, n. 7, p. 1621–1637, 2019. ISSN 14749092.

29 SILVA, J. L. da *et al.* Effects of low level laser therapy in cancer cells—a systematic review of the literature. **Lasers in Medical Science**, v. 35, n. 3, p. 523–529, Apr 2020. ISSN 0268-8921.

30 COURTOIS, E. *et al.* Mechanisms of photobiomodulation (pbm) focused on oral mucositis prevention and treatment: a scoping review. **BMC Oral Health**, v. 21, n. 1, p. 220, Dec 2021. ISSN 1472-6831.

31 DEL VECCHIO, A. *et al.* Laser photobiomodulation (pbm) —- a possible new frontier for the treatment of oral cancer: a review of in vitro and in vivo studies. **Healthcare**, v. 9, n. 2, p. 134, Jan 2021. ISSN 2213-0764.

32 DJAVID, G. E.; GOLIAIE, B.; NIKOOFAR, A. Analysis of radiomodulatory effect of low-level laser irradiation by clonogenic survival assay. **Photomedicine and Laser Surgery**, v. 33, n. 9, p. 452–459, 2015. ISSN 15495418.

33 BARASCH, A. *et al.* Effects of pre-radiation exposure to lllt of normal and malignant cells. **Supportive Care in Cancer**, v. 24, n. 6, p. 2497–2501, 2016. ISSN 14337339.

34 DJAVID, G. E. *et al.* Photobiomodulation leads to enhanced radiosensitivity through induction of apoptosis and autophagy in human cervical cancer cells. **Journal of Biophotonics**, v. 10, n. 12, p. 1732–1742, 2017. ISSN 18640648.

35 BARASCH, A. *et al.* Photobiomodulation effects on head and neck squamous cell carcinoma (hnscc) in an orthotopic animal model. **Supportive Care in Cancer**, v. 28, n. 6, p. 2721–2727, 2020. ISSN 14337339.

36 SILVA, C. R. *et al.* Photobiomodulation therapy combined with radiotherapy in the treatment of triple-negative breast cancer-bearing mice. **Journal of Photochemistry and Photobiology B**: biology, v. 220, p. 112215, July 2021. ISSN 10111344.

37 ANTUNES, H. S. *et al.* Long-term survival of a randomized phase III trial of head and neck cancer patients receiving concurrent chemoradiation therapy with or without low-level laser therapy (LLLT) to prevent oral mucositis. **Oral Oncology**, v. 71, p. 11–15, 2017.

38 REQUENA, M. B. *et al.* Dissolving microneedles containing aminolevulinic acid improves protoporphyrin ix distribution. **Journal of Biophotonics**, v. 14, n. 1, p. 1–14, 2021. ISSN 18640648.

39 KAPLAN, E.; MEIER, P. Nonparametric estimation from incomplete observations **Journal of the American Statistical Association**, v. 53, n. 282, p. 457–481, 1958.

40 PETO, R.; PETO, J. Asymptotically efficient rank invariant test procedures. **Journal of the Royal Statistical Society A**, v. 135, n. 2, p. 185, 1972. ISSN 00359238.

41 CHAN, T. F.; VESE, L. A. Active contours without edges. **IEEE Transactions on Image Processing**, v. 10, n. 2, p. 266–277, 2001. ISSN 10577149.

42 PARISET, E. *et al.* 53BP1 Repair kinetics for prediction of in vivo radiation susceptibility in 15 mouse strains. **Radiation Research**, v. 194, n. 5, p. 485–499, 2020. ISSN 19385404.

43 SPERANDIO, F. F. *et al.* Low-level laser therapy can produce increased aggressiveness of dysplastic and oral cancer cell lines by modulation of akt/mtor signaling pathway. **Journal of Biophotonics**, v. 23, n. 1, p. 839–847, Apr 2013. ISSN 1864063X.

44 SCHALCH, T. D. *et al.* Photobiomodulation is associated with a decrease in cell viability and migration in oral squamous cell carcinoma. **Lasers in Medical Science**, v. 34, n. 3, p. 629–636, 2019. ISSN 1435604X.

45 HOORELBEKE, D. *et al.* Cx43 channels and signaling via ip3/ca2+, atp, and ros/no propagate radiation-induced dna damage to non-irradiated brain microvascular endothelial cells. **Cell Death and Disease**, v. 11, n. 3, p. 194, 2020. ISSN 20414889.

46 MEER, F. J. Van der *et al.* Apoptosis- and necrosis-induced changes in light attenuation measured by optical coherence tomography. **Lasers in Medical Science**, v. 25, n. 2, p. 259–267, 2010. ISSN 02688921.

47 WANG, T.; BREWER, M.; ZHU, Q. An overview of optical coherence tomography for ovarian tissue imaging and characterization. **WIREs Nanomedicine and Nanobiotechnology**, v. 7, n. 1, p. 1–16, 2015. ISSN 19390041.

48 IFTIMIA, N. *et al.* Investigation of tissue cellularity at the tip of the core biopsy needle with optical coherence tomography. **Biomedical Optics Express**, v. 9, n. 2, p. 694, 2018. ISSN 2156-7085.

49 HALL, J. W.; FRIEDMAN, M. Histologic changes in squamous-cell carcinoma of the mouth and oropharynx produced by fractionated external roentgen irradiation. **Radiology**, v. 50, n. 3, p. 318–350, March 1948. ISSN 0033-8419.

50 BEGG, K.; TAVASSOLI, M. Inside the hypoxic tumour: reprogramming of the ddr and radioresistance. **Cell Death Discovery**, v. 6, n. 1, 2020. ISSN 20587716.

51 VALLE, I. B. do *et al.* Photobiomodulation drives pericyte mobilization towards skin regeneration. **Scientific Reports**, v. 10, n. 1, p. 1–15, 2020. ISSN 20452322.

52 KOCHNEVA, G. V. *et al.* Model of artificial metastasis of human epidermoid carcinoma a431 in nude mice for the examination of oncolytic activity of the vaccinia virus. **Russian Journal of Genetic**: applied research, v. 6, p. 469 - 476, 2016. ISSN 20790600.